A VHF BOUNDARY-LAYER RADAR

By

Scott N.M. Dullaway, B.Sc. (Hons)

Thesis

submitted for the degree of

MASTER OF SCIENCE

at the

UNIVERSITY OF ADELAIDE

(Department of Physics and Mathematical Physics)

January 1999

Contents

Abstract

This thesis is concerned with the development of a VHF wind profiler capable of measuring from a height of 300 metres up to 4 kilometres. This region of the troposphere contains the mixed-layer, which is more commonly known as the convective boundary layer region.

The different types of atmospheric detection equipment used to measure the boundary layer region of the atmosphere are reviewed, along with wind profiling observation techniques.

The factors considered during the development of the antenna arrays are described, which includes the beam patterns of antenna arrays, and the technical aspects of impedance matching from the individual antennas through to the transmission and acquisition system to minimise the effect of antenna ringing. The effects of scattering and ground clutter on the performance of boundary-layer VHF wind profilers are also discussed.

Results from initial tests of a single module of Yagi antennas of the system are shown, demonstrating the ability of the radar during the developmental stages for probing the boundary layer. A comparison of radar reflectivities with values calculated using radiosonde data from the Adelaide airport is also performed. An examination of pattern scales in the boundary layer is then carried out to determine the optimum configuration of the antenna arrays for spaced antenna mode operation.

This thesis then concludes with the the first results of the boundary layer radar in its optimum configuration. A study of pattern scales and the angular spectrum of scatterers in the lower troposphere was performed, and the comparison of results of campaigns of co-located high resolution GPS radiosondes and Omega Navaid radiosondes with the Adelaide Boundary Layer Radar are shown completing this research.

Altogether this thesis examines the potential of VHF radars in the application of boundary layer monitoring. These radars will not only have research applications due to their high spatial and temporal resolution for investigating the lower troposphere, but are potentially an important tool for meteorologists for continuous monitoring of the atmosphere in all weather conditions, even in remote locations.

Originality Declaration

This work contains no material which has been accepted for the award of any other degree or diploma in any university or other tertiary institution and, to the best of my knowledge and belief, contains no material previously published or written by another person, except where due reference has been made in the text.

I give consent to this copy of my thesis, when deposited in the University Library, being available for loan and photocopying.

Signed: ..... dated: 14 January 1999

Scott N.M. Dullaway, B.Sc. (Hons)

Acknowledgements

I would like to thank my supervisors, Dr Robert Vincent and Dr Iain Reid for their direction during my project. Dr Vincent's drive and encouragement to me were always a good motivator to complete this thesis.

I also thank Dr Peter May of the Bureau of Meteorology Research Centre for providing me with access to the radiosonde data from Adelaide airport and discussions on meteorological phenomena occurring in the boundary layer. Thanks also to Jeff Stickland of the Bureau of Meteorology for supplying the radiosondes for the intercomparison campaign of the sonde's results with the radar's results.

Dr Graham Elford and Dr Harish Chandra also provided useful insights into the larger field of atmospheric physics through our regular atmospheric physics group meetings.

A number of individuals have provided me assistance through my studies especially my fellow students Andrew MacKinnon, Jonathon Woithe and Florian Zink. They have always been willing to help with the development of this system, through to the analysis of data, which has been greatly appreciated.

There have also been many friends in the atmospheric physics group some of which have come and gone over the period of my studies, whom I also wish to thank including Dr Simon Allen, Andrew Badger, Karen Berkefeld, Dr Laurence Campbell, Dr Manuel Cervera, Dr Steve Eckermann, Dr Dorothy Gibson-Wilde, Stephen Grant, Dr Trevor Harris, Bridget Hobbs, Dr David Holdsworth, Ali Kazempour, Dr Patrick Klövekörn, Dr Sujatta Kovalam, Dr Drazen Lesicar, Dr David Low, Dr Chris Lucas, Dr Damien Murphy, Minh Nguyen, Dr Deepak Rajopadhyaya, Dr Andrew Taylor, Dr Brenton

Vandepeer, and Rupa Vuthaluru.

I would also like to thank the technical support given to the group by Simon Ludborsz, Shane Dillon, Alex Didenko, and Lesley Rutherford. The assistance given by ATRAD, Tomco, and Brian Fuller with Genesis is also appreciated during the testing of the transmitter and receiver systems. I am also grateful to Lyn Birchby and Dallas Kirby in the atmospheric administrative office whom always provided assistance when required.

Lastly, I would like to thank my family whom this thesis is dedicated to for their love and support throughout my studies. My sister Janelle, my parents, and my grandmother, all provided the support and encouragement I needed to complete this thesis. Thank you.

List of Figures

List of Tables

Chapter 1

Introduction To The Planetary Boundary-Layer

The planetary boundary layer (PBL) is the lowest region of the atmosphere. This region is the interface between the lower atmosphere's turbulent atmospheric flow, and the region above, the free atmosphere. The characteristic turbulence of the PBL requires that the frictional effects of the Earth's surface need to be taken into account for understanding it's dynamics.

The importance of the physical processes which regularly occur in this region can be seen due to the uniformity of the PBL from just a few metres above the surface (surface layer), up to the entrainment zone, which is where the relatively dry free atmosphere mixes with the moist boundary layer [*Holton* 1992]. Thorough mixing within the boundary layer results in a relatively uniform wind field and a constant decline in temperature with height, unless temperature inversions are present.

This convective mixing and transport of air parcels within the region are also important for the consideration of pollution management near heavily populated or industrial areas for two reasons. These include that heat pools can be formed in this region of the atmosphere from human activities at a locality, and an understanding of the dynamics of the atmosphere at that location needs to be obtained to determine whether there will be a safety hazard to nearby populations from pollutants being

dispersed in the atmosphere.

1.1 Introduction, Motivation & Scope

The primary goal of the research described in this thesis is the development of a VHF radar system which has the capability of probing from the lower levels of the convective boundary layer well into the the free atmosphere above the mixing layer. This system developed in the course of this research consists of small modules of 3-element Yagis. This enables the array to have a small aperture, but still have high directivity. This ensures that the beamwidths are narrow so that clutter is minimised, but that the Fresnel region of the radar is still low enough to enable probing at low levels of the atmosphere. The radar employs vertically directed beams using the spaced-antenna technique for measuring winds.

The recent surge in interest around the world in the development of radar systems for lower tropospheric investigations is due to a number of factors. The development of modular solid-state units and modern high-powered computer controllers opened up the field for vastly improved non-military development of high resolution interrogation, both temporally and spatially, of the lower region of the atmosphere. The reliability of these systems, and the ability to be fully automated for probing the atmosphere, to on-line processing of data and storage of results for remote retrieval has also contributed to their popularity.

This has spawned the growth in research in this area to enable more comprehensive investigations of the convective boundary layer to occur by radar.

Profiling of the boundary layer using UHF radars commenced in the late 1980's and has grown very rapidly with numerous systems now in operation around the world at frequencies of 400, 900, and 1300 MHz [*Ecklund et al.* 1990]. The large effect on the strength of the returns due to humidity enables UHF profilers to be used for hydrometeor and cloud dynamics studies [*Currier et al.* 1992].

The early work by the National Oceanic and Atmospheric Administration research

groups in the development of UHF wind profilers [*Ecklund et al.* 1990] showed the capabilities of UHF systems for studying hydrometeors in the boundary layer as well as wind profiling. The development of 915 MHz profilers through the late 1980's and early 1990's has been reviewed by *Carter et al.* [1995].

The development of UHF boundary layer radars before VHF systems occurred because of a number of desired features gained by using UHF. This included the high resolution available for probing the atmosphere when using sub-metre wavelengths, and the ability to be in the far-field of the small antenna arrays from only 50 to 100 metres above ground level.

A number of UHF radars are not aspect sensitive [*Cohn et al.* 1998], so tilted layers in the atmosphere will not affect the strength of radar returns as a function of angle. The relevant issue is that the atmospheric scatterers that these radars detect are usually not aspect sensitive, so radars which are aspect sensitive remain unaffected. A further benefit of having a small wavelength in comparison to the antenna modules for UHF systems is that you can form small beamwidths. This is useful for avoiding ground-clutter.

The most significant advantage of developing a VHF system over a conventional UHF boundary layer radar, is that at VHF the returned echoes from even heavy precipitation will not dominate the clear-air echoes to such an extent that the clear-air returns are lost. This effect frequently occurs with UHF systems for even moderate precipitation. Thus the flexibility of a VHF boundary-layer radar would potentially enable it to be used in investigations of the dynamics of the atmosphere including vertical velocities during precipitation within low-level clouds, and low-level atmospheric phenomena such as short time-scale microbursts to longer time-scale frontal activity, due to its all-weather conditions versatility. The problems of a UHF system regarding contamination from insect swarms and birds [*Richner et al.* 1998], would not be encountered with a VHF radar due to the increased size of the radar wavelength.

The pioneering development of a VHF boundary-layer system in France [*Crochet* 1993] showed significant hurdles have to be overcome before these systems could move

from the research environment into common use for monitoring of the atmosphere. These problems include :

1. The large physical size of the antenna arrays and relatively high mean transmitter powers which are needed to meet a high altitude initial objective, produces numerous problems including ringing of the antenna;

2. Clutter from the experimental site, and;

3. Equipment modifications needed to enable low altitude observations including receiver and antenna design.

This thesis is the result of an attempt to overcome a number of these problems during the development of a novel boundary layer profiler. The advantages of using VHF for all-weather monitoring are significant to the wider community through an improved ability to research atmospheric phenomena in the presence of precipitation, leading to a useful tool for meteorological services. The detection ability of wind shears at airports in all weather conditions by these radars is also of potential significance.

1.1.1 Outline of Thesis

Here the atmosphere is briefly described and then we focus on the boundary layer. This will involve explaining the processes which occur in the atmosphere around us. We then look at the different types of equipment which are used to observe the atmosphere. This includes the different techniques used to study the characteristics of the atmosphere.

The capability of a radar system depends significantly on the antenna array used. It is shown that there are a number of properties of the arrays which need to be carefully optimised in order to minimise clutter and noise and to maximise the signal returns. The antenna array arrangement also depends upon characteristics of the atmospheric scatterers. This is examined for optimising the antenna configuration and for reducing possible biases in the methods used to determine the winds.

In Chapter 4, preliminary results for the system obtained using a single module of Yagi antennas for both transmission and reception are discussed. This enables a comparison of radar results with the results from radiosondes launched at Adelaide airport. In particular we compare the atmospheric properties contributing to the potential refractivity of the atmosphere as determined by the radiosondes with the returned power echoes obtained by the radar.

An initial determination of the pattern scales in the boundary-layer is performed by transmitting on a single Yagi group or "module" and reception on three modules with different spacings for checking the cross-correlations to determine the size of the scatterers in the atmosphere.

In Chapter 5, the final configuration of the Adelaide boundary layer radar is described. Further investigations were then carried out to verify the correct separation by determination of the ground pattern scales from the full correlation analysis. These pattern scales were then studied to see if there was any relation between their size and their position within or above the convective boundary layer.

Recommendations for future work for the further development of this system, and investigations into the atmosphere are then outlined in Chapter 6.

1.2 The Atmosphere

The atmosphere is a fluid which is gravitationally held to the Earth's surface and pervades everything above it. It is a commonly held belief that the atmosphere was formed by the expulsion of volatile substances from the inner Earth by volcanic activity. The composition of gases was then modified over a long period of time to its present proportions initiated by the photo-dissociation of water, photosynthesis reactions and other biological activity. The root mean square velocity, v_{rms}, of the lightest molecules (e.g. hydrogen) in the upper atmosphere exceeds the Earth's escape velocity so these gases were continually lost to space.

It has been known for over a century that the temperature structure of the lower

atmosphere decreases with altitude. This is called the lapse rate, and is typically 7°C km^{-1} up to 10 km.

It was in 1902 that two meteorologists, Teisserence de Bort and Richard Assman independently discovered what we now call the tropopause, a layer of relatively constant temperature with height. This layer separates the troposphere, where temperature decreases with height, from the stratosphere, where the atmospheric temperature increases with height. A diagram of vertical temperature profile with height can be seen in Figure 1.1 from *U.S. Standard Atmosphere* [1976]. The most common method of defining the different atmospheric regions comes from the temperature profile. Each of these regions, being the troposphere, stratosphere, mesosphere, and the thermosphere, are each capped by a region of constant temperature with altitude except the thermosphere.

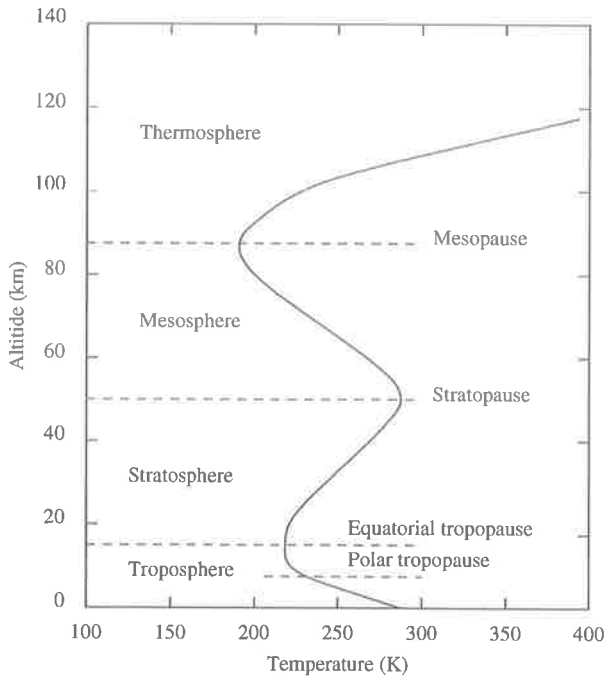

Figure 1.1: Temperature profile of the atmosphere.

The region of most interest to us for this study is the one closest to the Earth, the troposphere. It accounts for more than 80% of the mass and virtually all of the water vapour, clouds and precipitation in the Earth's atmosphere [*Wallace and Hobbs*

1977]. This is why the dynamical processes which occur in the troposphere dominates the *weather* that we encounter.

In all but the lowest region of the troposphere, the low levels of turbulence of air parcels except in the region of short time or space-scale phenomena such as thunderstorm activity, results in a free atmospheric flow, with horizontal velocities an order of magnitude larger than the vertical velocities.

The troposphere is a region of strong vertical mixing, especially in its lowest section. The capping layer, or tropopause, defines the abrupt changes in the constituent ratios between the troposphere and the stratosphere. The photo-chemistry which occurs in the stratosphere has a number of consequences. These include the creation of ozone and a temperature gradient which increases with altitude. This positive temperature gradient causes strong stability and consequently limited mixing occurs in the stratosphere. A consequence of these photo-chemical reactions and the tropopause separating the troposphere and the stratosphere is that the air above the troposphere is ozone rich, while the troposphere is ozone deficient. The stratospheric air is also very dry in comparison.

The thermodynamic state of the atmosphere has a large bearing on the structure of the atmosphere at any localised region. The equation of state for air is :

$$p = \rho RT \quad , \tag{1.1}$$

where p is the pressure, ρ is the density, R is the gas constant per mole, and T is the temperature.

Now since vertical motion in the atmosphere is small, the static equilibrium assumption requires that the gravitational force on air molecules must be balanced by the pressure gradient force. Thus the atmosphere is in hydrostatic equilibrium when :

$$\frac{dp}{dz} = -g\rho \quad , \tag{1.2}$$

where g is the gravitational acceleration, and z is the altitude of the air parcel.

Here we follow the deduction of the adiabatic lapse rate of an atmosphere by *Houghton* [1986]. For an atmosphere in hydrostatic balance, the first law of thermodynamics can be written as either :

$$dq = c_p \, d \ln T - R \, d \ln p \quad , \tag{1.3}$$

or

$$dq = c_v \, dT + p \, dV \quad , \tag{1.4}$$

where c_v is the specific heat at constant volume, and c_p is the specific heat at constant pressure.

Integrating (1.3), and taking the antilogarithms results in the potential temperature, θ, which is the temperature a parcel of dry air would have once compressed or expanded to p_0, the standard pressure of 1000 hPa, from a pressure p and temperature T.

An important conserved quantity the potential temperature, θ, can be developed

$$\theta = T \left(\frac{p_0}{p} \right)^{\kappa} \quad , \tag{1.5}$$

where $\kappa = \frac{R}{c_p}$.

Differentiating (1.1) results in :

$$p \, dV + V dp = \frac{R \, dT}{M_r} \quad , \tag{1.6}$$

where M_r is the molecular weight of the air.

Now for a perfect gas :

$$c_p - c_v = \frac{R}{M_r} \quad . \tag{1.7}$$

Then substitution for a perfect gas of Equation 1.4 into Equation 1.6, and substitution of $p \, dV$ from the hydrostatic equation, for the case where there is no transfer of heat to or from the parcel, results in Γ_d, the adiabatic lapse rate for a dry atmosphere.

$$-\frac{dT}{dz} = \frac{g}{c_p} = \Gamma_d \quad . \tag{1.8}$$

When $-\frac{dT}{dZ}$ is less than Γ_d the atmosphere is stable, and when it is greater, the atmosphere is unstable.

The thermodynamic properties of unsaturated air are similar to those for dry air. However in the lower atmosphere saturation does occur when unsaturated air rises and cools. When this process occurs the relative humidity increases until it reaches 100%, which will be at the condensation level.

Houghton [1986] similarly showed that for saturated air, the saturated adiabatic lapse rate, Γ_s, is approximately :

$$\Gamma_s = -\frac{dT}{dz} = \Gamma_d \left(1 + \frac{LeM_{rv}}{\rho RT}\right)\left(1 + \frac{LeM_{rv}}{\rho RT}\frac{\epsilon L}{c_p T}\right)^{-1} \quad , \tag{1.9}$$

where e is the partial pressure of the water vapour, M_{rv} is the molecular weight of the water vapour, L is the latent heat, and ϵ is 0.622, the ratio of molecular weight of water to air.

The vertical motion of air parcels can thus be determined by the stability of the saturated air with its liquid water. Stable conditions in the atmosphere are similarly found when $-\frac{dT}{dZ}$ is less than Γ_s, and unstable conditions exist when $-\frac{dT}{dZ}$ is greater than Γ_s.

When adiabatic displacement of a parcel occurs, the buoyancy frequency N, also known as the Brunt-Väisälä frequency, is used as a measure of the static stability of the atmosphere :

$$N^2 = g\frac{d\ (\ln\ \theta_0)}{dz} \quad . \tag{1.10}$$

There are a number of methods of displaying the water vapour in the atmosphere, as listed by for example *Wallace and Hobbs* [1977]. These include using the mixing ratio, w :

$$w \equiv \frac{m_v}{m_d} \quad , \tag{1.11}$$

where m_v is the mass of water vapour, and m_d is the mass of dry air.

The pressure due to the water vapour in the air, e, is given as :

$$e = \frac{w}{w + \epsilon} p \quad , \tag{1.12}$$

When the air is saturated, the saturated mixing ratio w_s becomes :

$$w_s \equiv \frac{m_{vs}}{m_d} \quad , \tag{1.13}$$

$$w_s \simeq 0.622 \frac{e_s}{p} \quad , \tag{1.14}$$

where m_{vs} is the mass due to saturated water vapour in a given volume of air, and e_s is the pressure due to saturated water vapour in the air.

Finally, the relative humidity, RH is defined as :

$$RH = 100 \frac{w_{sd}}{w_s} \quad , \tag{1.15}$$

where w_{sd} is at temperature T_d and pressure p, while w_s is at temperature T and pressure p.

1.3 The Planetary Boundary-Layer

The planetary boundary layer (PBL) is the thin layer of atmosphere closest to the Earth's surface. The top of the planetary boundary layer at mid-latitudes is normally at an altitude of around 1 km in winter at mid-latitudes and up to 3 km in summer. This layer consists of strong mixing throughout the region due to the turbulence resulting from the frictional effects of the Earth's surface on the atmosphere, and due to surface heating. This frictional effect causes a significant vertical shear of the wind with height.

Even though the region is quite thin by volume, it still accounts for about 10% of the atmosphere by mass. This region also plays an important part in the vertical transfer

of momentum in the atmosphere and consequently needs to be carefully considered for understanding the dynamics of the troposphere as a whole.

This convective region is broken into two divisions, the surface layer which is the lowest few metres of the atmosphere, and the Ekman layer named after the Swedish oceanographer V. W. Ekman. The Ekman model of determining the wind field in the boundary layer deviates considerably from actual boundary layer winds as summarised by *Holton* [1992]. Holton showed that the structure and amplitude of the turbulent eddies responsible for the vertical momentum transport in the boundary layer need to be known to accurately model the wind velocity field.

The atmospheric turbulence is what causes the thorough mixing in this region as air parcels are disrupted producing uniform regions of momentum, potential temperature, and moisture in the PBL.

Air parcels have a number of horizontal forces acting on them, including the Coriolis force, pressure gradient force and frictional forces. Here we follow the description of these forces given by *Wallace and Hobbs* [1977].

The Coriolis force, C, is an apparent radially directed force with its sense dependent upon the planetary rotation and the zonal motion of the winds. Westerly flows have an outward directed force, and eastward flows result in an inward directed force.

Now,

$$C = -fk \times V \quad , \tag{1.16}$$

where f is the Coriolis parameter,
k is the unit vector in the vertical direction, and
V is the velocity vector of the wind.

The Coriolis parameter f is :

$$f = 2\Omega \sin \phi \quad , \tag{1.17}$$

where $\Omega = 2\ \pi$ rad day^{-1}, and ϕ is the geographical latitude of the air parcel on the Earth.

The pressure gradient force, P, is the force on a parcel of air due to an incremental decrease in pressure on different faces of the air parcel.

$$P = -\frac{1}{\rho}\nabla p \quad , \tag{1.18}$$

where ∇ is the gradient operator.

The frictional force, F, which is the drag on an air parcel is :

$$F = -aV \quad , \tag{1.19}$$

where a is a positive coefficient dependent upon the wind speed, roughness of the underlying surface, and the static stability.

The balancing of the three forces, the Coriolis force, the pressure gradient force, and the frictional force, depending upon the stability of the atmosphere determines the speed and direction of the wind field.

The Ekman layer equations for determining the departure of the wind field from the geostrophic balance in the boundary layer are :

$$K_m \frac{\partial^2 u}{\partial z^2} + f(v - v_g) = 0 \quad , \tag{1.20}$$

$$K_m \frac{\partial^2 v}{\partial z^2} - f(u - u_g) = 0 \quad , \tag{1.21}$$

where K_m is the eddy viscosity,
u_g and v_g are the geostrophic velocities.

Holton stated that vertical shear of the geostrophic wind, which is where the wind field is parallel to the isobars of pressure, would cause deviations from the Ekman solution within the boundary layer. The Ekman solution is the spiral curve used to determine the velocity variation as a function of height. He also noted that circulations due to instability for a neutrally buoyant atmosphere would result in a decrease in the angle between the boundary layer wind and the geostrophic wind.

The Mixing Length Theory which was devised by Prandtl and Von Karmen, enables an estimation of the magnitude of the eddy viscosity, which is determined by the nature of the atmospheric flow as converse to the nature of the fluid, in the planetary boundary layer. Turbulence results in the instantaneous velocity, U, in a fluid to fluctuate about a mean velocity $\overline{U}$, by an amount corresponding to the turbulent eddies U' :

$$U = \overline{U} + U' \quad . \tag{1.22}$$

The Mixing Length Theory states that a parcel of fluid may be moved vertically by a distance l', the mixing length, before there is a change in the mean horizontal velocity. Thus the change of the turbulent eddies with height, z, is :

$$U' = -l' \frac{\partial \overline{U}}{\partial z} \quad . \tag{1.23}$$

When there is neutral vertical stability in the atmosphere, then $N = 0$ for where $\Gamma = \Gamma_d$. The buoyancy effects are minimal and the turbulent eddies should be of similar dimensions in all three dimensions, thus :

$$w' = -l' \frac{\partial \overline{V}}{\partial z} \quad , \tag{1.24}$$

where $\overline{V}$ is the mean horizontal velocity field, and w' is the vertical velocity component associated with the turbulent eddies. The velocity notation used in this thesis is u and v represent the zonal and meridional winds, and w the vertical velocity.

There are numerous meteorological phenomena which are only applicable to the planetary boundary layer due to their small depths. The type of phenomena encountered in any locality depend upon the topography of that region. A common feature of localities near coastal strips are sea breezes and land breezes.

Sea breezes are a common result in the afternoon as the surface temperature of the land usually exceeds the sea temperature, resulting in the air rising over the land. The cooler, moister maritime air is then drawn inland across the coast.

Land breezes generally occur during the night and in the early morning when the sea temperature exceeds the land temperature, resulting in the air rising over the ocean and air being drawn at low-levels out to sea.

Other low-level atmospheric phenomena can include katabatic winds and anabatic winds along the slopes of hills, and also shallow winter-time frontal activity. These are all phenomena which a boundary layer radar can study.

1.4 Summary

This chapter has outlined the goals of this thesis through the development of the VHF Adelaide Boundary Layer Radar.

The introduction to the atmosphere as a whole, and the convective boundary layer in particular are to enable an understanding of the radiosonde data received from Adelaide airport, and also at the location of the boundary layer radar during the radiosonde campaigns conducted at Buckland Park, which is the University of Adelaide's field site for the Atmospheric Physics Research Group. The field site is located nearly 40 km north of the city of Adelaide at 35 S 138 E.

In chapter 2, the equipment and techniques used for ground based atmospheric probing and *in situ* probing of the atmosphere are discussed.

In chapter 3, the technical details concerning the development of the antenna arrays and matching of the array's impedance and bandwidths for the Adelaide boundary-layer radar are discussed.

A pilot study of the VHF boundary layer radar was then conducted with results shown in chapter 4. The comparison of the radar's results with results from radiosondes launched at the Adelaide airport were used to confirm the sensitivity of the radar to fluctuations in the refractive index of the atmosphere.

Testing for proof of concept of the VHF boundary-layer for Spaced Antenna measurements of atmospheric winds is shown in chapter 5. A study of the pattern scales of the boundary layer to verify the correct spacing of the antenna modules for wind

determination is also described in chapter 5.

The conclusions drawn from the results of this thesis, along with recommendations for future research of the atmosphere using the commissioned Adelaide boundary-layer radar are then summarised in chapter 6.

The ability to study atmospheric phenomena which are not only restricted to the PBL but also penetrate both the PBL and the troposphere are necessary to fully understand everyday meteorological phenomena. The continuous monitoring that radar systems can give of the atmosphere is a valued goal for both researching and monitoring of the "weather".

Chapter 2

Atmospheric Observation: Equipment and Techniques

2.1 Introduction

There are numerous methods of investigating the atmosphere. This chapter introduces a number of ground-based remote sensing techniques. *In situ* methods using balloon launches for measuring the meteorological conditions of the atmosphere, are also considered.

2.2 MST Radars and Observation Techniques

This section looks at the operation of electro-magnetic radar systems for probing the atmosphere and the theory behind their operation. The term radar stands for *ra*dio *d*etection *a*nd *r*anging of targets. In the field of atmospheric physics, the target is the air itself and meteorological phenomena within that medium. The term MST radars stands for *mesosphere-stratosphere-troposphere* radars, as these are the regions of the atmosphere that the radars are able to probe.

We will first look at what causes reflections of electro-magnetic radiation in the atmosphere. We will then proceed to discuss different radar systems which can be

used for monitoring the convective boundary, and the principles of their main forms of operation.

2.2.1 Scattering of EM Waves by the Atmosphere

The scattering mechanisms of radar systems are due to two fundamental phenomena, precipitation and fluctuations in the refractive index of the atmosphere.

Weather radars, as discussed by *Doviak and Zrnić* [1993], usually operate at low elevation angles, and are used in an azimuthal scanning mode. They are principally used to detect precipitation.

Atmospheric radars or wind profilers are primarily used for detecting clear air turbulence and changes in refractive index due to fluctuations in water content, pressure and temperature of air parcels. The radio refractive index is given by *Tatarskii* [1961] as being approximately :

$$n - 1 = \frac{3.73 \times 10^{-1} e}{T^2} + \frac{77.6 \times 10^{-6} p}{T} \quad , \tag{2.1}$$

where

p = atmospheric pressure (hPa),

e = partial pressure of water vapour (hPa), and

T = absolute temperature (K).

The first term on the right is the contribution due to the density fluctuation of water vapour due to the bound electrons. The second term is due to the density fluctuations from dry air.

In the boundary layer the first term generally dominates due to the relatively high humidity of this region. The second term becomes dominant in a region extending from the upper troposphere through to the stratopause.

The scattering and reflection of radar pulses occur due to fluctuations in the index of refraction, n, which itself is dependent upon the density of molecules and their polarisation within the atmosphere. When irregularities exist in the refractive index on the scale of a half radar wavelength, the Bragg condition for scattering and reflection

of the radar signal is satisfied. The irregularities in the refractive index can be produced by turbulence or from stratification of the atmosphere into layers [*Briggs* 1980]. These regular variations of temperature and humidity causing the stratification of the atmosphere can result in partial reflection where the strength of the returned power of a radar echo varies with zenith angle [*Röttger and Liu* 1978]. The radar reflectivities can thus be determined by the vertical gradient of the generalised refractive index, M, as given by *Gage and Balsley* [1980] :

$$M = -77.6 \times 10^{-6} \frac{p}{T} \left(\frac{\partial \ln \theta}{\partial z} \right) \times \left[1 + \frac{15500\, q}{T} \left(1 - \frac{1}{2} \frac{\frac{\partial \ln q}{\partial z}}{\frac{\partial \ln \theta}{\partial z}} \right) \right] \quad , \tag{2.2}$$

where

θ = potential temperature (K),

q = specific humidity.

Equation 2.2 can also be rewritten as :

$$M = M_{Dry} + M_{Wet} \quad , \tag{2.3}$$

where

$$M_{Dry} = -77.6 \times 10^{-6} \frac{p}{T} \left(\frac{\partial \ln \theta}{\partial z} \right) \quad , \tag{2.4}$$

and

$$M_{Wet} = -77.6 \times 10^{-6} \frac{p}{T} \left(\frac{\partial \ln \theta}{\partial z} \right) \times \left[\frac{15500\, q}{T} \left(1 - \frac{1}{2} \frac{\frac{\partial \ln q}{\partial z}}{\frac{\partial \ln \theta}{\partial z}} \right) \right] \quad . \tag{2.5}$$

By comparing the components of the generalised refractive index with the Brunt-Väisälä frequency defined in (1.10) , it is seen that they are directly proportional, and both are dependent upon the stability of the atmosphere. The atmospheric stability term is given by $\left(\frac{\partial \ln \theta}{\partial z} \right)$. It is also known that the structure parameter of refractive index, C_n^2, is proportional to M^2 through [*Gage et al.* 1980]:

$$C_n^2 = \frac{a_n^2\, \alpha'\, Ri_{crit}\, \epsilon_{turb}^{\frac{2}{3}}\, M^2}{N^2} \quad , \tag{2.6}$$

where

a_n^2 is a constant,

α' is the ratio of the eddy diffusivities,

Ri_{crit} is the critical gradient Richardson number, and

ϵ_{turb} is the eddy dissipation rate within a turbulent layer.

The reflection of radar waves by the atmosphere can be due to isotropic scattering from turbulence or anisotropic scattering from aspect-sensitive scatterers. A study of irregularities in the troposphere by *Vincent and Röttger* [1980] showed that Fresnel or partial reflections of radar signals occurs in regions of high stability.

The Fresnel scatter model describes the occurrence of multiple specular reflectors in the radar volume. The numerous studies of specular models are important to VHF radars but not for UHF boundary-layer radars due to the atmospheric scatterers detected by VHF radars being aspect sensitive.

Isotropic scattering from clear air turbulence is believed to be the dominant source of reflections for radars operating at large ($> 10°$) off-vertical angles, while for vertical beams specular reflections are thought to dominate [*Tsuda et al.* 1997].

Fresnel reflection or scattering is a process that leads to a specularlike reflection from coherent surfaces of intense gradients in refractive index, *Gage et al.* [1981]. Fresnel reflection is due to inhomogeneities lying in a thin layer, while Fresnel scattering is a volume-scattering process. The narrow spectral widths of echoes produced by these scattering mechanisms leads to narrow arrival angles, clearly distinguishing this type of scattering from isotropic scattering mechanisms, as discussed by *Gage and Green* [1978].

2.2.2 UHF Boundary-Layer Radars

UHF radar systems for monitoring the boundary layer have become common in the 400 to 1300 MHz region due to their good height resolution and their ability to commence probing from heights as low as 100 metres. UHF radars are also very sensitive to hydrometeors as discussed in *Ecklund et al.* [1990], for example.

It is the combination of high resolution and sensitivity to precipitation of UHF radars which gives these systems their wide usage in studies of the evolution of hydrometeors within non-precipitating clouds as well as fall velocities within the atmosphere including virga where the precipitation is completely evaporated before it reaches the ground. The penalty for this however is that clear air echoes are completely swamped by the strength of returns from moderate to heavy precipitation. This was shown in *May et al.* [1994]. *Cohn et al.* [1995] did find an observation where a clear-air reflective layer was enhanced when precipitation passed through it. There is however no explanation for this isolated instance.

The contributions of the radar returns from clear air and hydrometeors as taken from a diagram in *Rajopadhyaya* [1994] is seen in Figure 2.1. The contributions to the radar reflectivity on a 50 MHz VHF radar, with a wavelength about 6 metres, will be similar for both clear air and hydrometeors. However the sensitivity of UHF radars to precipitation means that echoes from hydrometeors dominates by up to 50 dB over the clear air echoes, which can only be detected in the presence of light precipitation.

To determine the true hydrometeor fall velocities for UHF radars, the clear-air velocity contributions need to be removed from the spectra. This can be achieved by comparing the Doppler spectra of the UHF radar with an even higher frequency profiler which would also be sensitive to precipitation [*Williams et al.* 1998]. Since the two radars have a different sensitivity to Bragg scattering, they will produce different reflectivity for the clear-air velocities of the spectra, while producing similar reflectivity from Rayleigh scattering for the precipitation echo [*Gage et al.* 1998]. This enables the clear air and precipitation velocities to be each distinguished. This could also be calculated from radars which have been scaled using the dBz reflectivity factor scale. This is where the echo power has been scaled to equalise the observed Rayleigh scattered power on radars of different wavelengths. The use of another instrument, an acoustic bird-call listening system, can be used to assess the presence of birds [*Van Zandt et al.* 1998], however the problem of contamination due to insects and the nocturnal activity of bats still needs to be fully addressed. The work of *Merritt* [1995]

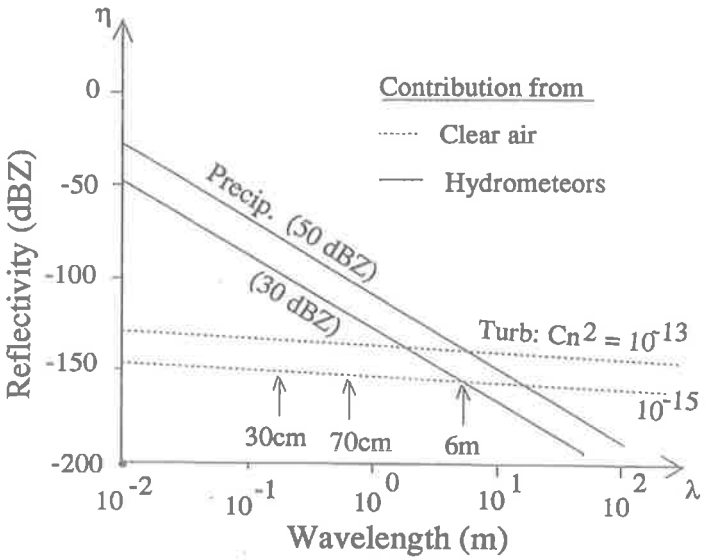

Figure 2.1: Figure from *Rajopadhyaya* [1994] showing the relative radar reflectivities due to clear air turbulence and hydrometeors as a function of operating frequency. The increased sensitivity of UHF systems to precipitation compared with VHF is shown. The corresponding wavelength for the UHF frequency range is between 0.3m and 3m. The wavelength for the VHF frequency range is between 3m and 30m.

has shown, however, that the intermittent nature of bird and bat echoes can be significantly reduced through the development of routines that compute average radar Doppler spectra which use statistical averaging methods for removing flier contamination.

UHF wind profilers can be used for detecting and classifying different rain types through detection of the melting layer height in cold environments where there is a sharp increase in the fall speed [*Ohno et al.* 1998]. These systems are able to measure profiles of the falling speed, reflectivity and the spectral width of the precipitation echo. A weakness of these systems is that sometimes the maximum sampling range is too small to detect the height of the melting layer. This can result in the incorrect classification of stratoform rain as convective precipitation.

The use of UHF wind profilers to examine turbulence by *Rogers et al.* [1996] and *Angevine and Grimsdell* [1998] showed that estimates of turbulent dissipation rates could be extracted from profiler measurements. Limitations due to nonstationarity,

inhomogeneity, and scaling affected measurements, however.

Determining the height of the convective boundary layer through finding the peak of the reflectivity can be automated [*Angevine* 1998], however, depending on how well the top of the PBL is defined the chosen peak may not be the peak which corresponds to the top of the PBL.

2.2.3 VHF Boundary-Layer Radars

The previous use of VHF radars has primarily been the probing of the atmosphere from 2 km to 20 km to determine the vertical and horizontal wind field. They have also been a powerful tool for studying wave motions of the atmosphere both in the troposphere through to the mesosphere [*Woodman* 1981]. These radars operate through their sensitivity to turbulent irregularities in the refractive index of the neutral atmosphere for the troposphere, stratosphere and mesosphere, and through the presence of free electrons in turbulence or meteor trails in the lower ionosphere [*Gage* 1981].

The two basic methods of measuring wind velocities with MST radar systems, Doppler beam-swinging (DBS) and Spaced Antenna (SA) technique, have been reviewed by *Briggs* [1968*a*], *Briggs* [1968*b*], *Briggs* [1980], *Briggs* [1993], *Hocking* [1983*b*], *Larsen and Röttger* [1989], *Liu et al.* [1990], and *Röttger* [1984].

The DBS technique as described by *Röttger* [1984], uses the change in frequency of the returned echo from beams pointed at various angles and their associated radial components to determine the velocity of irregularities. A vertical beam is used to determine the vertical wind and then a minimum of two off-vertical directions are used to determine the horizontal wind. The selected altitude is determined from the time from transmission to delay, and the associated vertical component of an off-vertical beam from the round trip of the radar transmission.

The limitations of UHF radars of obtaining an atmospheric return from the clear air during periods of precipitation resulted in a move to study the ability of VHF radars for investigating the convective boundary layer. The other advantages of VHF are that clutter from non-atmospheric objects such as insect swarms, birds, bats and

other small air-borne objects would not produce the same order of interference as it does for UHF, due to the wavelength dependence of scattering.

Fillol et al. [1997], discussed the problems of using a VHF system for investigating the atmosphere with oblique beams when the beamwidth is large due to using an antenna array which is very small. This includes the problem of beam broadening and shear broadening which was first verified by *Hocking* [1983*a*]. This showed that the spectral width for tilted beams was larger than for a vertical beam of the same polar half-width. At a given range, the echoes will be due to scatter in a number of range bins resulting in contamination which can not be easily removed. This may result in these systems required to perform extra vertical sampling during acquisitions to accurately determine the vertical velocity of the atmosphere and then successfully separate the different altitude data within range gates. This problem of small antenna sizes resulting in wide beams can be seen in Figure 2.2 for the mini-radar consisting of an array of 4 coaxial-colinear antennas of 6 elements.

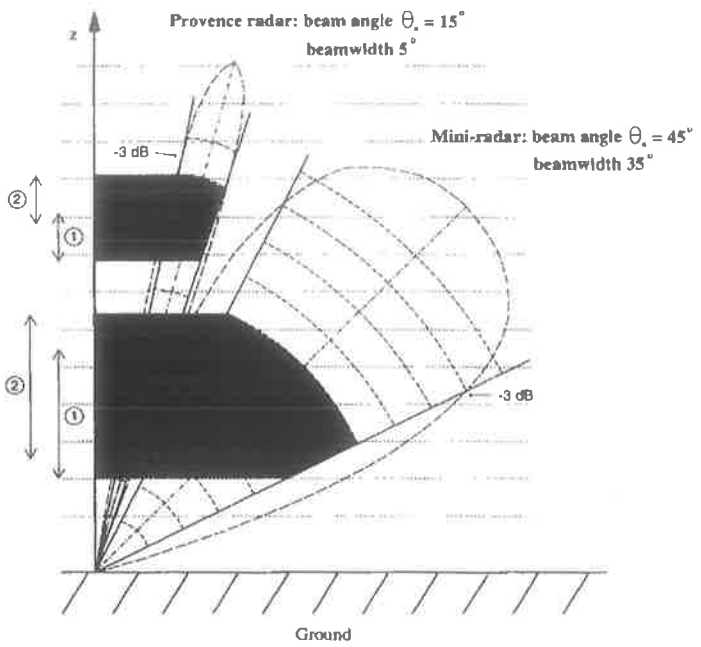

Figure 2.2: Figure from *Fillol et al.* [1997] demonstrating the problem large beamwidth VHF boundary layer systems have when operating with oblique beams for contamination from adjacent range gates.

This contamination from adjacent heights for oblique wide beam radars has resulted in the French (Fillol, Broche and Crochet), working to develop indirect methods to determine the atmospheric reflectivity and wind velocity profiles, which they have reported requires further investigation to retrieve the wind profiles in a routine manner.

2.2.3.1 The Doppler Technique

The DBS technique is frequently used by radar systems with narrow beamwidths. The implications for boundary layer radars of off-vertical beams has already been mentioned.

This method enables a determination of the wind through the phase changes of the backscattered signal to the radar. This rate of change of the phase gives the scatterers' velocity along the direction of the beam, the radial velocity (v_{rad}) :

$$v_{rad} = -\frac{\lambda}{4\pi}\frac{d\phi}{dt} \quad , \tag{2.7}$$

where λ is the wavelength of the propagating radiation, and ϕ is the phase of the signal.

It is necessary that the average value of the wind within a radar volume be used to find the mean wind. Through the use of vertical beams, the vertical velocity can be found, which then enables the horizontal velocity to be found for any particular azimuth by :

$$v_{rad} = v_h \sin\theta + w\cos\theta \quad , \tag{2.8}$$

where

v_h = horizontal velocity,

w = vertical velocity,

θ = the tilt angle of the beam from the vertical.

This then enables the meridional and zonal angles to be calculated once the vertical velocity is determined and two off-zenith beams have been used.

2.2.3.2 Spaced Antenna Analysis

The SA technique has been recently described by *Briggs* [1984]. This technique uses the movement of the diffraction pattern of the backscattered signal from irregularities to determine the horizontal movement of the medium for each range gate.

The auto and cross-correlations from pairs of receiving antennas i and j shown in Figure 2.3, enable the spatio-temporal correlation function for the full correlation analysis (FCA) to be parameterised. These FCA parameters include the fading time $\tau_{0\cdot5}$ where the lag of the mean auto-correlation function equals $0 \cdot 5$. The cross-correlation maximum ρ_{0ij} and its associated lag $\tau_{ij}^{'}$, and τ_{ij} is where the auto-correlation function equals the zero-lag cross-correlation.

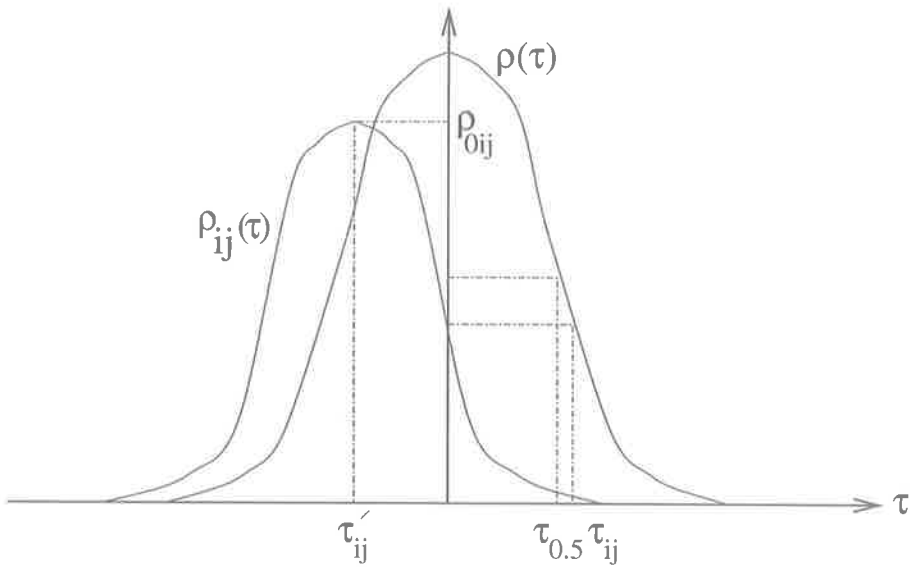

Figure 2.3: Auto and cross-correlation parameters of the FCA technique for a pair of antennas.

The pattern scale is determined as the average size of the characteristic ellipse, which is the ellipse formed where the cross-correlation function in the horizontal plane is 0.5.

The ground velocity of the pattern detected by the timeshifts of the signal fading at receiver pairs enables a determination of the apparent velocity of the scatterers. The true velocity, which takes into account the random changes occurring in the pattern

as it moves and the anisometry of the moving patterns can be calculated by the FCA technique. The FCA technique requires a minimum of three non-colinear spaced receivers.

Another method, the interferometric technique, forms an interferometer by receiving on separate groups of antennas. These techniques both determine the angle of arrival of backscattered signals using cross-spectral techniques. The Doppler shift of the signals is used to find the radial velocity of the scatterers. This then enables the three dimensional wind field to be determined.

With the DBS, the signal power changes as the pointing angle changes. Similarly the FCA technique also enables the scatterers' aspect sensitivity to be calculated. This is necessary to find the pattern scales of scatterers in the atmosphere, as the spacing of antenna arrays for SA needs to be of the order of the pattern scales to enable the true velocity to be correctly determined without biasing from the triangle size effect [*Golley and Rossiter* 1970] and [*Holdsworth* 1995].

It has since been shown by *Briggs* [1980], *Van Baelen et al.* [1990], and *Vincent et al.* [1987] that the SA and DBS techniques are essentially the same, if the different biases introduced by the two techniques are correctly removed.

There are still differences between the techniques which result in the SA technique being used in preference to DBS. These were discussed by *Cohn et al.* [1998], and include an increased aspect sensitivity of reflectivity for SA over DBS, and the concept that DBS assumes a uniform wind field which is not true in the PBL, which SA avoids through its probing of a single radar pulse volume for each height.

2.3 Acoustic Sounders

Acoustic sounders are a method of probing the boundary layer up to cloud layers which are not precipitating. They have excellent vertical resolution and enable measurements of the temperature structure, gravity waves, wind, and temperature to be made. A description of acoustic sounding experiments over the past twenty years and their

theory of operation has been given by *Crescenti* [1997].

The principle of operation of acoustic sounders is the transmission of a 1000 Hz to 4500 Hz pulse either by a dedicated transmitter, or a transceiver, which is a combined transmitter and receiver, which is then backscattered by the atmosphere. The scattering of these pulses by temperature inhomogeneities from turbulence is then received.

When a single transceiver is used, the intensity of the backscattered signal is purely dependent upon the thermal structure of the atmosphere which enables a temperature profile of the atmosphere to be determined. The entire wind field is able to be determined when three transceivers are used. This is accomplished by orienting two antennas so that they are at oblique angles, normally 15° to 30° from the vertical at right angles to one another, and the third transceiver is vertically oriented. The horizontal and vertical wind fields are then able to be calculated from the radial components.

The weakness of these systems is that in periods of precipitation or even non-precipitating periods of high turbulence with strong winds, the system's performance is extremely limited. This is due to the generation of noise by these meteorological disturbances.

2.4 Radio-Acoustic Sounding Systems

The development of radio-acoustic sounding systems (RASS) using Doppler tracking of an acoustic pulse by an electromagnetic radar proved to be a significant advance on the original sounders. RASS determines the temperature from measurements of the velocity of the speed of sound, V_s :

$$V_s = AT^{\frac{1}{2}} \quad , \tag{2.9}$$

where

T = absolute temperature, A = a constant dependent on the relative humidity.

The process which RASS uses involves the vertical transmission and propagation of an acoustic pulse in the atmosphere. This pulse creates variations in the local index of refraction due to disturbing the density of the air. This pulse then acts like a good radar target for the co-located radar due to the choice of an acoustic pulse length λ_a, at the radar's optimal reflectivity of:

$$\lambda_a = \frac{\lambda_r}{2} \quad , \tag{2.10}$$

where λ_r is the radar pulse length.

As *Frankel and Peterson* [1976] describe, the co-location of the RASS speakers and the radar enable the acoustic pulse to be easily tracked by the radar. This enables the propagating acoustic wavefront to act as a large spherical reflector due to the approximately spherical acoustic wavefront propagation, that focuses the radars signal back to its antennas. Other reasons included scattering of the radar signal from successive wavefronts when a high enough repetition pulse is used with the sounder. This enables a higher data sampling rate for improved time and height resolution of the temperature profile from the measured virtual temperature profile of the atmosphere.

Importantly the acoustic wavelength must be one-half of the radar's transmitted wavelength if Bragg scattering is to occur, so that the returned signal strength is coherently integrated from each acoustic wavefront.

The ability of wind profiling radars in conjunction with RASS to remotely sense the temperature profile of the atmosphere has been shown to be effective for 50 MHz radars up to an altitude of 5 to 9 km [*May et al.* 1988]. The maximum range is restricted by the size of the intensity profile on the ground, which is a limitation on the size of the radar antenna array, as the horizontal advection of the pulse by the wind could result in the spot missing the radar's receiving array [*Clifford et al.* 1978].

A method to improve the accuracy of measurements of the atmospheric temperature profile to that of a typical radiosonde, by using a chirped atmospheric pulse was first proposed by *Masuda et al.* [1992]. This method reduces the error in the Doppler frequency shift due to the finite widths of the acoustic and radar pulses.

There are significant advantages of RASS when used with VHF BL radars. This includes using larger wavelengths which results in less absorption by the atmosphere. A consequence of lower absorption is an increased altitude range available to VHF BL radars integrated with RASS over UHF systems.

2.5 Radiosondes

Balloon-borne radiosondes have existed for the last sixty years for obtaining temperature, pressure and humidity profiles of the atmosphere, from near ground level up to altitudes of nearly 30 km. The winds are determined by tracking the position of the balloon by either radar or some navigation system such as Omega from the propagation of the radiosonde assuming that in the horizontal direction that it was moving with the mean wind and not a short term fluctuation.

Wind calculations are performed using two basic methods. Radiosondes using VLF signals transmitted by the Omega or Loran-C navigational aid (navaid) beacons work via retransmitting the navaid signal. The base station is then able to determine the radiosonde position from the reference signal from the navaid and the delay in the signal from the radiosonde. The velocity of the wind is then easily calculated from the change in position with time of the sonde's position. The Omega radiosondes are no longer available as the Omega navaid beacons were shut down in September 1997.

Another type of radiosonde is the high resolution GPS system. This system uses a GPS receiver which measures the L1 carrier shift frequencies [*Väisälä* 1996]. The wind velocity is able to be calculated from the Doppler shifts once account is taken of the satellite motion.

The sonde and the base station both receive the GPS satellite network signal. The sonde then determines its relative movement to the satellites from the Doppler shifted carrier frequencies of the satellites. The Doppler data is then relayed to the base station by a UHF signal. The satellite's motion then still needs to be removed before the winds can be calculated.

The base station computes the wind velocity via the Differential GPS (DGPS) concept using local carrier phase Doppler shift measurements to the satellites. The DGPS technique removes bias errors incorporated into the satellite signal by determining the error between that computed and the actual known location of a reference position. This measured bias is then used to correct all of the local GPS receivers' data. From the GPS times and the downloading of the satellite ephemerides, the wind is then calculated by combining the Doppler measurements with the satellite and the radiosondes measurements.

The determination of the wind vectors still has many artifacts due to the balloon-radiosonde's relative motive. This velocity vector due to the effect of the pendulum motion swamps the atmospheric winds and needs to removed. The problem of pendulum motion of the balloon-radiosonde system is minimised through filtering of the velocity components using a low pass filter corresponding to the reception interval of data from the sonde. This also enables small breaks in the data to be easily interpolated.

At least four satellites are required for determination of the radiosonde velocity in three dimensions. The accuracy in determining the wind velocity is dependent upon the number of satellites visible to the systems, and improves with the number of satellites in view.

2.6 Summary

This chapter reviewed the equipment and techniques most commonly used for investigating the convective boundary layer. Advances in sounding equipment to enable the integration of RASS with VHF boundary layer radars will enable a broad spectrum of parameters to be determined by these highly flexible and portable systems.

The advantages of VHF over UHF boundary layer systems through reduction in interference from insects, birds, and bats, and the ability to receive clear air echoes in

the presence of precipitation make them highly useful for applications such as aerodrome weather systems which need to be on-line in all weather conditions. The ability to receive the precipitation echo as well, will also enable studies of hydrometeors and micro-cloud dynamics with these systems. There is also the increased height coverage of VHF BL systems with RASS over UHF systems due to absorption of the shorter wavelength by the atmosphere.

In addition the different equipment and techniques can still be used to complement one another as they enable a wide range of possible combinations to occur. Each technique has advantages and disadvantages, so where one device has a weakness, another can be utilised for completeness in investigating the atmosphere.

Chapter 3

The Adelaide VHF Boundary-Layer Radar

The design factors which needed to be considered during the development of the radar system included

1. Small antenna size to ensure that the lowest height range was in the far field of the antenna;
2. Wide bandwidths to enable sampling at low altitudes with good range resolution;
3. Relatively narrow beamwidths for future developments including beam-steering, and also to minimise clutter; and
4. Optimum antenna spacing and orientation to minimise biasing of wind determinations.

3.1 Introduction

There are a number of factors where need to be taken into account when considering the antennas of a SA boundary layer system. These factors include

1. The antennas need to have as high a directivity as possible so that the overall array is still small. The choice, taking into account cost, was a strong deciding

fact in the choice of 3-element Yagi antennas. Good-front to back power ratios ensured that ground planes were not required, thus keeping down cost and making the system more transportable.

2. The array must be easily assembled and disassembled for transportability. This resulted in the development of the frameworks for locating the antennas.

3. The antennas and the circuitry used to combine the signals to and from each antenna and subsequent module had to be tunable to within very small tolerances due to the small signal strengths being used in transmission for the radar, and to reduce reflections.

4. The circuitry should be zero phased correctly to ensure accurate control of the beam pointing direction.

This chapter looks at the characteristics of the radar system's components which restrict the sensitivity of detection of weak atmospheric phenomena. There are five main areas where unwanted signals are introduced, or where loss of the transmitted signal can occur even for a seemingly functioning radar.

The problems to be overcome, include

1. Miss-phasing or miss-matching of the antenna arrays, within the receive path and with the receivers;

2. Incorrect spacing of the antenna arrays for local conditions;

3. Slow fading from low-level local ground clutter;

4. Spurious echoes from aircraft, and;

5. The atmospheric detection problem occurs for all radars when there is a lack of radar targets where $M^2 \rightarrow 0$. It was shown in equation 2.2, that M^2 depends on the vertical gradients of humidity and potential temperature. Then, it is possible for M^2 to be quite large in a humid environment, even if the static

stability is neutral. However, when there is both a constant increase in potential temperature with height in a stable atmosphere, and a constant decrease of humidity with height, the scenario where $M^2 \rightarrow 0$ occurs. This results in a lack of detection of signals if the radar system does not have automatic gain control capability.

If there are constant phase differences between antenna modules, or even individual antennas within a module then the beam will be off-zenith, and there will be horizontal contamination of vertical data, with a corresponding minor decrease in the measured horizontal winds relative to the true winds. If the impedance of any component is changed, such as through damage to a connection to an antenna, then the power transmitted to that module will decrease, and the pattern characteristics for transmission and reception will not be as expected, resulting in a wider beamwidth.

The radar signal when scattered by the irregularities produces a diffraction pattern on the ground. The Spaced Antenna (SA) technique samples the moving diffraction pattern and the resulting time series of the complex electric field are used to deduce the vertical and horizontal winds. The spacing of the antenna modules in the SA method is important, as the size of the antenna spacing should be the same as the ground diffraction pattern scale if wind calculations are to be accurate as discussed by *Briggs* [1984]. If the spacing is too wide the signals from adjacent antennas are poorly correlated and random statistical errors are large. When the spacing is too small, you have $\tau' \sim 0$, as observed in Figure 2.3. These small correlation times result in large relative errors in them so derived measurements are also prone to large errors. If the triangle is not an equilateral, then this incorrect spacing results in the triangle size effect as first noted by *Kelleher* [1966].

Since the path between the antenna arrays and local ground structures can have a continuously changing refractive index, then there would be slow fading resulting from this ground clutter which can have a very strong return relative to any atmospheric return.

The removal of aircraft echoes is required to prevent contamination of winds in that interval of time at that range gate.

Different atmospheric conditions can result in significant changes in the power received. To fully utilise the dynamic range of radar systems it is useful to have automatic gain control to enable weak echoes to be optimally detected without saturation of the receivers. A second method is to modify the radar parameters to have multi-mode operation, where different pulse lengths and hence mean powers, are used in a consecutive sequence.

3.2 The Antenna System

The use of small array modules is important so that the lowest height measurements performed are not in the Fresnel or near-field pattern. The small array modules also enabled signal ringing to be minimised in comparison to large antennas and antenna feed cables.

The antenna system for the Adelaide Boundary Layer Radar consists of 3 element Yagi antennas with a dipole length of half a wavelength of the transmitted radio frequency. The director and reflector for the antenna enable the antenna to have a high directivity and enable use without a ground plane due to the front to back ratio of 12 dB. These features are highly useful in minimising equipment required for a transportable VHF radar system.

It was decided to make the basic element a group of 4 Yagis, as shown in Figure 3.1. Each Yagi is spaced by a $0 \cdot 7\lambda$ separation to reduce the beamwidth which is referenced as the half-power half-width beamwidth of 36° for a single three-element Yagi antenna as seen from the top dotted line in Figure 3.2, to a narrower beamwidth for the whole group of 21°. This increased the gain of the set-up array.

As part of this project it was decided to use a framework for setting up the Yagis which was constructed from water pipe with 3-way corner joints for locating the Yagi poles. This enabled easy movement of the modules relative to one another, and also was

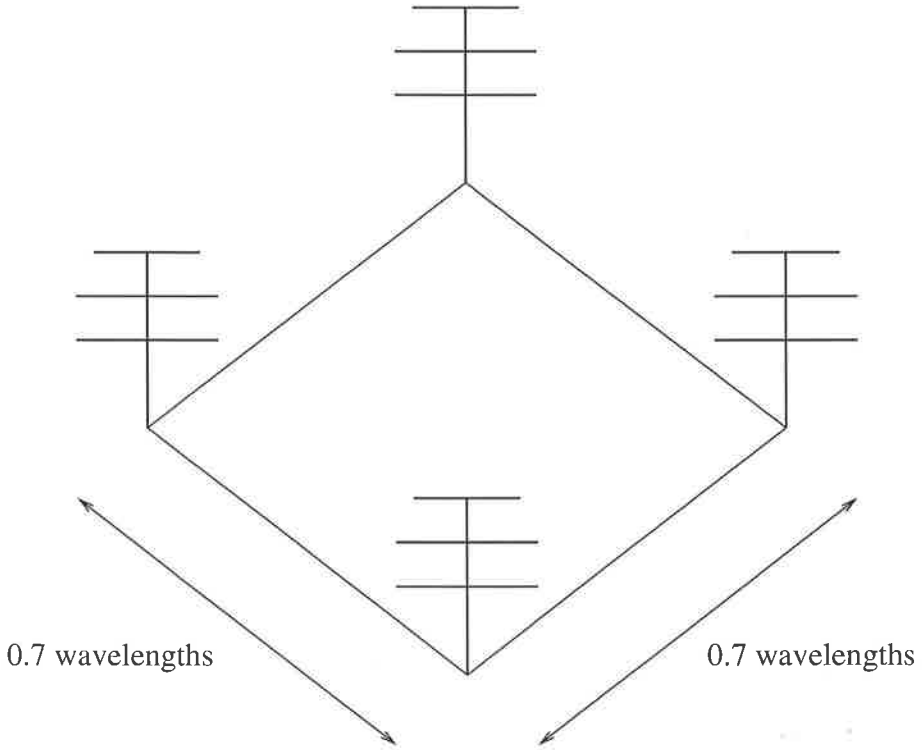

Figure 3.1: Antenna layout for a single module of Yagis.

simple to dismantle and reconstruct for portability. Guy wires are however essential for holding the antennas taut to restrict movement in the wind.

The active element of the antenna is tapped along its length at 200 Ω and then needs to be matched to the coaxial cable characteristic impedance of 50 Ω. This impedance is transformed and balanced through a balun attached directly to the driven element. The group of four Yagis are then combined and matched for a 50 Ω output which is connected to the receivers.

During the set up of the antenna arrays, these circuits need to be carefully constructed as it is not only important that the antenna arrays are physically set up with the correct spacing and vertical alignment, but all of the components have to be correctly phased to ensure that the radar is looking at the volume of atmosphere intended. This is achieved through ensuring that individual antenna elements, cables and combiner boxes are all matched. One method of checking this is to use a signal generator together with a vector voltmeter. Verifying that the input reference signal

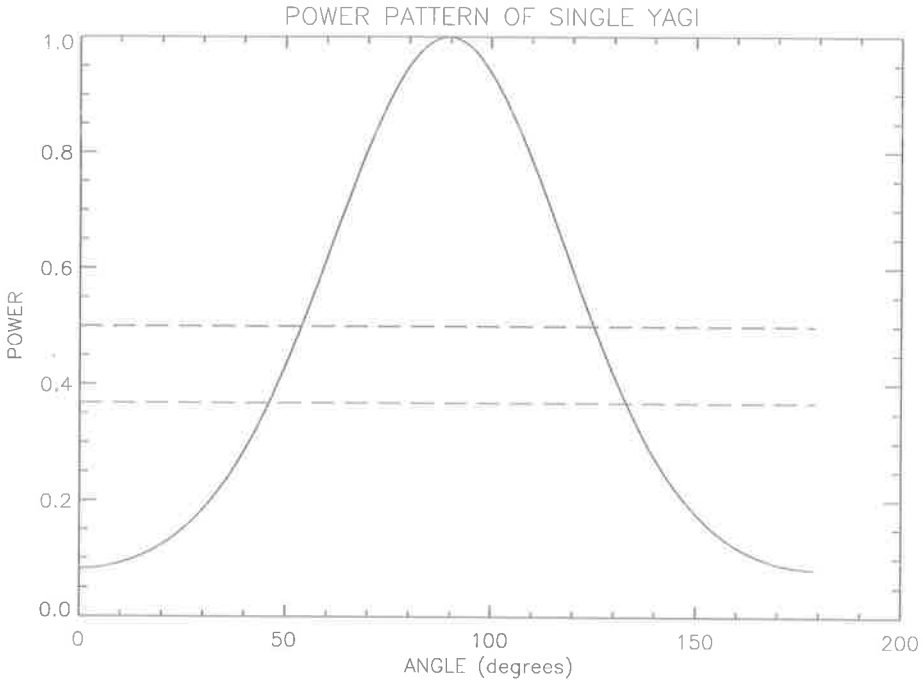

Figure 3.2: Theoretical Power pattern of a single Yagi antenna. The top dotted line is the half-power level, and the bottom dotted line is the e^{-1} power level.

has the same relative magnitude and phase at all of the outputs of the combiner boxes ensures a vertically pointing beam.

The setup of the signal generator and vector voltmeter used to check that the individual components within the signal path were correctly phased relative to one another is shown in Figure 3.3. Fifty ohm terminators were placed on the inputs and outputs of the circuits during testing as all components are tuned to 50 Ω.

The electrical lengths of cables can also be quickly checked by using the signal generator with an oscilloscope.

3.3 Antenna Ringing and Circuitry for its Removal

To ensure that the beam pattern formed by a group of Yagis is of the expected form, and in the direction chosen, then the individual antennas within a module must then be in-phase relative to one another and of equal impedance. Antenna ringing, which

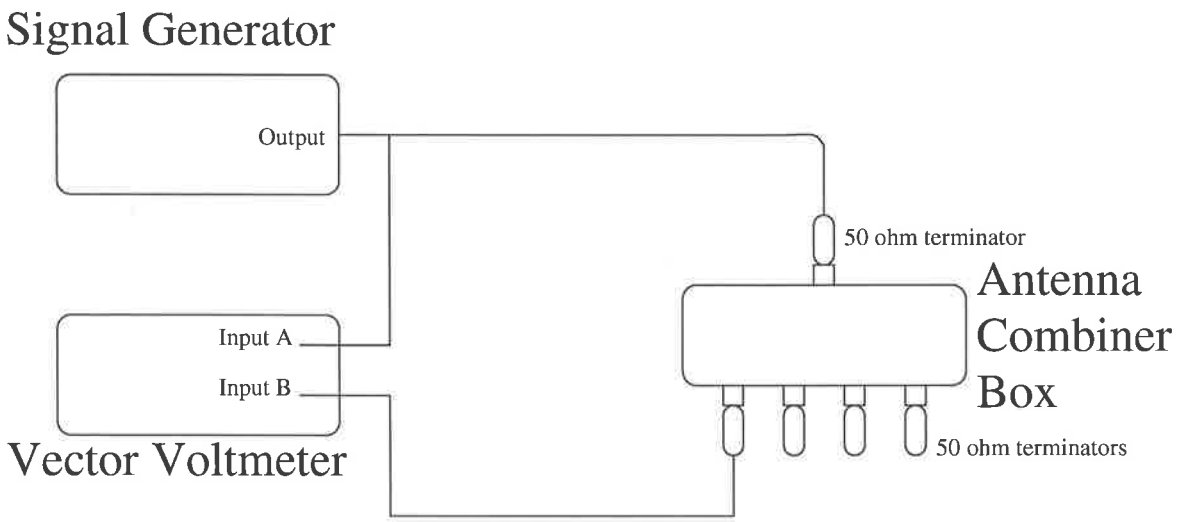

Figure 3.3: Method using a signal generator and a vector voltmeter to correct the relative phasing of circuitry used to match antenna array components.

is where electric energy is reflected around a circuit, is a consequence of impedance mismatching between different elements of the system. This results in a very strong coherent signal which can swamp any atmospheric signal from low levels. Careful construction of matching circuits used in the splitting of signals and tuning of modules and antennas needs to be performed. It is also important that such equipment is protected from the extremes of weather to ensure reliable operation at all times.

Military specification MIL-213 low-loss coaxial cable was used between the antennas and the transmitter/receivers, to ensure that the characteristic impedance was as close to 50 Ω as possible to minimise impedance mismatches which would result in signal reflection at connections, and for maximising weak signal detection.

3.3.1 Coaxial Cable Tuning Circuits

The baluns for tuning individual antennas, and the splitter box for connecting a group of module of antennas together, underwent several design changes during their development. Initially, coaxial cable was used to match the impedances of the system to the antennas. This however was not suitable for tuning of elements or splitters if impedance changes occurred due to weathering of any antennas or elements. The

incursion of moisture into connections quickly resulted in corrosion which modified the impedances resulting in significant ringing of the antennas.

The coaxial cable matching circuits were also not optimal due to their reduction of the bandwidth for the Yagi module. This is shown in Figure 3.4. Since the circuits are difficult to accurately tune, this contributes to the narrow bandwidths of the circuit and restricts sampling at low altitudes through antenna ringing.

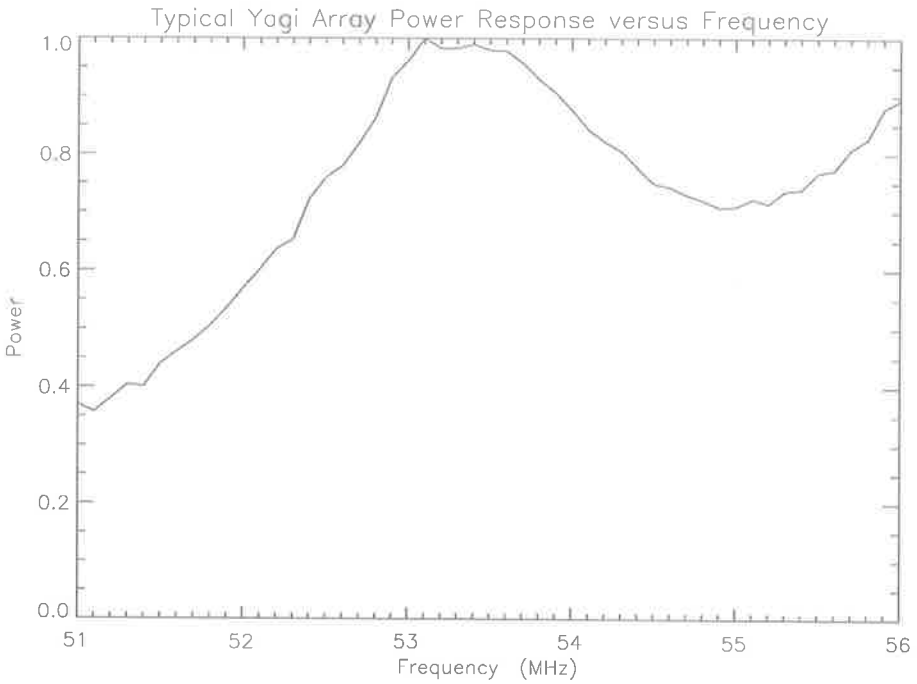

Figure 3.4: Power response of a typical combiner box with frequency using coaxial cable for matching circuit components.

3.3.2 LC Tuning Circuits using Coiled Wire Inductors

The next method of impedance matching utilised LC circuits. A problem with using coiled wire inductors is, that at high radio frequencies, there is a high mutual impedance between the inductors and other circuit components. To ensure that the circuit impedances are close to desired when working at Radio Frequencies (RF), it is important to have the connections between different circuit components as short as

possible.

3.3.3 LC Tuning Circuits using Toroidal Wound Inductors

The design finally chosen utilised toroidal wound inductors in an LC circuit. The characteristics of the toroids enabled two desirable features to be obtained. First they enabled a large bandwidth of a few megahertz around the radar's transmitted frequency of 54.1 MHz. This was determined by connecting a vector impedance meter into the baluns at the antennas, and also into the combiner boxes to measure the power response of the circuit by scanning through the frequency range near the selected frequency of 54.1 MHz.

Constructing the 4 to 1 baluns using a wire wound toroid in a T-matching circuit with a variable capacitor enabled the impedance of the antenna to be precisely matched to the characteristic impedance of the coaxial cable. This enabled the impedance to be balanced, and since both the inductive and capacitive components could be adjusted then the magnitude and phase of the resultant impedance could be accurately set.

This final circuit design also enables a module to still effectively function even if the impedance of a single antenna varies widely from the desired values. This occurs since even when the rest of the circuit for the module is no longer correctly tuned, the miss-matching is only minor due to the isolating effect of the toroidal wound inductors in conjunction with the isolation resistors. Second, this design enabled antennas and entire modules to be both quickly and accurately retuned to 50 Ω and 0° with an accuracy of ± 0.1 Ω and ± 0.1°. The circuitry for this design for the baluns can be seen in Figure 3.5, and for the splitter boxes in Figure 3.6.

Table 3.1: Circuit components for baluns.

Component	Value
Ferrite Core Inductor	4:1 wound (VHF core)
Capacitor	5 to 65 pF (500 V D.C.)

The tuning of the baluns and combiner boxes for a module of antennas is achieved by connecting a vector impedance meter to the output of the components. Then

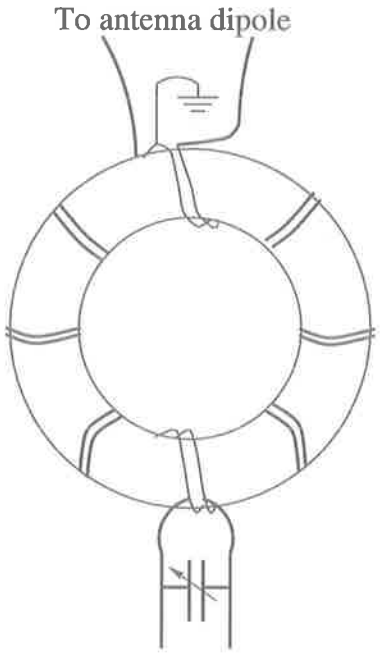

Figure 3.5: Circuit diagram for balun tuning box.

Table 3.2: Circuit components for combiner box.

Component	Value	
Resistors	100 Ω	(4 Watts)
Ferrite Core Inductor	4:1 wound	(50 MHz)
Coiled Inductor	5 turns	(60 Ω)
Capacitors C1	470 pF	(500 V D.C.)
Capacitor C2	33 pF	(500 V D.C.)
Capacitor C3	5 to 65 pF	(500 V D.C.)

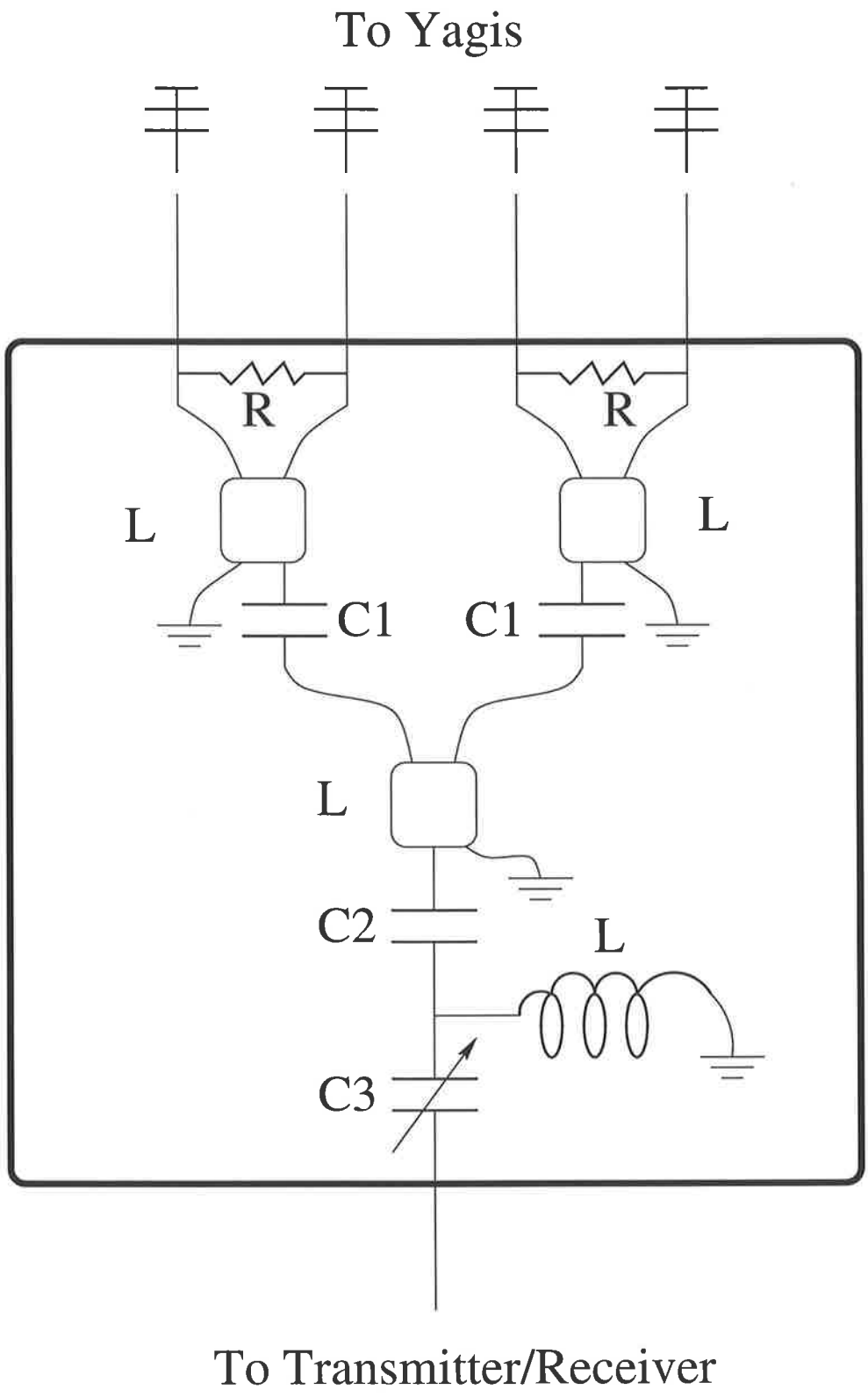

Figure 3.6: Circuit diagram for splitter/combiner box.

through adjusting the coils of the inductors and adjusting the variable capacitors, the desired impedance magnitude and phase tolerances can be selected.

The function of the baluns is to match the 200 Ω impedance Yagi active element to the 50 Ω characteristic impedance of the coaxial cable. The combiner boxes enable the four 50 Ω Yagis to be then matched to the transmit/receive equipment. The bandwidths of the modules were checked to ensure they do not limit the operation of the radar, as the bandwidth should be determined by the receiver filters for optimum matching to the radar pulse. A typical power response of a module with frequency is seen in Figure 3.7. The bandwidth of the modules can be seen to be well in excess of 4 to 6 MHz.

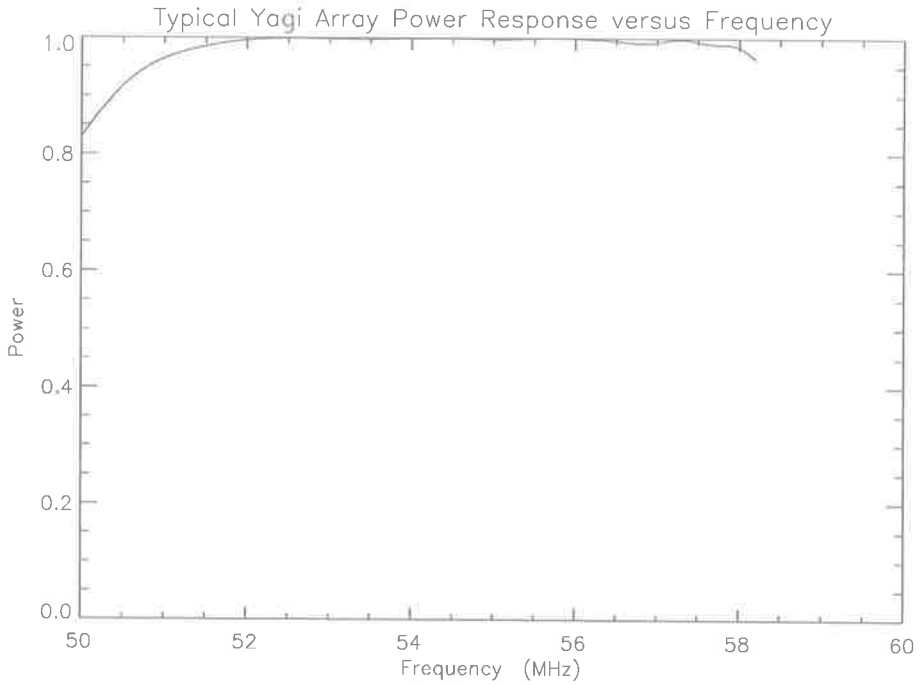

Figure 3.7: Power response of a typical combiner box with frequency.

3.4 Ground Clutter

Ideally, ground clutter has zero Doppler shift and therefore should not affect the analysis of fading signals. The clutter component will produce a D.C. offset which will be

subtracted from the raw signal before processing. However, small fluctuations in the density of air along the paths between the reflecting objects and the radar will cause small changes in the refractive index resulting in slow fading. Another problem with ground clutter is that the signal strength can be so strong that the receivers become saturated, and no useful data can be obtained.

Ground clutter can be removed either at the time of recording through hardware design and initial processing which interacts with the chosen range of radar parameters, or through signal processing after recording, either on- or off-line.

There are a number of techniques to remove clutter, by signal processing of the raw data. One technique described by *Sato and Woodman* [1982], enables signals to be extracted from data even in the presence of clutter 50 dB larger than the wanted atmospheric return. This technique works if the Doppler shift of the signal echo is large enough that the signal is not lost in the unfading clutter component at zero Doppler shift. This method involved a nonlinear parameter technique which estimated the spectral parameters of the fading clutter components for the signals removal.

During development of the present system, initial tests showed that ground clutter was not a major effect for this radar when transmitting with a vertical beam in spaced antenna mode.

This enabled the ground clutter to be removed from the data. The data is recorded as a complex time series. The two components which constitute the phase signal components are termed the in-phase and quadrature components. To remove the ground clutter from the signal thus required the slow fading component of both time series to be separately removed. This was achieved through the implementation of a third order polynomial fit. An example of the ability for the easily applied algorithm to remove the clutter from the raw time series can be seen in Figure 3.8.

The fit removed the slowly varying component of the ground clutter. This application of removal of ground clutter is only feasible when the time series has the same duration as the slowly fading ground clutter, otherwise multiple order polynomials would need to be automatically tried to find the best removal of the ground clutter.

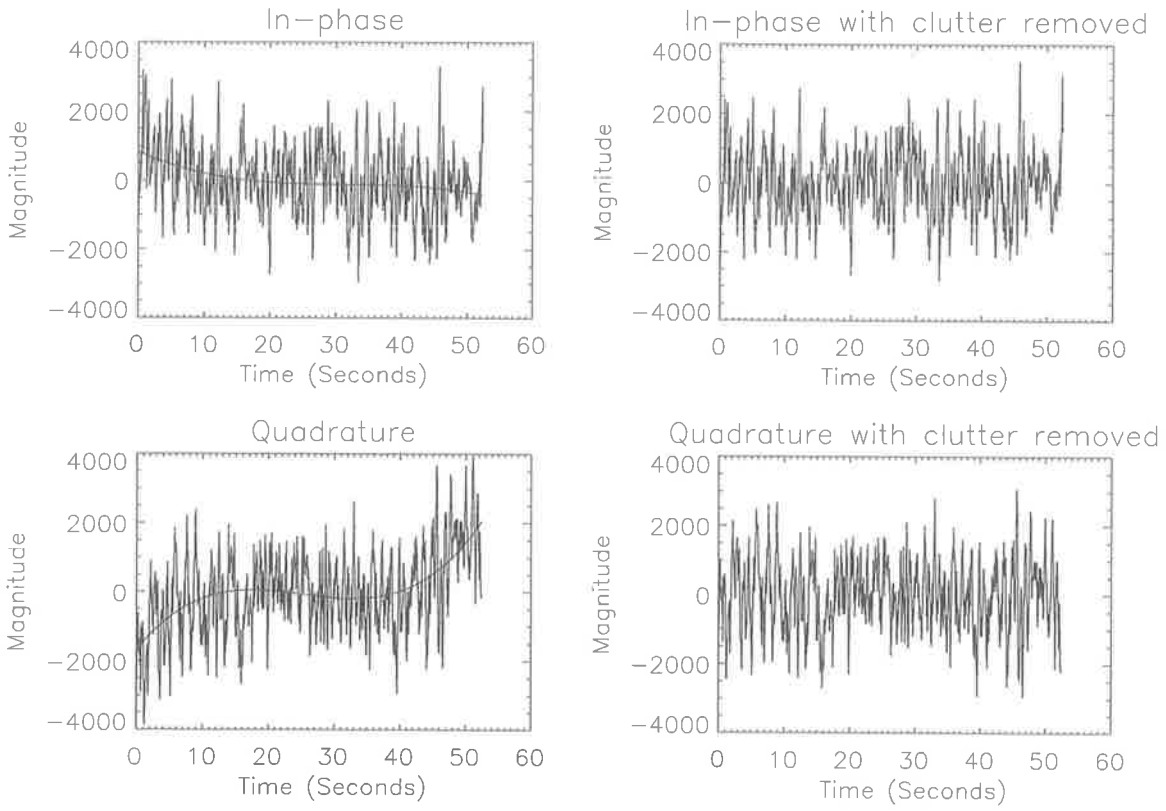

Figure 3.8: Typical complex raw time series. The application of a third order polynomial fit to the in-phase and quadrature components of the time series can be seen in the left diagrams, with the resultant time series with the clutter removed shown in the right diagrams.

This technique is very simple and quick in its ability to be applied before analysis of the raw data occurs, enabling on-line processing to occur in real time.

3.5 Optimal Antenna Spacing

It is desirable to know how irregularities scatter power as a function of zenith angle and azmiuth, which is called the aspect sensitivity of the atmospheric scatterers. By calculating the aspect sensitivity of atmospheric scatterers, the horizontal scales of these irregularities can be found. Knowledge of how atmospheric irregularities scatter energy as a function of angle is important for determining the effective pointing angle of the radar beam [*Briggs* 1992], especially so when using off-vertical beams. The stronger returns from scatterers within the beam but closest to the vertical dominate. This causes the effective beam angle to be closer to the vertical than expected through antenna positioning and phasing, which can be corrected for if the aspect sensitivity of the scatterers is known.

The importance of determining the aspect sensitivity of scatterers increases as the beamwidth increases. Components entering through a broad beam contribute to the radial Doppler shifts for vertical beams of spaced antenna radars even though the beam may only extend a few degrees off-centre of the selected radial. This results in large beamwidths producing a mis-calculation of the true radial wind components. This effect produces a restriction on the beamwidth, otherwise significant contamination of the atmospheric motion occurs.

An important feature of using a VHF radar for probing the lower troposphere is that within the convective boundary layer there should be a uniform volume distribution of scatterers as long as good mixing has occurred. The significance of the scatterers for off-vertical beams increases when considering the effects of different aspect sensitivities with altitude. We will show in Chapter 5, that at the top of the boundary layer, and also within the free air region above it, scatterers can be stratified into thin horizontal layers smaller than a range gate of the radar.

These layers can act like mirrors, producing a strong return for the probing radar if the layer is perpendicular to the radar beam. When the angle of the layer to the radar beam varies from being orthogonal the returned echo strength will quickly decrease as the angle increases. If the layers are tilted they would then be responsible for introducing contamination between the horizontal and vertical winds of vertically pointing beams.

Following the description of the aspect sensitivity of atmospheric scatterers by *Briggs* [1992], the angular power spectrum in polar co-ordinates $W(l,m)$, is

$$W(l,m)\,\mathrm{d}l\,\mathrm{d}m = \frac{KM_sR}{h^2}G_T(l,m)G_R(l,m)\sigma(l,m)\,\mathrm{d}l\,\mathrm{d}m \quad , \tag{3.1}$$

where

K is a constant,

M_s is the density of scatterers,

h is the height of the layer,

σ = scattering cross-section of scatterer for back-scatter,

G_T = gain of transmitting antennas,

G_R = gain of receiving antennas,

The total received power is

$$\int_{-1}^{+1}\int_{-1}^{+1} W(l,m)\,\mathrm{d}l\,\mathrm{d}m = \frac{KM_s}{h^2} \times \int_{-1}^{+1}\int_{-1}^{+1} G_T(l,m)G_R(l,m)\sigma(l,m)\,\mathrm{d}l\,\mathrm{d}m \quad . \tag{3.2}$$

Then the two-dimensional auto-correlation function for the complex wave field is

$$\rho(\xi,\eta) \propto \int_{-1}^{+1}\int_{-1}^{+1} G_T(l,m)G_R(l,m)\sigma(l,m) \times \exp[2\pi i(l\xi+m\eta)]\mathrm{d}l\,\mathrm{d}m \quad , \tag{3.3}$$

and through dividing (3.3) by the transmitter and receiver polar diagrams, the scattering cross-section is

$$\sigma(l,m) \propto \frac{1}{G_T(l,m)G_R(l,m)}\int_{-1}^{+1}\int_{-1}^{+1} \rho(\xi,\eta) \times \exp[-2\pi i(l\xi+m\eta)]\mathrm{d}\xi\,\mathrm{d}\eta \quad . \tag{3.4}$$

When the aspect sensitivity is a function of zenith angle s only

$$2\pi \int_0^1 W(s) s \, \mathrm{d}s = \frac{2\pi K M_s}{h^2} \int_0^1 G_T(s) G_R(s) \sigma(s) s \, \mathrm{d}s \quad , \tag{3.5}$$

$$\rho(r) \propto \int_0^1 G_T(s) G_R(s) \sigma(s) J_0(2\pi r s) s \, \mathrm{d}s \quad , \tag{3.6}$$

$$\sigma(l,m) \propto \frac{1}{G_T(s) G_R(s)} \int_0^\infty \rho(r) J_0(2\pi r s) r \, \mathrm{d}r \quad , \tag{3.7}$$

where r is the separation between antennas in wavelengths, J_0 is the Bessel function of zero order.

Now if the scatterers have spherical symmetry on average, or they are very small compared to the wavelength, then the aspect sensitivity will be constant for all zenith angles. Thus if $\sigma(s) = constant$, then the zenith angle dependence of the returned power will be dependent upon the transmitting and receiving antenna arrays polar diagrams. Thus if the antenna array polar diagrams are Gaussian with a e^{-1} half-width, s_0, then

$$G_T(s) \propto \exp\left(-\frac{s^2}{s_0^2}\right) \quad , \tag{3.8}$$

$$G_R(s) \propto \exp\left(-\frac{s^2}{s_0^2}\right) \quad , \tag{3.9}$$

which gives the returned power as

$$W(s) \propto \exp\left(-2\frac{s^2}{s_0^2}\right) \quad . \tag{3.10}$$

Thus substituting (3.8, 3.9 and 3.10) into (3.6) gives

$$\rho(r) \propto \int_0^1 \exp\left(-2\frac{s^2}{s_0^2}\right) J_0(2\pi r s) s \, \mathrm{d}s \quad , \tag{3.11}$$

which gives the spatial correlation function for the case where scatterers were isolated through a mechanism such as a thin horizontal layer of turbulence as

$$\rho(r) = \exp\left(-\frac{1}{2}\pi^2 s_0^2 r^2\right) \quad . \tag{3.12}$$

The spatial correlation function is then calculated for a module of four three element Yagi antennas with a spacing of 0.7 λ and a e^{-1} half-width of 23.3°, and is plotted in Figure 3.9. This derivation by *Briggs* [1992] assumed that the scatterers are isotropic. It is seen in the diagram that the spatial correlation falls to 0.5 for a spacing of 1 wavelength for isotropic scatter. Since aspect sensitive scatterers results in a higher spatial correlation with separation than isotropic scatterers, then the spacing for the antenna modules is the smallest possible and would need to be increased for a mix of anisotropic and isotropic scatter.

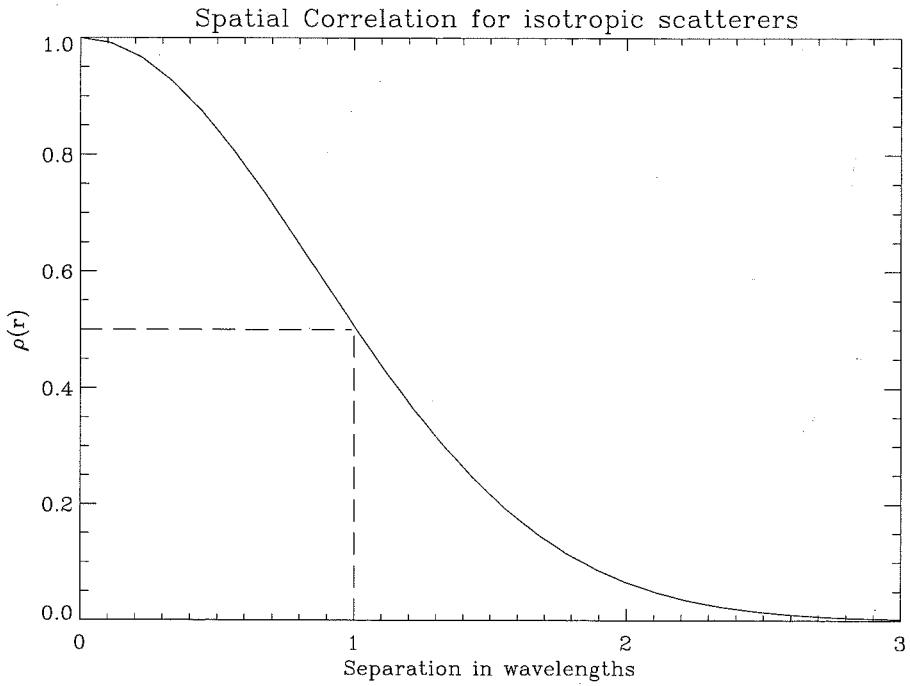

Figure 3.9: Spatial correlation function with separation of antenna modules.

Similarly Briggs showed that when the transmitter and receiver polar diagrams are of a Gaussian form then the aspect sensitivity of non-isotropic scatterers can be found from the spatial correlation functions since:

$$\sigma(s) \quad \propto \quad \exp\left(-\frac{s^2}{s_1^2}\right) \quad , \tag{3.13}$$

$$G_T(s) \propto \exp\left(-\frac{s^2}{s_2^2}\right) \quad , \tag{3.14}$$

$$G_R(s) \propto \exp\left(-\frac{s^2}{s_3^2}\right) \quad , \tag{3.15}$$

where

s = sin(zenith angle),

s_1 = sin(aspect sensitivity of scatterers),

s_2 = sin(transmitter beamwidth),

s_3 = sin(receiver beamwidth),

then the angular power spectrum is

$$W(s) \propto \exp\left(-\frac{s^2}{s_4^2}\right) \quad , \tag{3.16}$$

where

$$\frac{1}{s_4^2} = \frac{1}{s_1^2} + \frac{1}{s_2^2} + \frac{1}{s_3^2} \quad . \tag{3.17}$$

Then

$$\rho(r) = exp\left(-\frac{1}{2}\pi^2 s_4^2 r^2\right) \quad . \tag{3.18}$$

This enables s_4 to be determined from Equation 3.18, and then s_1 is then able to be calculated from Equation 3.17.

3.6 Summary

The circuitry used for matching the antenna arrays is important for minimising antenna ringing and for its broad bandwidth which is important for the detection of weak signals and for future additions including dual frequency transmissions.

The restriction on the minimum height which can be probed depends on a number of features including ensuring that you are in the far field of the radiation pattern of the radiated beam for the antenna aperture, the length of the transmitted pulse to ensure a strong enough signal is transmitted without exceeding the duty cycle of the transmitter, and the blanking of the receivers during transmission and for a short interval after switching the antenna arrays from the transmitter.

From experiment it is seen that the minimum usable height is about 300 metres, though the ringing of the antennas even when well matched is seen in the data and needs to be removed in the same method as the ground clutter for the lowest range gate.

Further advancements to the radar system design, including the introduction of beam-steering, require that the aspect sensitivity of the scatterers be accurately known to determine the effective pointing angle of the radar beam.

Chapter 4

Preliminary Results of The Adelaide Boundary-Layer System

A pilot study of the ability of a VHF radar system to investigate the convective boundary layer was performed with a single module consisting of four Yagi antennas. This was performed to determine the viability of small groups of Yagi antennas for detecting weak echoes from the boundary layer.

First, the returned power was measured using one module of Yagis for both transmission and reception. This was followed by an investigation into the dominance of the wet and dry components of the general refractive index in the lowest four km of the troposphere. Finally, three modules of antennas were used to investigate the pattern scales of irregularities in the lower troposphere. This was performed to determine the optimum spacing of antenna modules for SA wind profiling.

The location of the radar site at Buckland Park relative to Adelaide and the Gulf of St. Vincent is shown in Figure 4.1. The launch site for the radiosondes during this study occurred at Adelaide airport.

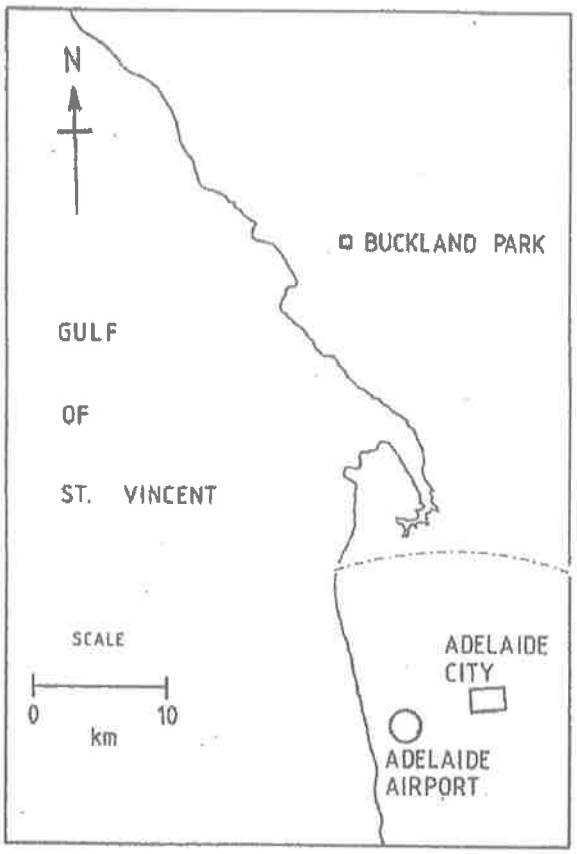

Figure 4.1: Map of Buckland Park from *May* [1986]. The relative locations of Buckland Park, the city of Adelaide, Adelaide airport, and the Gulf of St. Vincent are shown. The dotted line represents the northern limit of the urban area. The urban area extends almost half-way from Adelaide's central business district to Buckland Park.

4.1 September 1995 - Single Module Observation

A single module of four Yagi antennas was used in an initial test of the feasibility of a VHF boundary layer radar. A short run lasting 1.4 hours was held on 13 September 1995 from 15.0 to 16.4 Central Standard Time (CST).

A pulse length of 1 μs was used for this study. The raw data were analysed with results obtained from 400 metres up to 4 km in 200-m range intervals. Figure 4.2 shows a preliminary analysis of the received signal strengths, with strong ground clutter and antenna ringing occurring up to 800 metres. There are also times between 15.4 and 16.0 CST when an external noise source was present. It was received for short bursts and thus appears throughout the entire height spectrum. There is an aircraft detected around 15.1 CST near 3 km, and between 16.0 and 16.2 CST from 3 km down to 600 metres. This would most likely be due to an aircraft flying through the sidelobes and main lobes of the power pattern of the radar. The field site is in a low-flying area and often used by trainee pilots.

Of most interest in this signal strength plot is the phenomena which occurs between 1 km and 1.6 km. A layer of strong returns pervades the data run due to a region of rapid change of the refractive index, possibly associated with a rapid decrease in the humidity with altitude. This region corresponds to the top of the mixed-layer.

As an initial test of the system, the signal strength and vertical velocities were obtained using the correlation technique of *Woodman and Guillén* [1974]. The auto-correlation function of the received signal was calculated to determine the signal strength and the noise to enable the SNR to be calculated. This was performed by fitting a Gaussian across zero lag to find both the signal strength and the superimposed noise spike upon it. Figure 4.3 (from [*Low* 1995]), displays an autocorrelation function with its associated parameters.

Since a single module was used with a vertically pointing radar beam, then the radial velocity will approximately correspond to the vertical velocity of air parcels if there is no contamination due to horizontal velocity from tilted layers. Contamination

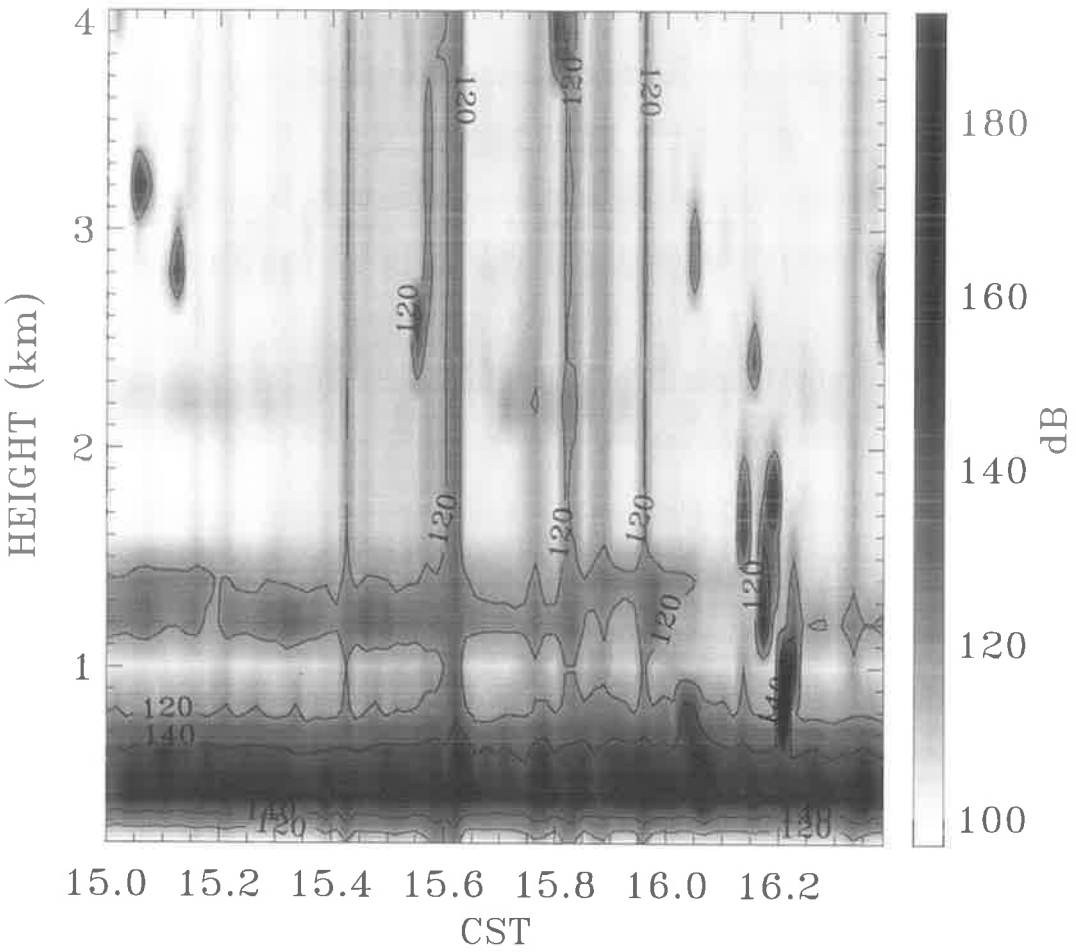

Figure 4.2: Returned echo signal strengths obtained using a single module of Yagi antennas. The amplitude of the returned power profile is a relative scale.

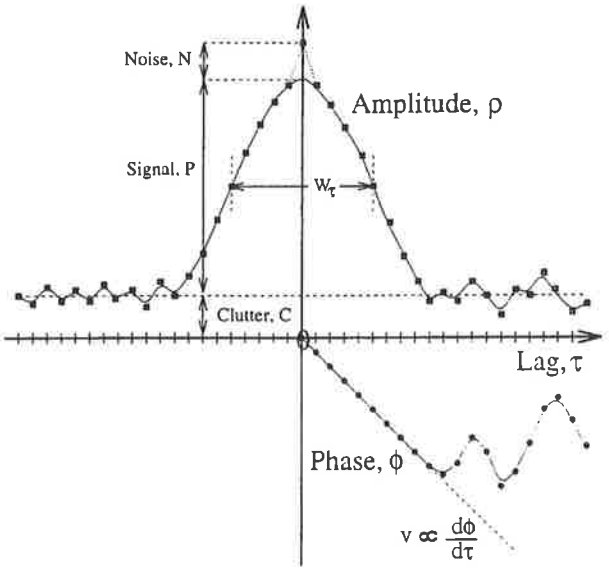

Figure 4.3: Figure from *Low* [1995] displaying a typical autocorrelation function with its measurement parameters, including the width W_τ which is a measurement of the echo lifetime and the turbulent velocity variance.

of the horizontal velocity into the calculation of the vertical velocities occurs due to the finite width of the beam. Even if there is no horizontal motion of a tilted layer, there would still be an effect on the spectral width of the echoes.

The vertical velocity of the air parcels was then calculated from the Doppler shift of the frequency of the returned signal. The Doppler shift, f_D, is first calculated from the change of the phase between the zeroth and first lag of the auto-correlation function:

$$f_D = \frac{1}{2\pi}\frac{\Delta\phi}{\Delta t} \tag{4.1}$$

$$\approx \frac{1}{2\pi}\frac{\partial\phi}{\partial t} \quad , \tag{4.2}$$

where $\frac{\partial\phi}{\partial t}$ is the rate of change of the phase.

The vertical velocities, V_r, were then able to be calculated

$$V_r = -\frac{\lambda f_D}{2} \quad . \tag{4.3}$$

The average vertical velocity is plotted in Figure 4.4, along with the signal to noise ratio averaged for the 1.4 hour data run. The bars indicate the sample standard deviation at each height.

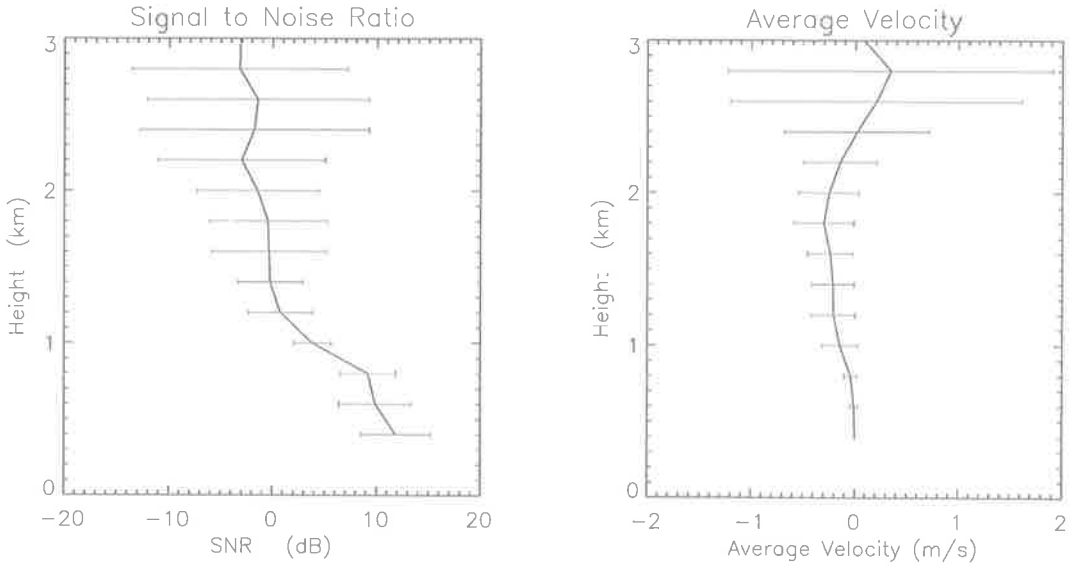

Figure 4.4: Signal to Noise Ratios and Average Vertical Velocity using a single module of Yagi antennas on 13 September 1995 from 15.0 to 16.4 CST.

It can be seen from the SNR that on average the signal strength exceeds the noise up to the top of the boundary-layer, and even up to 3 km does not drop below -4 dB. The lowest heights up to 800 metres have an SNR above 10 dB, but this is not a true representation due to the ground clutter and antenna ringing which contaminated the returns from the lower heights.

The average vertical velocity profile shows limited up- and downdrafts over this period with neither exceeding 40 cm s^{-1} over the data run. In the region of the top of the mixing-layer there tended to be a light downdraft evident, which might be due to subsidence of higher humidity air parcels in the locality due to the proximity of the radar to St. Vincent Gulf.

These preliminary results using only a single module of antennas were extremely encouraging and lead into further refinements of the system for better detection of atmospheric phenomena before utilising the full array.

4.2 March 1996 - Single Module Observation with Radiosonde Comparisons

It is necessary with any newly developed equipment to undertake an examination of results with accepted equipment and techniques to ensure that results are consistent. Consequently, a comparison of results from balloon-borne radiosondes was performed with a single module of the VHF BL-radar. The balloon launches occurred around 07:30 local time daily at Adelaide airport which is some 36 km from Buckland Park, as seen in Figure 4.1.

In this campaign a vertical Doppler beam was used to calculate the returned power profile and the SNR from 12:00 on the 20th of March to 12:00 on the 24th of March. The radar returned power profiles were then compared with the reflectivities from soundings to calibrate the radar, and to also find the dominant components affecting the refractive index in the regions of interest.

A time-height cross section of the received power is shown in Figure 4.5. The antenna module was placed in a very cluttered environment and initially ground clutter rejection techniques were not employed, which resulted in very strong non-atmospheric echoes in the lowest 1 km. There is also another strong return from what is most likely the top of the convective boundary layer. It can be seen that this layer changed significantly with height over the four days. Initially, the layer was located near 2.5 km on March 20, then dropped to around 1.5 km two days later, before rising above 2 km from 12:00 to 20:00 on March 22. Only a small amount of data were received between 3 km and 4.2 km, because of low SNR resulting from just one antenna module for both reception and transmission.

It can also be seen in Figure 4.5 that the passage of the galactic centre which occurs about 0600 local time in March each day, does not cause a dramatic increase in the returned power which would degrade the SNR as the power pattern of the antenna modules used for reception has a relatively wide beamwidth. This is important as very narrow vertical beamwidths with high gains are prone to signal degradation during

the passage of the galactic centre, or when any other form of sky noise enters the main or sidelobes of the radar.

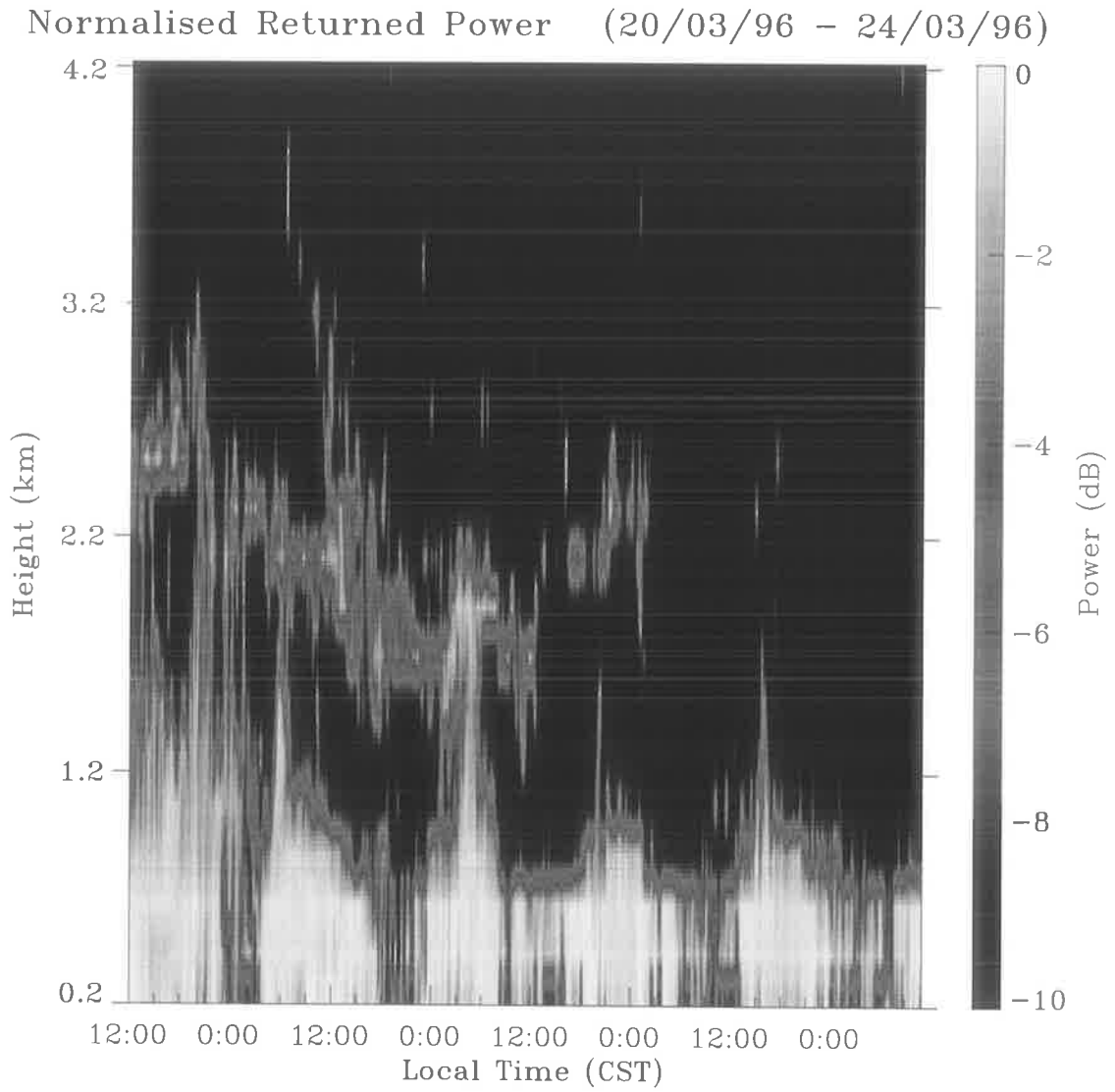

Figure 4.5: Returned power profile derived from a wide beamwidth single module from 20/03/96 to 24/03/96.

The signal to noise ratio was averaged from 07:00 to 08:00 local times to coincide with the radiosonde data from Adelaide airport. The results are plotted in Figure 4.6.

The power profiles calculated from the radar system's data were first range corrected by multiplying by r^2, and then averaged over a period of one hour centred on

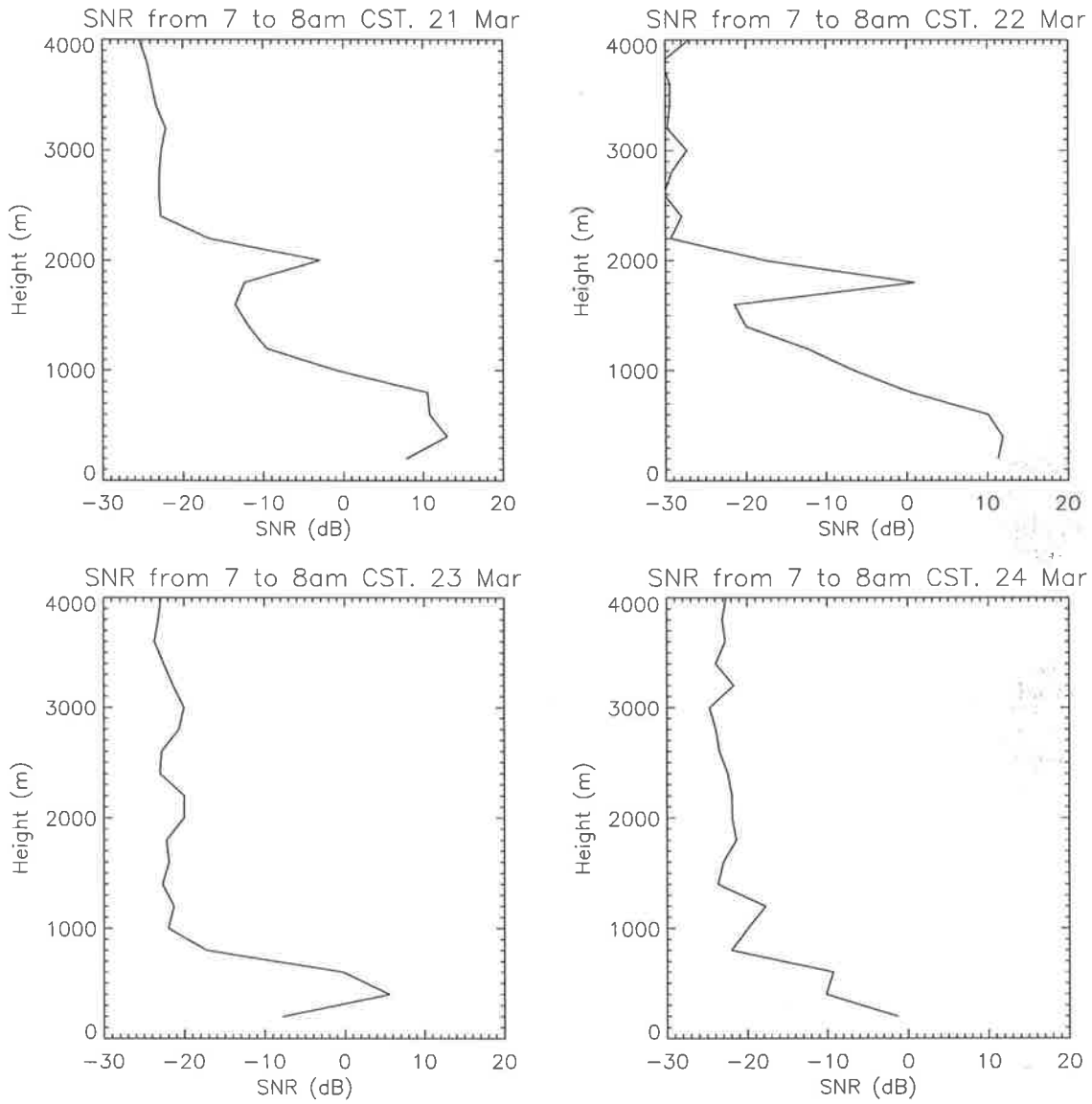

Figure 4.6: Signal to Noise Ratios for the campaign from 20/03/96 to 24/03/96

the time of launch of the radiosonde. The range correction is due to the decrease in the radar beam intensity with altitude. This occurs through a decrease of the intensity as a function of r^{-2} due to the increase of the surface area of the propagating wavefront, which is then scattered from the clear air turbulence and is again decreased as a function of r^{-2}. This results in a decrease in the intensity of the signal at r^{-4}, however for volume scatter as the range increases so does the volume which scatters the radar signal, by a factor of r^2. Thus the final affect of range on the decrease in the echo strength is r^{-2}. The range-corrected power returns are plotted in Figure 4.7, using arbitrary units.

The combination of incomplete removal of ground clutter from the data and an early prototype of the antenna array matching circuitry which has produced antenna ringing in the lowest height, has resulted in low echo strength in this range gate. The enhanced echoes in the power profile occur as expected at the same altitude as the local maxima of signal to noise ratio. The magnitudes of the SNR and range-corrected power are significantly stronger on the 21 st and 22 nd of July near 2 km than on the final two days.

The vertical velocity variances, shown in Figure 4.8, were also calculated and averaged over a ten minute period to determine the variation of the vertical winds with time. The two lowest heights of 200 metres and 350 metres contain contamination from ground clutter. It was found that changes in the vertical velocity were minimal over short intervals of time and were generally less than 0.005 m^2s^{-2} for both low altitude and for the top of the mixing layer where the returned signal strength was high enough for the signal to noise ratio to almost continuously exceed the cutoff threshold of -10 dB.

The comparison of the potential refractive index and the range corrected power returns is achieved using sonde launches at the Adelaide airport for the 21 st through to the 24 th of March 1996. The dry and wet components of the potential refractive index are calculated as outlined in section 2.2.1, and are plotted in Figure 4.9, along with the total potential refractive index.

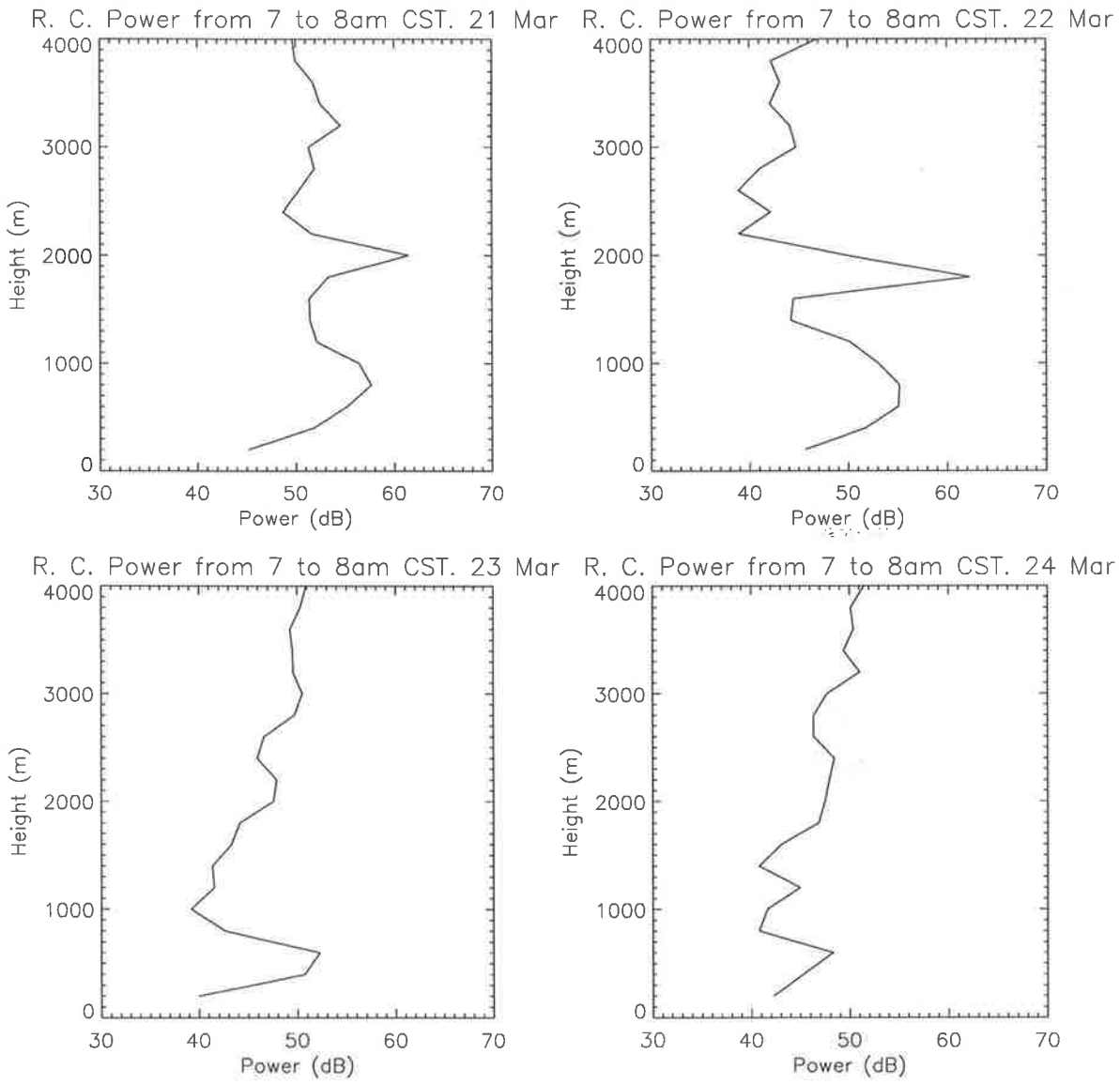

Figure 4.7: Range Corrected Power for the campaign from 20/03/96 to 24/03/96 for the times of radiosonde launches at Adelaide airport.

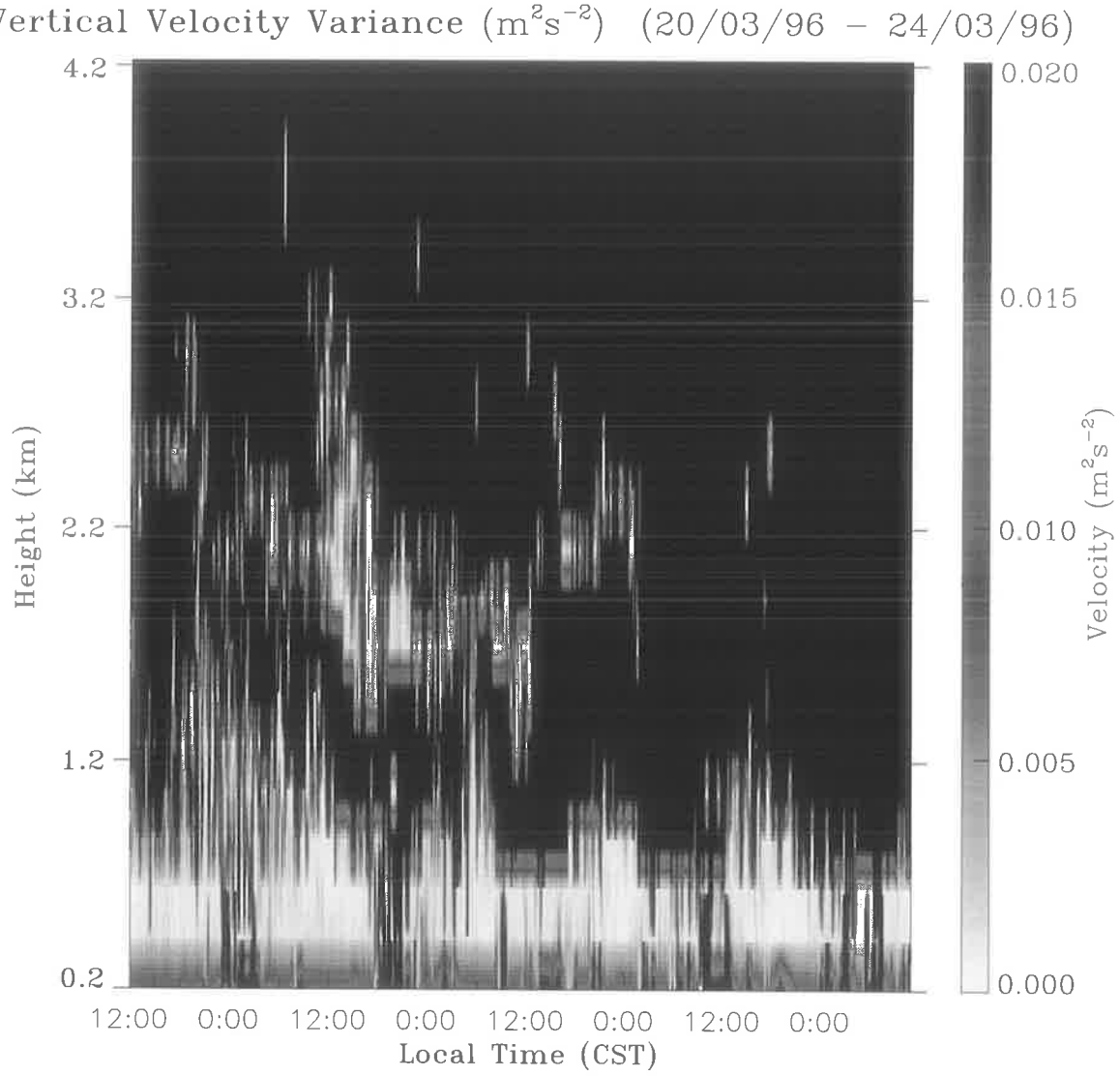

Figure 4.8: Vertical Velocity Variance derived from a wide beamwidth single module from 20/03/96 to 24/03/96

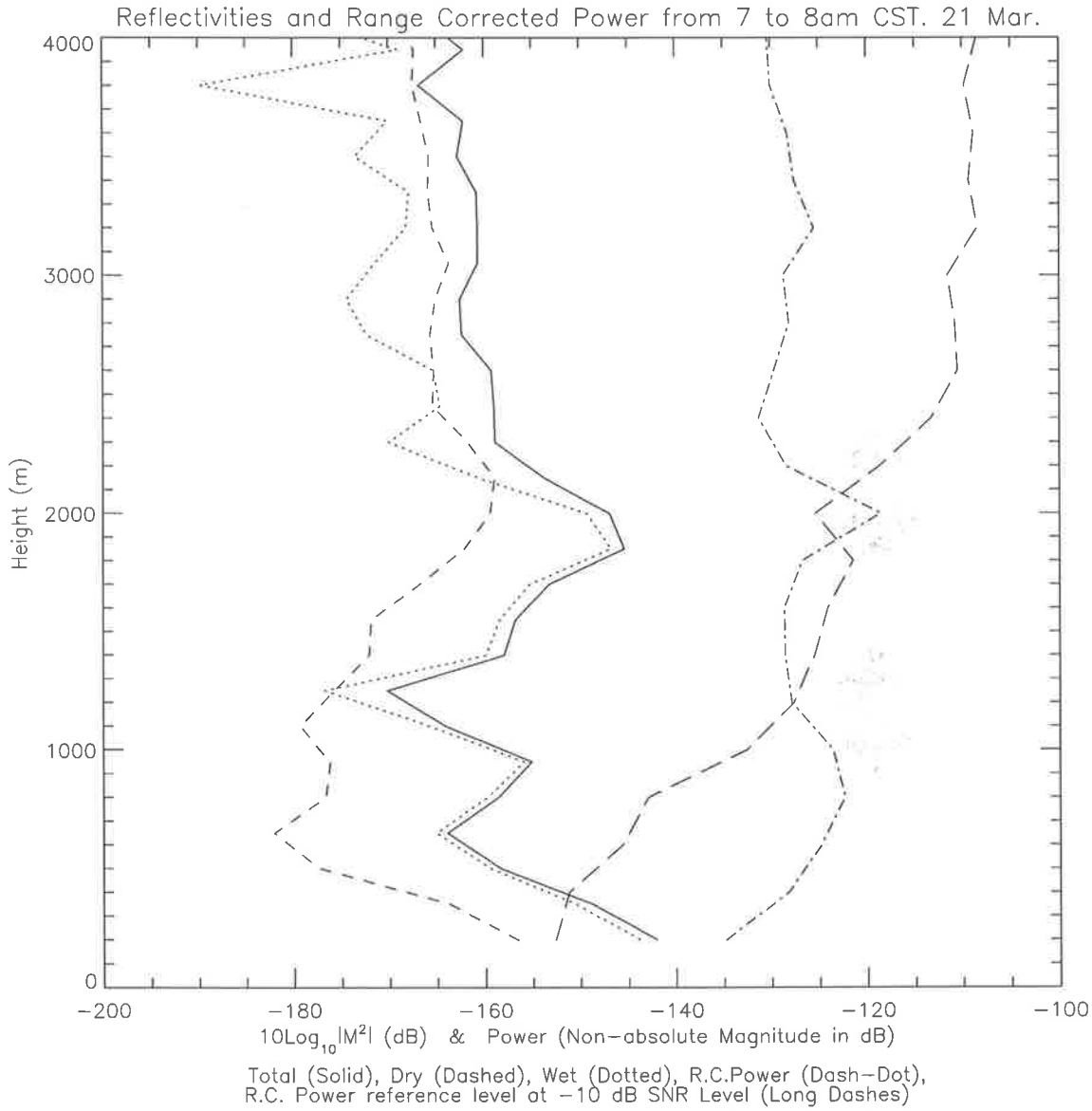

Figure 4.9: Reflectivities and Range Corrected Power for 21/03/96

The two components display similar characteristics, although the wet term dominates by about 15 dB in the lowest 2 km of the atmosphere, and the two terms contribute approximately equally in the lower troposphere above 2 km. It can also be seen that the range corrected power peaks near the largest values of $\overline{M^2}$, at 2 km.

The gradients in $\overline{M^2}$ are dominated by fluctuations in the wet term which corresponds to the fluctuations occurring in the specific humidity, as shown in Figure 4.10.

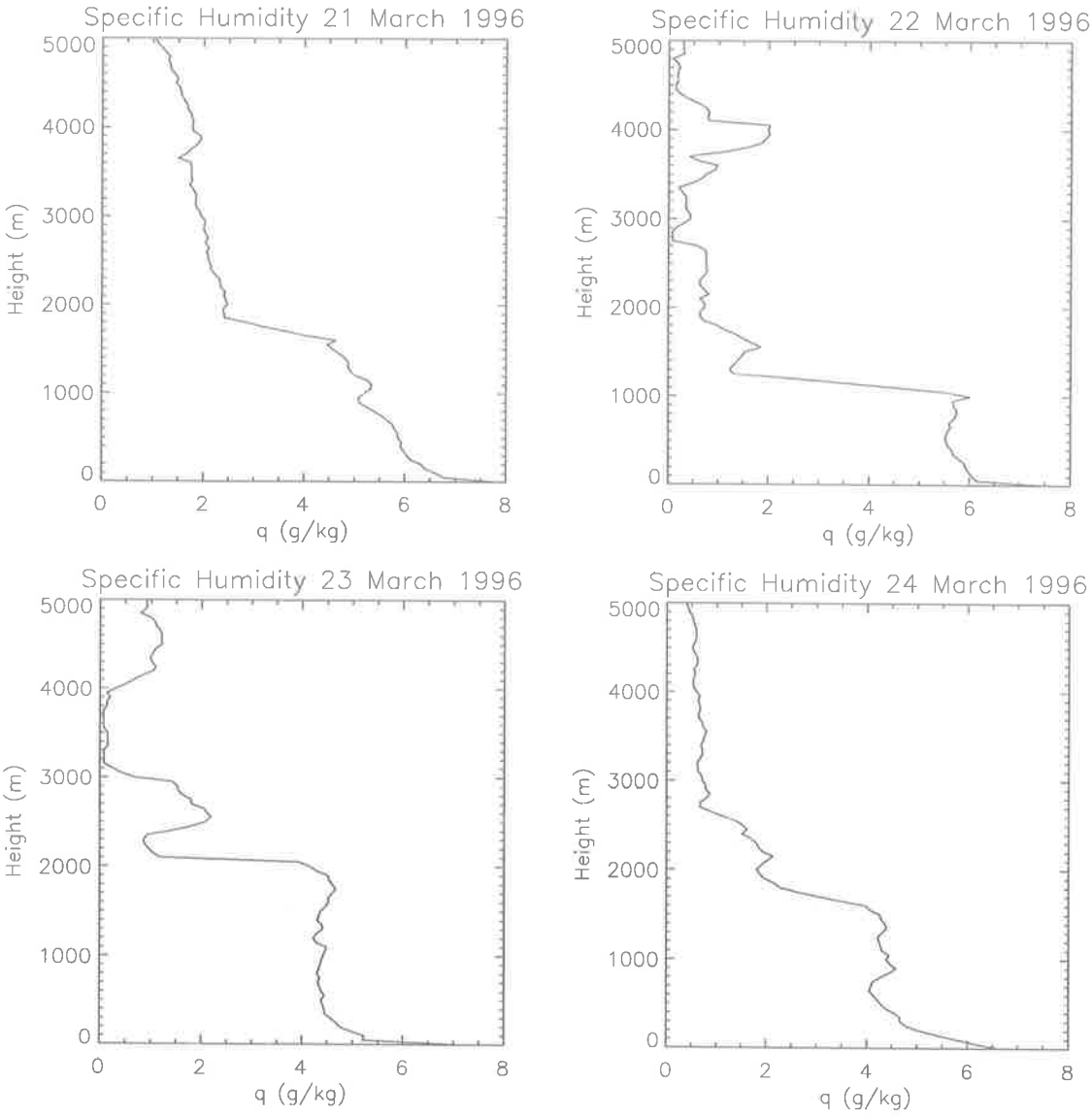

Figure 4.10: Radiosonde specific humidity from 20/03/96 to 24/03/96.

Figure 4.11 shows the state on March 22. This diagram illustrates the differences which can occur due to spatial separation of the radiosonde launch site and the radar site. Again there is a strong power return at the top of the mixing layer about 1.8 km, but the radiosonde measurements show a 300 metre height difference in their determination of the top of the mixing layer. This is similar to findings of *Hocking and Mu* [1997], who generally found excellent correlations between sonde data from Adelaide airport and radar measurements from Buckland Park, but on occasions found very poor correlations.

When comparing results between the two systems the large spatial separation, 35 km, between the two sites needs to be considered, as there may be considerable differences in the local weather between the two locations.

The third launch on March 23 in Figure 4.12, and Figure 4.13 for the final launch of March 24, have very low SNR in the periods around the launch times. It is shown that the received signal power for the -10 dB SNR level is larger than the signal strength at heights above 700 metres. It can still be seen in Figure 4.12 that the peaks in the received power at 2.0 and 2.8 km correspond to the peaks in the reflectivity, and similarly the peaks in Figure 4.13 around 2 and 3.1 km in the reflectivity are matched by corresponding peaks in the received echoes. The weak returns from the last two days could also be partly attributed to the small gradient in potential temperature at the top of the mixing-layer as shown in Figure 4.14.

Radiosonde results from Adelaide airport were then investigated for March 20 to April 6 to see if the days chosen show a typical signature pattern for early Autumn in Adelaide. In Figure 4.15, it can be seen that the four days chosen are typical, with the air temperature falling up to about 1.5 km to 2.5 km where a temperature inversion of about 5°C generally occurs. The temperatures from March 23 to 27, also show that there was a low level nocturnal inversion and that the heating of the surface had not exceeded the nocturnal inversion temperature by 07:30 local time.

The potential temperatures for the same period March 20 to April 6 are shown in Figure 4.14 and the specific humidities in Figure 4.16, which indicates that there

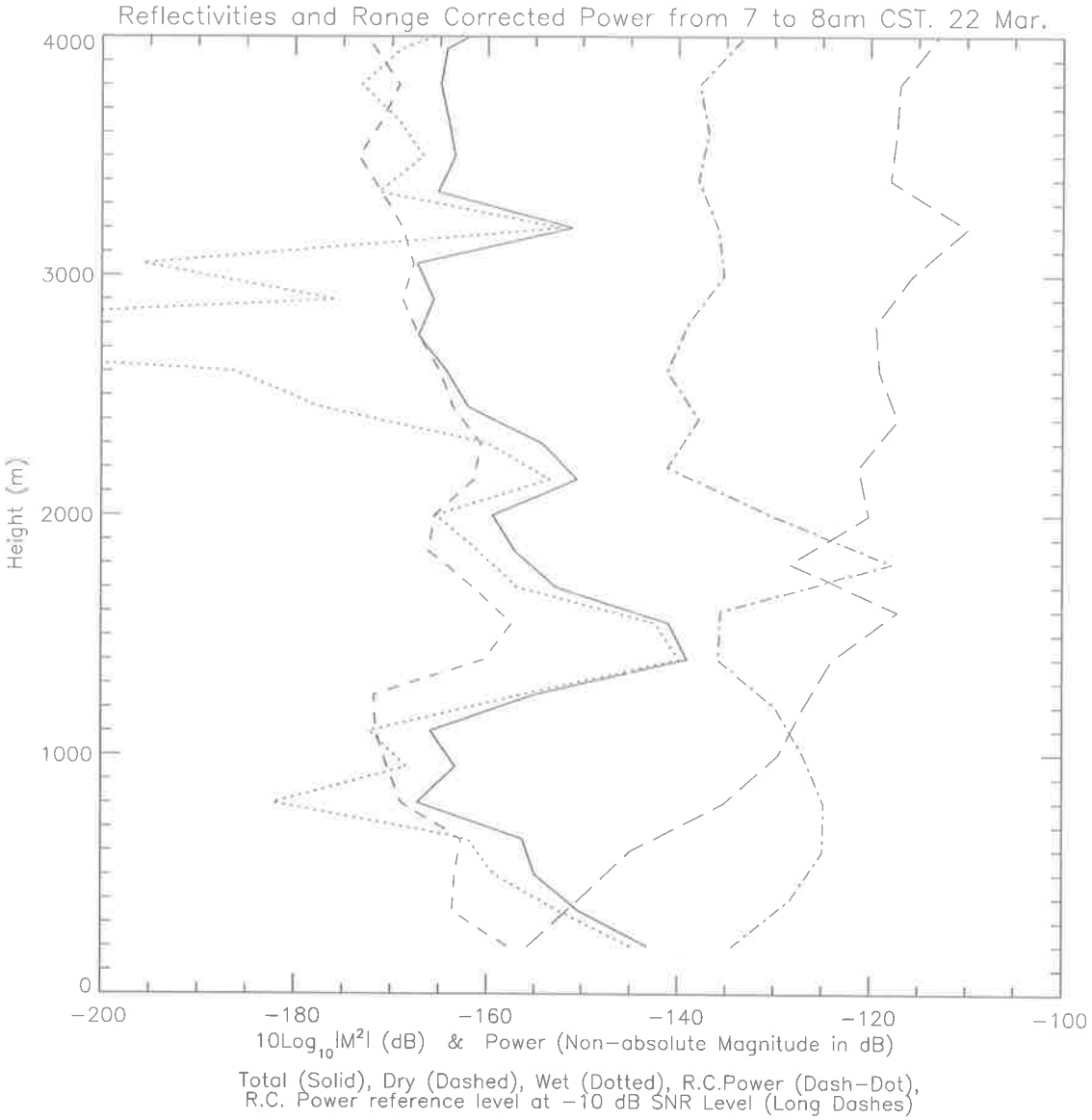

Figure 4.11: Reflectivities and Range Corrected Power for 22/03/96

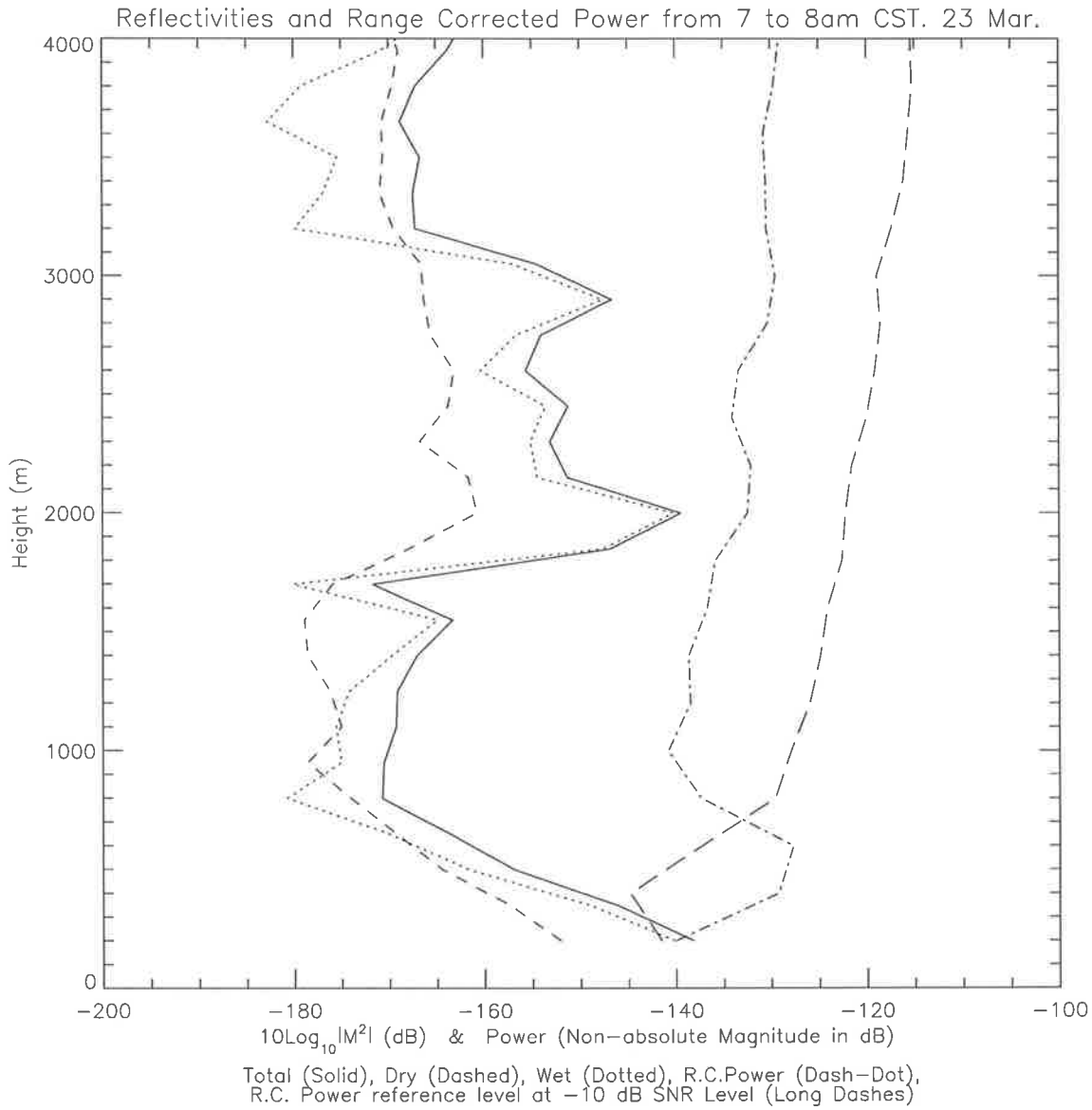

Figure 4.12: Reflectivities and Range Corrected Power for 23/03/96

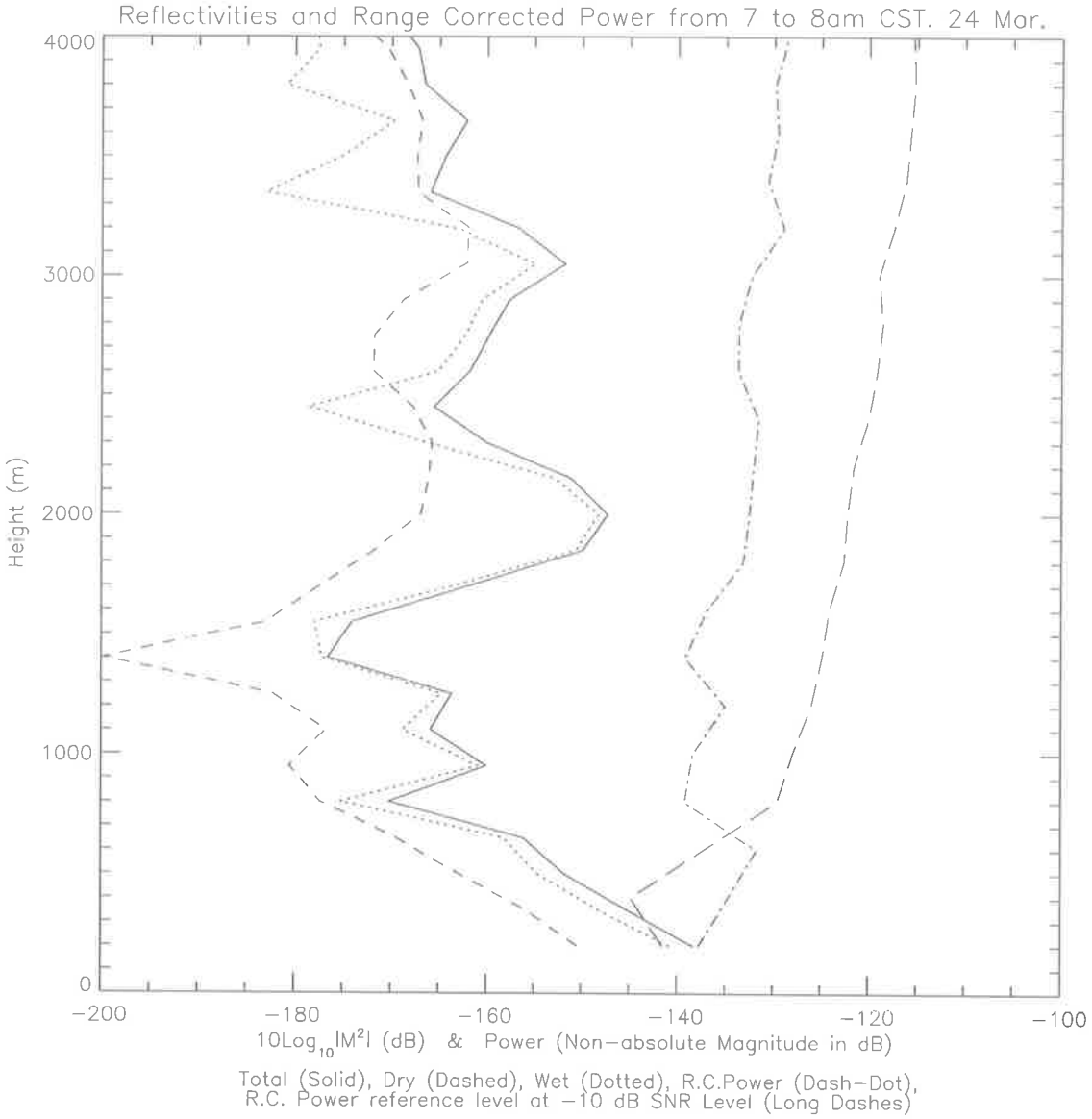

Figure 4.13: Reflectivities and Range Corrected Power for 24/03/96

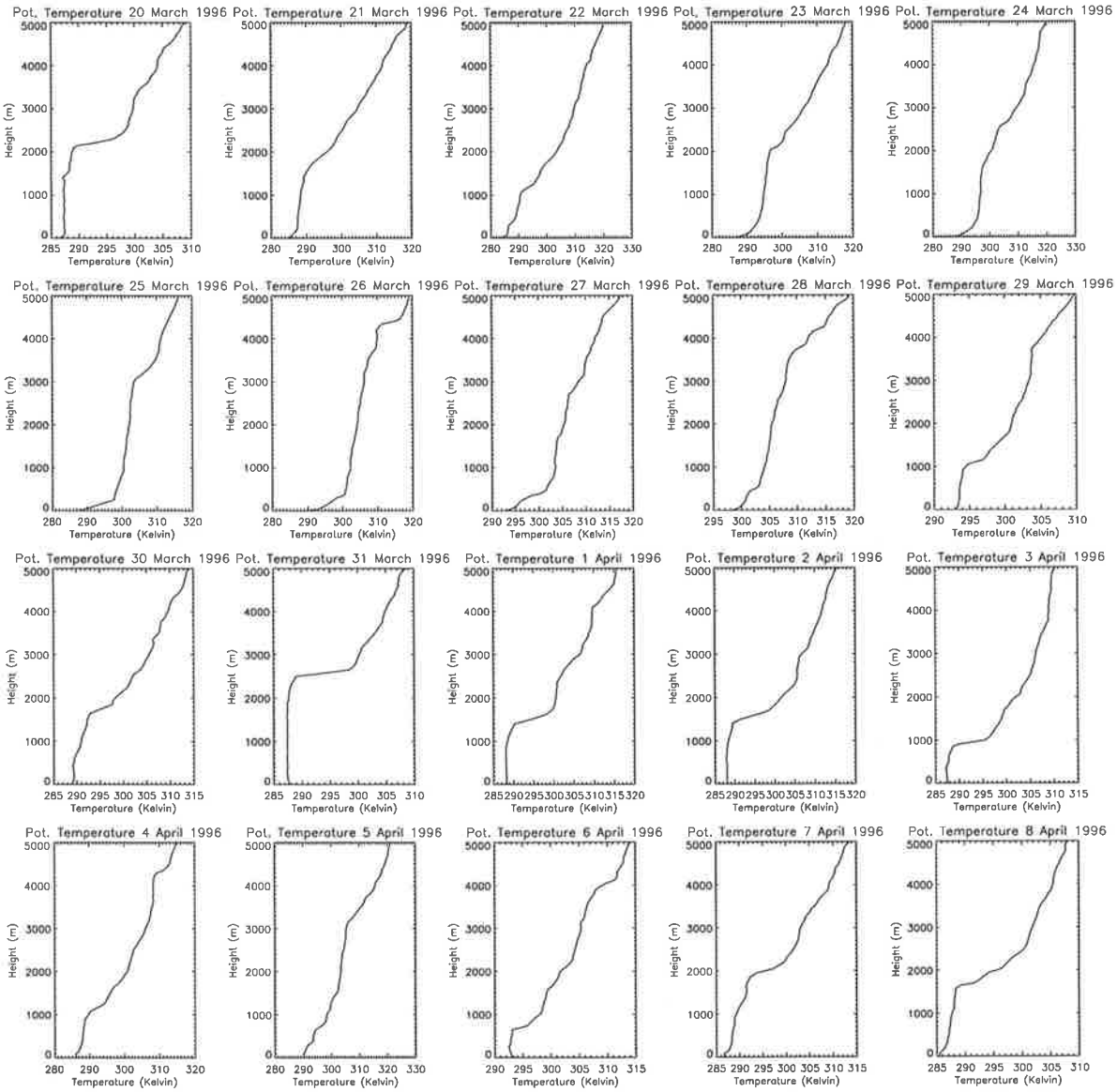

Figure 4.14: Potential temperatures from 20/03/96 to 06/04/96

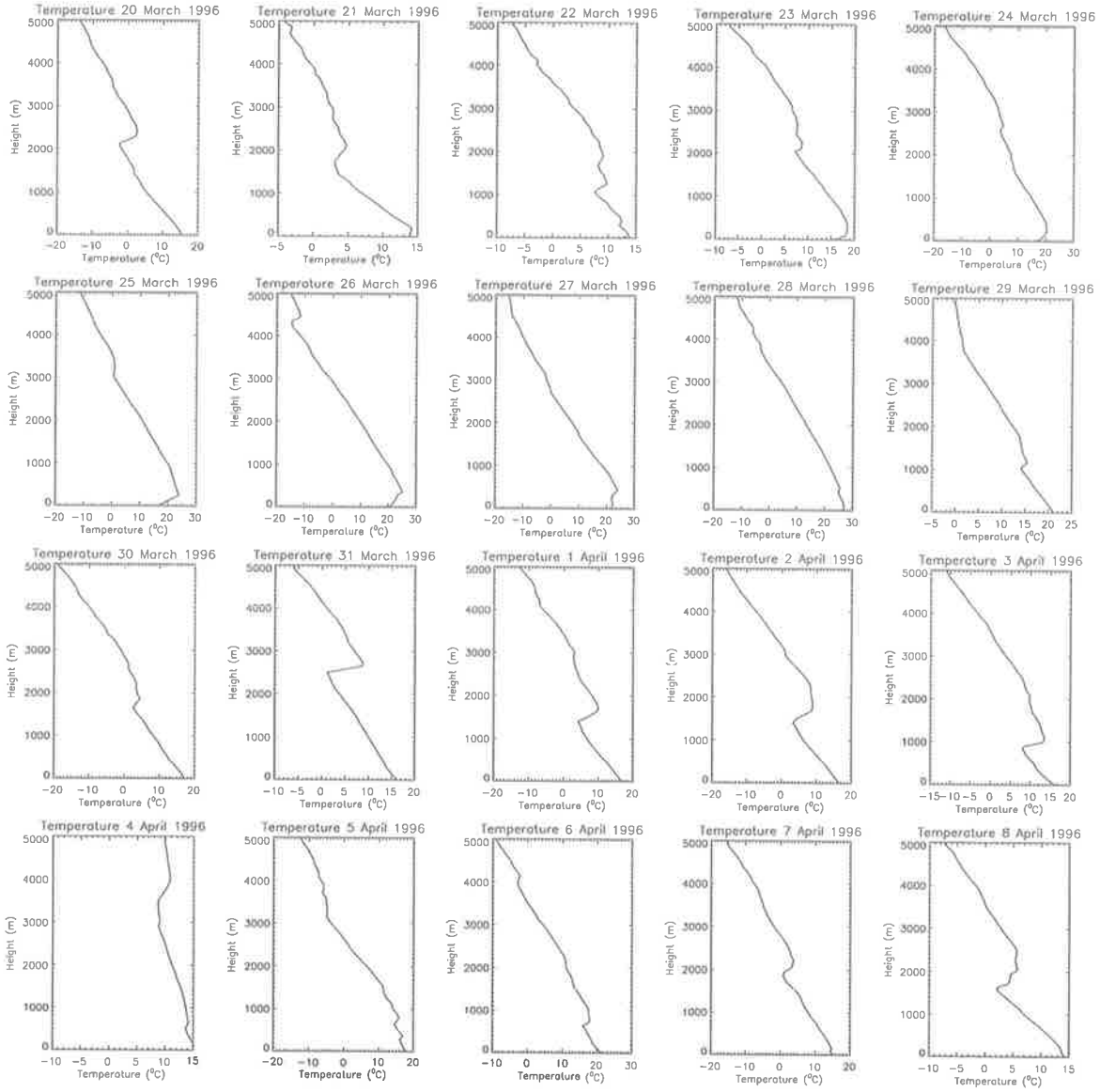

Figure 4.15: Radiosonde determined temperatures from 20/03/96 to 06/04/96.

is strong mixing occurring up to the top of the convective boundary layer, as the potential temperatures and specific humidities are close to being constant with height.

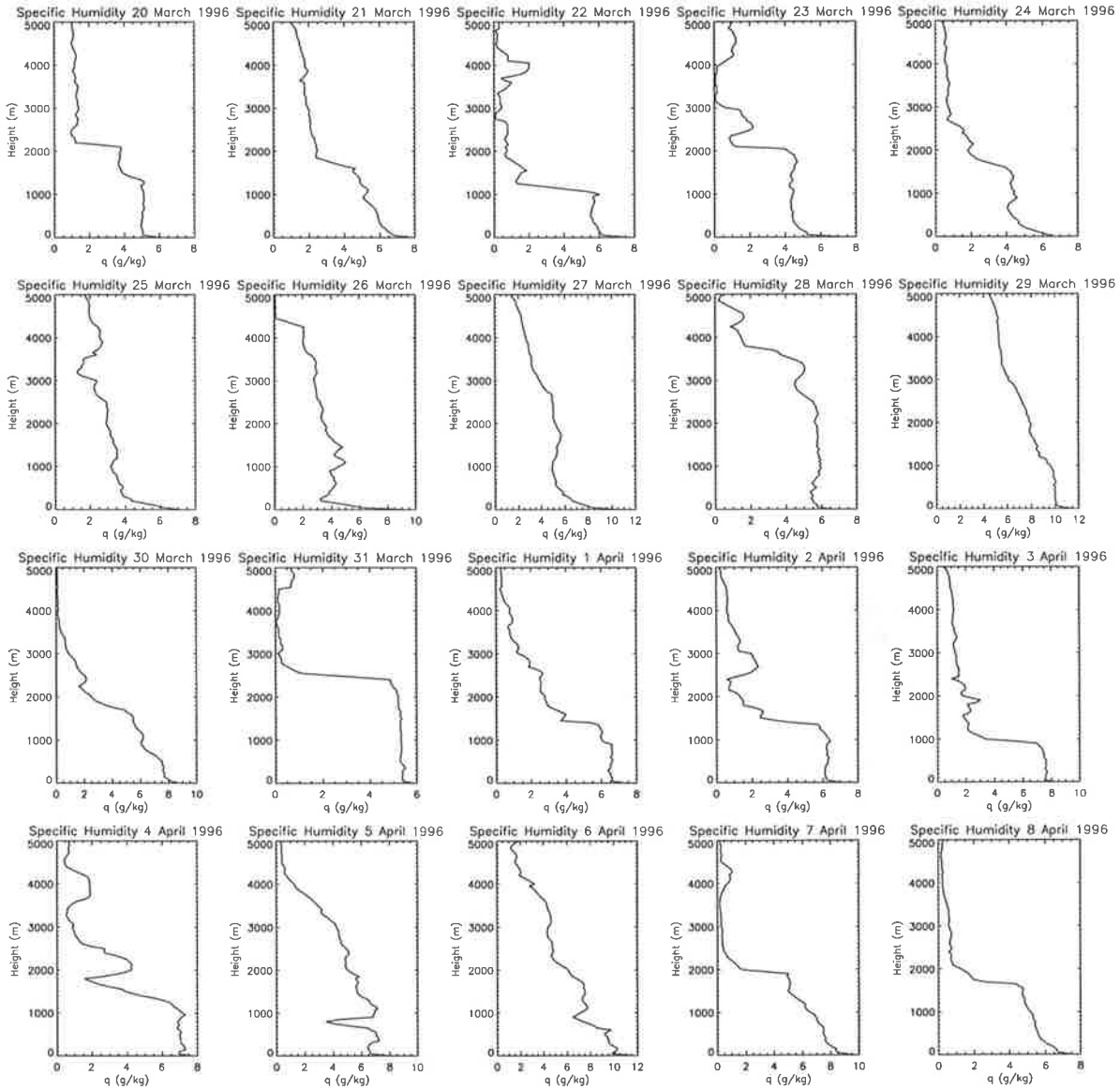

Figure 4.16: Specific Humidity from 20/03/96 to 06/04/96

4.3 Pattern Scale Measurements for Antenna Spacing

For optimum determination of winds by the SA method, the antenna spacing is required to be the same as where the spatial correlation falls to $\sim 0 \cdot 5$, as this spacing

will enable the "true" velocity to be correctly determined [*Briggs* 1984].

If the spacing is too close the cross correlation at zero lag is too high and there is a tendency to underestimate the velocity, sometimes called the triangle size affect *Golley and Rossiter* [1970] and *Holdsworth* [1995]. On the other hand, if the spacing is too large the zero-lag correlation is small and errors are large. Optimum spacing is where $\rho = 0 \cdot 5$ [*Briggs* 1984]. From computation in the last chapter theory would suggest the antenna array module spacing is $r \sim 1\lambda$. Experiment is the best way to determine the optimum module spacing.

After three sets of modules of antennas were completed, an experiment was set up to find the size of the pattern scales for reflections from the lower atmosphere. In this experiment the three modules were placed in a linear configuration with the centrally located module used for transmission, and the other two modules in reception mode only. The layout of the experiment is seen in Figure 4.17.

To determine the pattern scale the cross-correlations were taken between the three sets of antennas corresponding to spacings of 1.5 λ, 3.0 λ, and 4.5 λ. This arrangement is displayed in Figure 4.18.

The height coverage is from 300 metres to 1550 m with 150 m range gates. Since this experiment only had one 350 W transmitter just one array module was used for transmitting, which resulted in weak return echoes.

When the cross-correlation drops to 0.5, the antenna modules should have the same spacing as the pattern scales for that region of the atmosphere. Incomplete removal of ground clutter and the noise spike, as discussed earlier, can be seen in the second lowest height range. Even with these effects particularly on the lowest two heights, it can be seen in Figure 4.18 that the cross correlation function drops below 0.5 for the 1.5 λ antenna spacing for heights above 600 metres.

Results at this stage are rather inconclusive, however using the knowledge from the last campaign on the incomplete removal of ground clutter in the lowest two heights, these should be disregarded. Similarly in the last campaign it was determined for a single transmitter that returned echoes were very weak above 1.2 km except for range

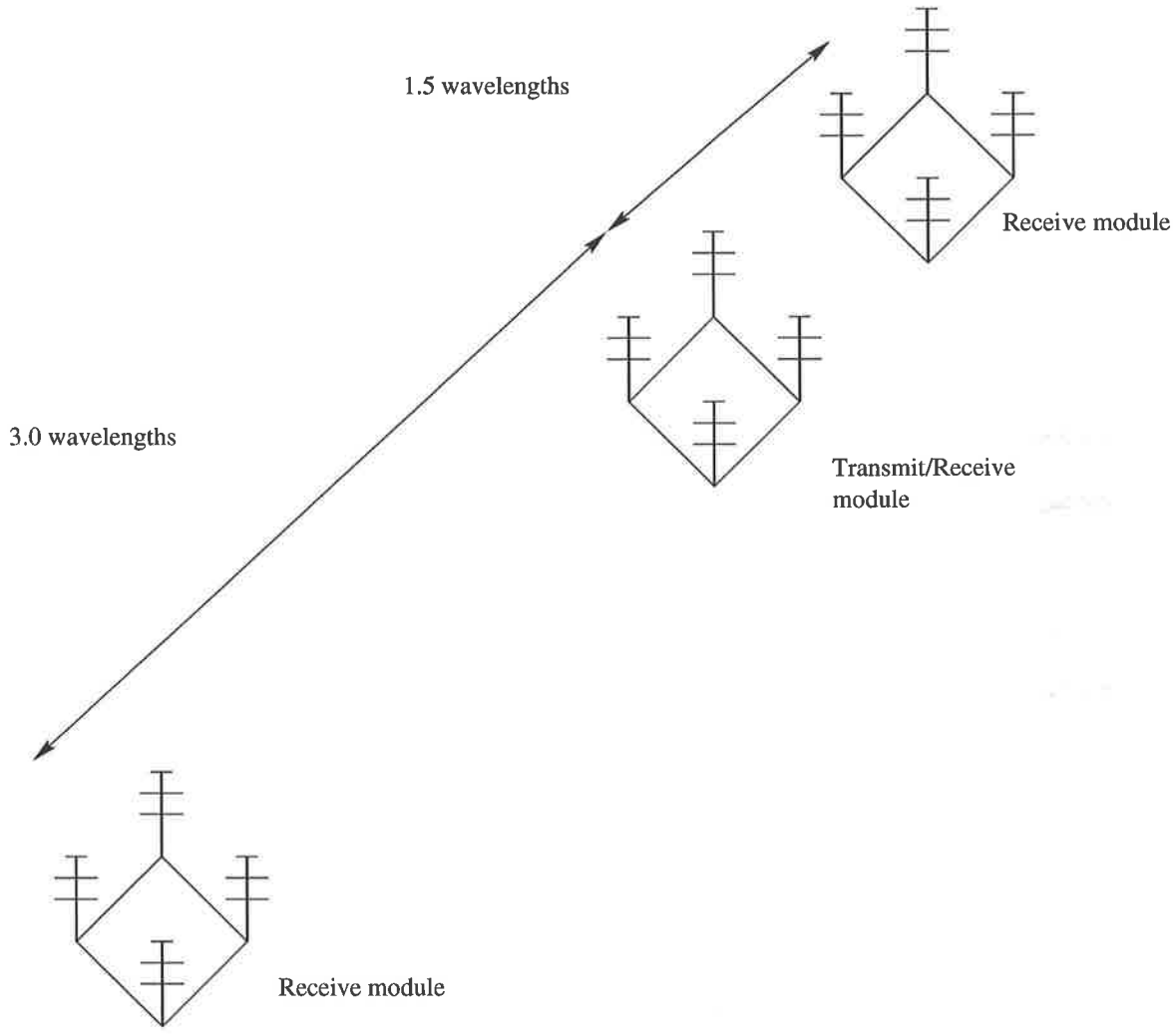

Figure 4.17: Configuration of antenna modules for determining pattern scales in the lower atmosphere.

gates near the top of the convective boundary layer. For these reasons heights 3 to 6 which corresponded to 600 metres up to 1050 metres were the focus for determining the correct antenna spacing. It can be seen that the correlation is $0 \cdot 5$ in the 600m height for an antenna spacing of $1 \cdot 5\lambda$. In the three heights from 750m to 1050m the correlation has dropped below $0 \cdot 5$ by $1 \cdot 5\lambda$ and continues to decline for larger antenna spacings.

It was seen in section 3.5 that the optimal antenna spacing for isotropic scatter is 1λ and that this spacing increases when specular scatter or a combination of isotropic and specular scatter is present. The tests to determine the best spacing were all larger than 1λ due to physical size constraints of the antenna system. However, it was still able to be determined with this constraint that the best antenna module separation would be greater than 1.5 λ due to the presence of specular scatter for a spaced antenna analysis campaign for wind determination.

4.4 Summary

There were a number of developments during this pilot study. The returned power from atmospheric scatterers from the different experiments in late 1995 through to 1996 using a single antenna module for transmitting on, are a good indication of the future performance of the full radar system.

The removal of extraneous signals has now been established from the preliminary results, including echoes from aircraft from the nearby airforce base which frequent the area from their enhanced signal strengths and motion through range gates, and ground clutter removal through its slow fading.

The calculation of the antenna spacing for the cross-correlation function dropping to 0.5 between antenna module pairs in the boundary layer will allow an appropriate spacing of the antenna modules at 1.5 λ. This should enable horizontal winds to be optimally calculated, minimising the triangle size effect on the full correlation analysis.

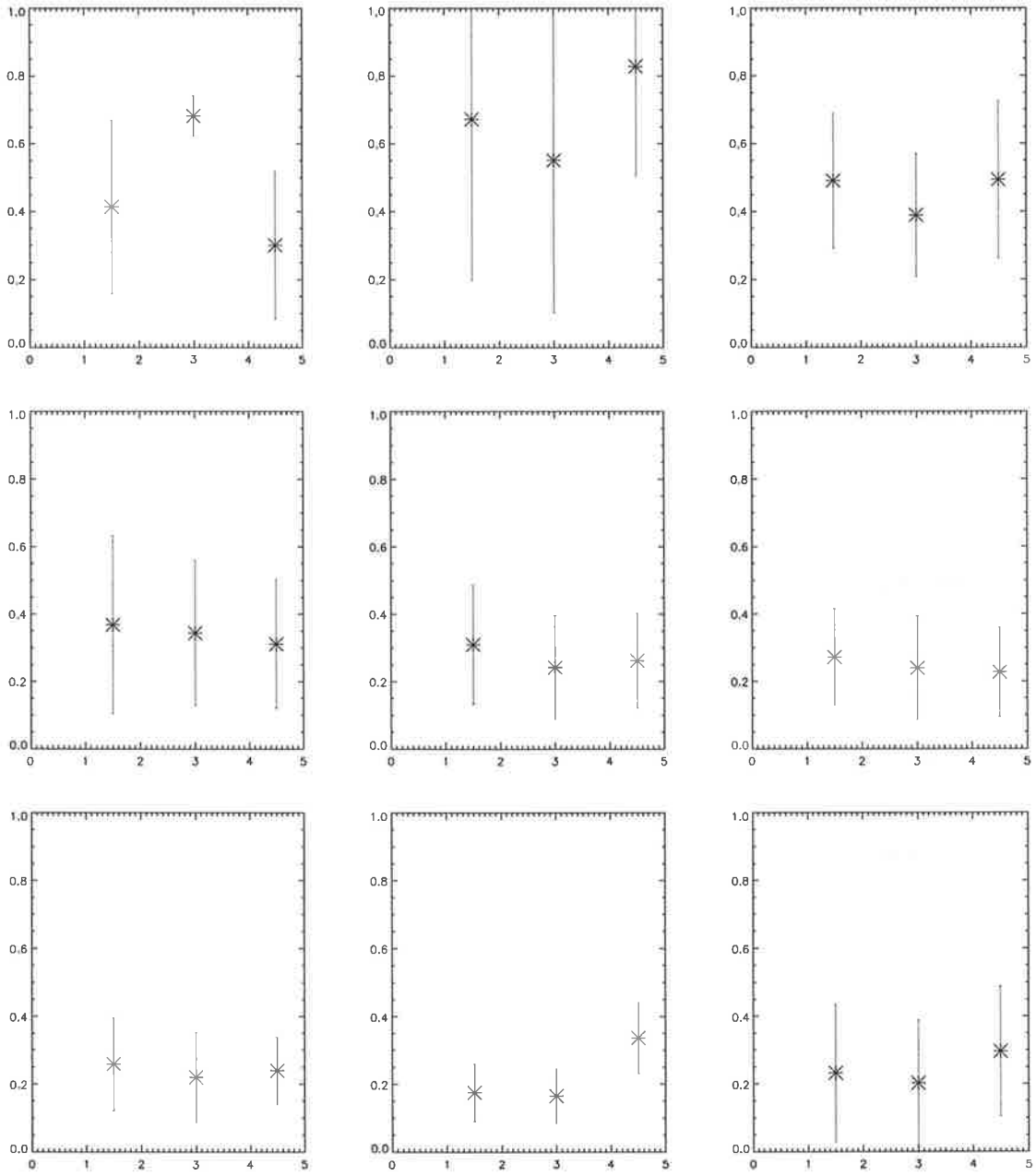

Figure 4.18: Spatial-Correlations between antenna modules. Starting from the top left plot the height is 300 m increasing in 150 m intervals up to 1550 m. When the correlation is 0.5 the spacing of the antenna modules is the same as the pattern scales of the atmospheric irregularities. The y-axis is the cross-correlation, and the x-axis is the spacing between antenna modules measured in wavelenths.

This chapter reports initial measurements made to test the concept of lower atmospheric studies at VHF. In the experiments reported here, only one 350 W transmitter was available.

Chapter 5

Campaign with Final Configuration of Radar

Four different campaigns were conducted in 1997 using the boundary-layer radar in Spaced Antenna mode. The primary goals of these campaigns were to establish the range of the new system for wind detection in the atmosphere, and to also measure the pattern scales of the boundary layer to confirm that the antenna modules were correctly spaced to minimise triangle size effect.

The first campaign in March 1997 calculated the SNR in the atmosphere to determine the range limitations of the radar. The meridional and zonal wind components were also computed to see if there were any correlation with high winds producing stronger SNR returns.

The final three campaigns were an investigation into the pattern scales of the atmosphere through a joint campaign of the boundary-layer radar and co-located radiosonde launchings. These campaigns compared the radiosonde measurements of mixing ratio and potential temperature with the radar data to determine the top of the mixing-layer. The pattern scales were calculated and analysed in conjunction with the radiosonde reflectivity and the radar SNR and echo strengths for studying which components were capable of resolving the cap of the boundary layer and the commencement of the entrainment zone.

5.1 First Adelaide Boundary-Layer Spaced Antenna Experiment

Upon completion of the upgrade of the system with all three transmitter modules and receivers tested, the radar system was arranged so that each antenna module was individually connected through a transmit/receive switch to a separate transmitter and receiver.

The three antenna modules were set up in the spaced antenna configuration, as seen in Figure 5.1, with $1 \cdot 5\lambda$ spacing as determined through the observations conducted in Chapter 4, as the best separation through being the spacing where the spatial correlation of the antennas drops to $0 \cdot 5$ at zero lag. Since all three modules are used for transmission then the beamwidth of the full array for transmission will be determined by the spacing of the modules. For this case the 1.5 λ spacing between the antenna array modules at 54.1 MHz results in a transmitted beamwidth of 12° (from Figure 2 of [*Vincent et al.* 1998] in Appendix B).

The experiment conducted in March 1997 was the first utilisation of the full array of three modules. The campaign was conducted from 09:49 CST on 14 March 1997 to 22:27 CST on 16 March 1997. The radar was run continuously over this period, using the parameters for the radar given in Table 5.1.

Table 5.1: Radar parameters for the campaign of 14/03/97 to 16/03/97.

Parameter	Setting
Pulse Repetition Frequency	20 000 Hz
Number of Coherent Integrations	1 024
Number of Data Points	1 024
Enable Phase Inversion	Yes
Acquire Data on Channels	1,2,3
Contiguous Data Sets	10
Initial Gain Values Rx 1,2,3	71,71,71
Sampling Start Height	200 m
Sampling Resolution	150 m
Sampling Range	3 000 m
Transmitter Pulse Length	150 m
Receiver Filter Setting	2 MHz

The raw data recorded were stored on the local hard disk of the computer controlling the radar for an off-line analysis of the data performed using the full correlation analysis.

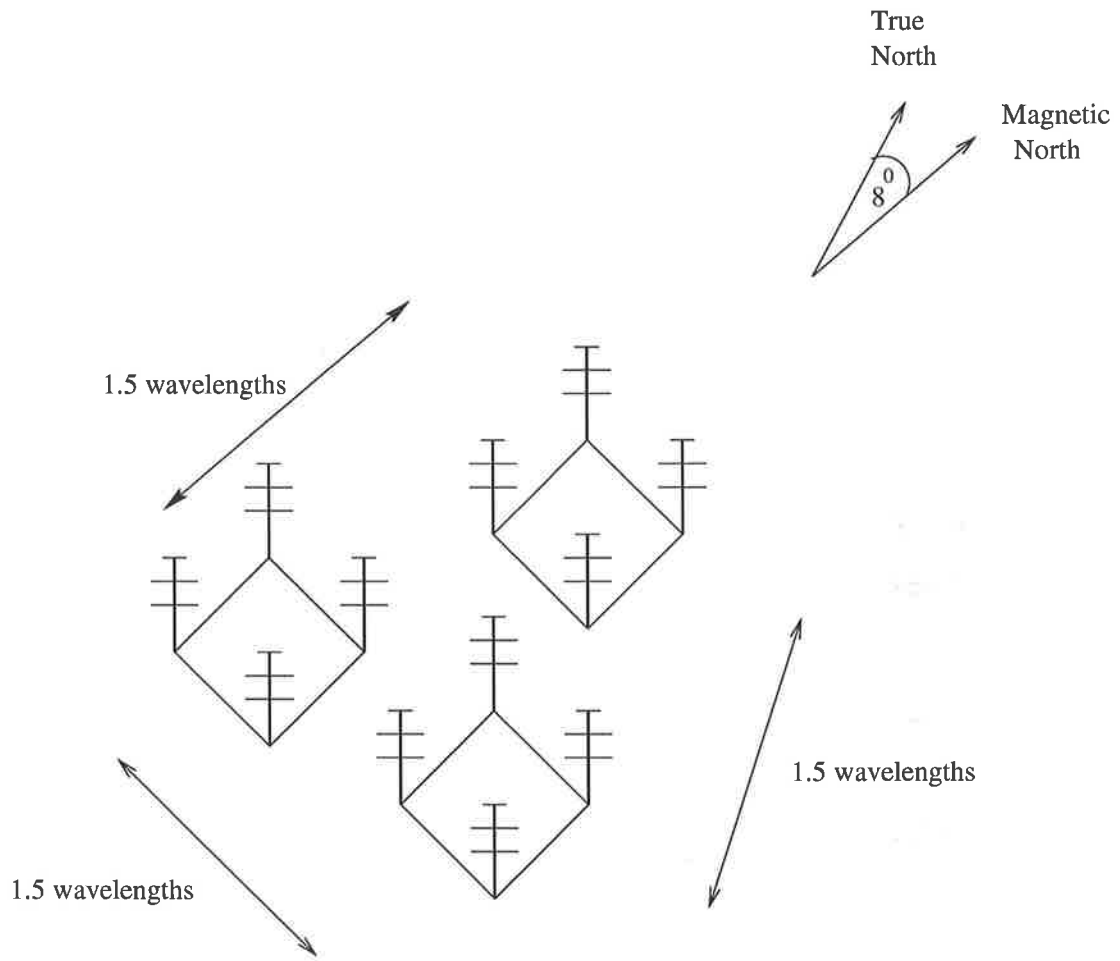

Figure 5.1: Final Spaced Antenna configuration of the Boundary Layer Radar.

In this campaign the SNR was first calculated, the results of which are displayed in Figure 5.2. It is observed in Figure 5.2 that there is an enhancement of the returned echo at about 1.5 km altitude which is an indication of the height of the top of the boundary layer.

The first measurements of winds in the boundary layer were then calculated, with some interesting results. The FCA true velocities were averaged over a ten minute period. The plot of the meridional velocity can be seen in Figure 5.3, and the zonal

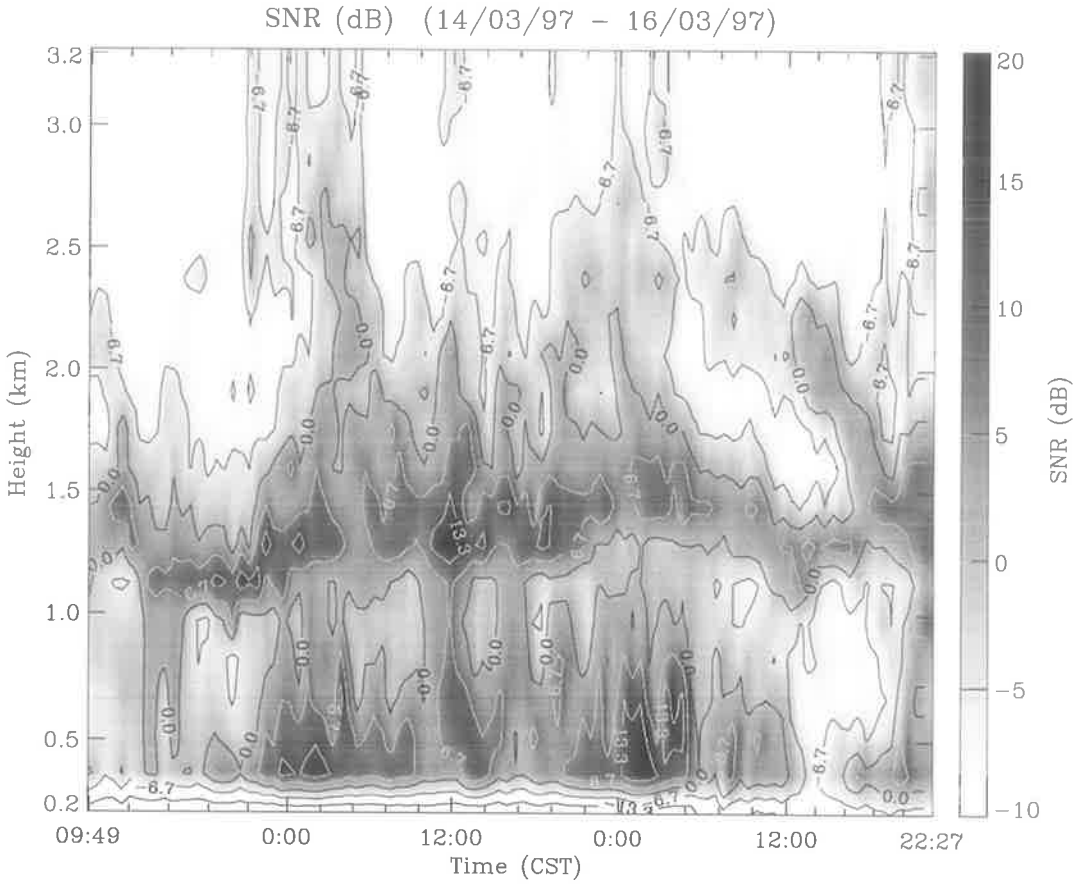

Figure 5.2: Signal to Noise Ratio for Campaign from 09:49 14/03/97 to 22:27 on 16/03/97

velocities for the campaign are displayed in Figure 5.4.

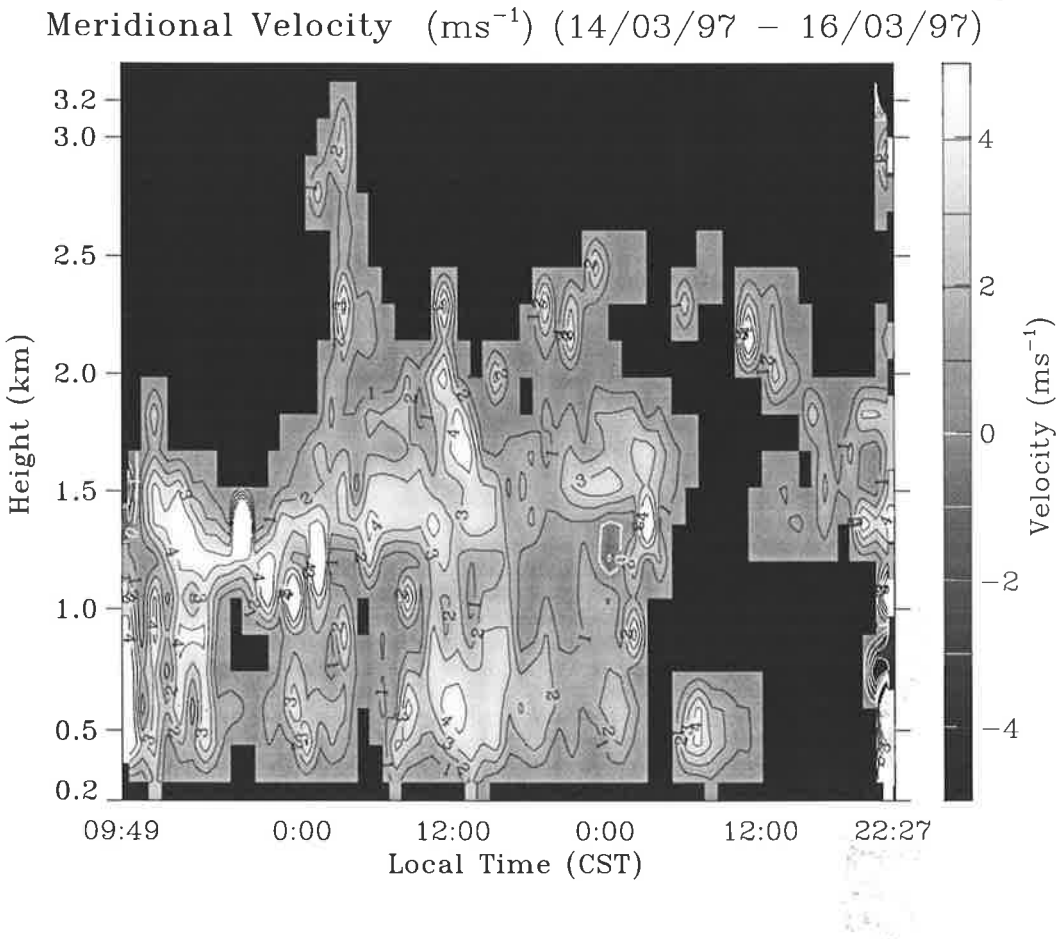

Figure 5.3: Spaced Antenna analysis derived Meridional Velocities from 14/03/97 to 16/03/97

The winds are only displayed for altitudes where the analysed data does not violate any of the FCA rejection criteria. These rejection criteria include low echo strength, low SNR, too slow fading, poor fitting of auto- or cross-correlation functions, or large variations between the apparent and true wind velocities. When either one or a combination of these criteria occurred no winds are displayed.

Results are received consistently up to 2.3 km, and there are short periods where winds can be measured up to 3.2 km. At the top of the boundary layer there was a constant eastward wind, frequently exceeding 4 ms^{-1}, and a weaker northward wind which also was typically strongest at the top of the mixed layer.

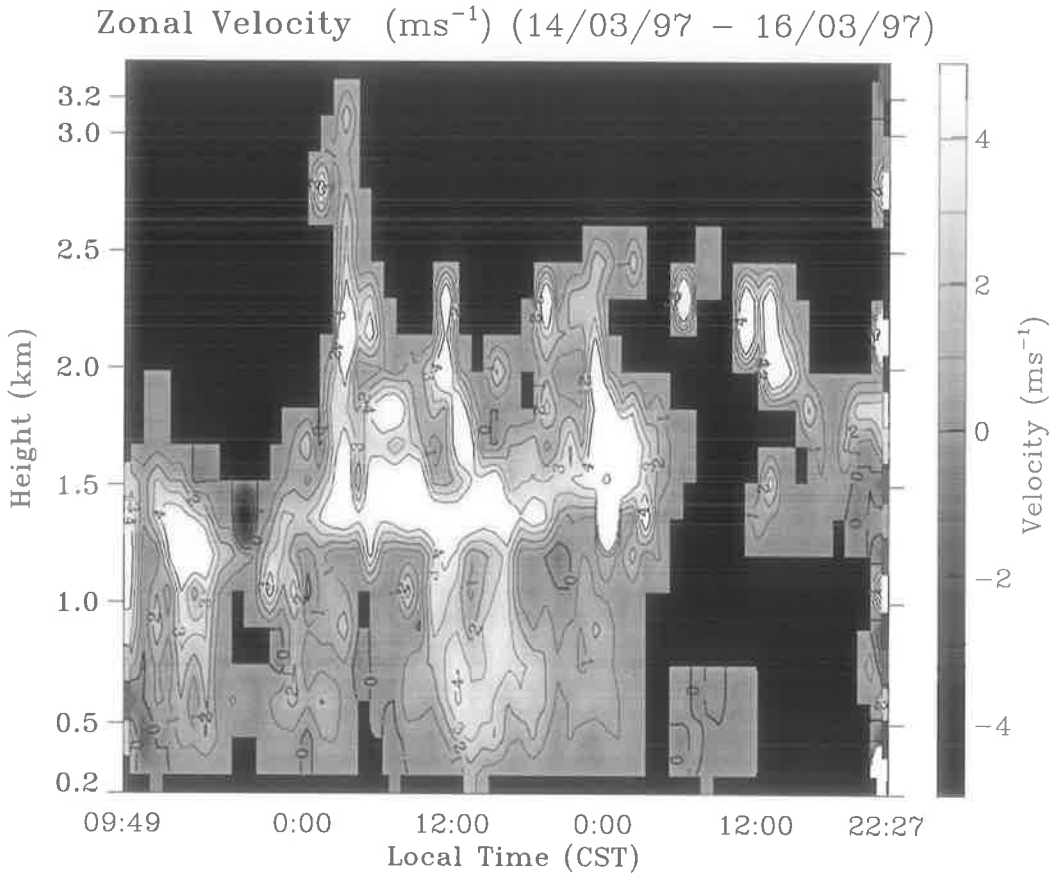

Figure 5.4: Spaced Antenna analysis derived Zonal Velocities from 14/03/97 to 16/03/97

It can be seen that there is clearly a strong increase in the SNR when the horizontal winds strengthen. This is probably more evident during low humidity periods than at other times. This is because in a dry atmosphere the returned power of the radar would be expected to be decreased, as seen by the dominance of the density fluctuations of the water vapour in Equation 2.1, and strong signals would only be expected from strong regions of clear air turbulence, or from moist layers. Strong turbulence, however, would occur as the horizontal winds themselves strengthen in the lower atmosphere due to the frictional effects within the boundary layer.

These initial results with the radar in its final configuration were very encouraging, and led to three campaigns being carried out during winter and spring 1997 where the radar scattering was compared with the radiosondes launched at Buckland Park. These are described in the next section.

5.2 Co-Located Adelaide Boundary-Layer Radar and Radiosonde Campaigns

In the period of late July to September 1997, three separate campaigns were conducted to verify the results of the VHF Boundary Layer Radar. In these campaigns radiosondes were launched at the site of the radar to test the performance of the VHF BL radar.

The first campaign ran from 12:36 CST on 31/07/97 to 15:22 CST on 01/08/97 using GPS radiosondes. The second campaign used Omega Navaid Radiosondes, and ran from 18:48 CST on 12/09/97 to 15:06 CST on 14/09/97. The final campaign also used Omega Navaid Radiosondes and was conducted from 15:20 CST on 26/09/97 to 06:05 CST on 27/09/97.

The meteorological conditions varied considerably between the three campaigns. The first campaign was conducted when a strong high-pressure region of 1035 hPa was centred over the region. The second campaign had a cut-off low propagate through the region during its conduct, and there were periods of heavy precipitation. The third

campaign was similar to the first, though this time the high-pressure cell was weak.

5.2.1 Experiment Description

During the three campaigns the radiosondes were all launched at approximately 3 to 4 hourly intervals.

The methods used to track both the GPS and Omega sondes used in the three campaigns are described in section 2.5.

The GPS sondes used a 60-second smoothing algorithm, while the Omega sondes had a 240-second filter. This is used to remove the pendulum motion of the sonde package beneath the balloon. The shorter period over which the GPS sondes are smoothed enables a better vertical resolution which equates more closely with the radar's 150 metre range gates.

The boundary layer radar was set up with its three modules configured in the spaced antenna format with 1.5 λ spacing as as shown in Figure 5.1.

5.2.2 Results

The radar results were compared with the sonde results in *Vincent et al.* [1998], for wind comparisons between the two systems. As shown in that paper, the agreement is excellent. Here we focus on the pattern scales of scatterers in the atmosphere, and the characteristics of the boundary layer related to signal strengths returned to the radar.

5.2.2.1 Campaign 1: July 31 to August 1, 1997

During this campaign the radar's results were averaged for 1 hour around the launch time of the sondes. The results for the first campaign can be seen in Figures 5.5 to 5.13. Results for the radar are displayed in the same figures as for the sondes.

The pattern scales calculated from the radar data are plotted along with the angular widths for the scattering irregularities as calculated from the techniques explained in

section 3.5. The SNR and the range-corrected power for the boundary layer radar are both shown, with the range corrected power plotted with the potential refractive index as calculated from the radiosonde data. The specific humidity and potential temperature from the sonde data are also shown to help determine the depth of the mixed layer.

Diagrams for the pattern scale, signal to noise ratio, and range corrected power have error bars drawn corresponding to one standard deviation of the respective results for each height.

In Figure 5.5, it can be seen that data were obtained from the lowest range gate of 300 metres up to the top gate of 3150 metres with signal to noise ratios only dropping below -10 dB in the uppermost range gates. With the ground-clutter removal procedures employed and data rejection during processing of the data using the full correlation technique, the lowest range at 300 metres has only a limited amount of data accepted as a result of receiver saturation and clutter removal.

The specific humidity and potential temperature profiles from the sonde data indicate through their approximate constancy with height that there is relatively good mixing occurring above the strong super-adiabatic layer in the lowest 100 m from ground level, up to the thermal inversion at about 2.1 km, which is located at the top of the boundary layer.

This inversion at about 2.1 km has a significant effect on the potential refractive index, as expected from the results shown in chapter 4 looking at the dry and wet contributions to the potential refractive index. There is a a direct correlation between the changes in refractive index calculated from the sonde and the increase in range corrected power as computed from the radar data. It should be noted that the radiosonde may pick up very small spatial and temporal fluctuations, which would be smoothed out as a result of averaging the radar data within one hour of the sonde launch. There will also be differences based on the separation of the location of the sonde and the radar volumes, as the sonde will drift horizontally away from the volume of atmosphere directly probed by the radar.

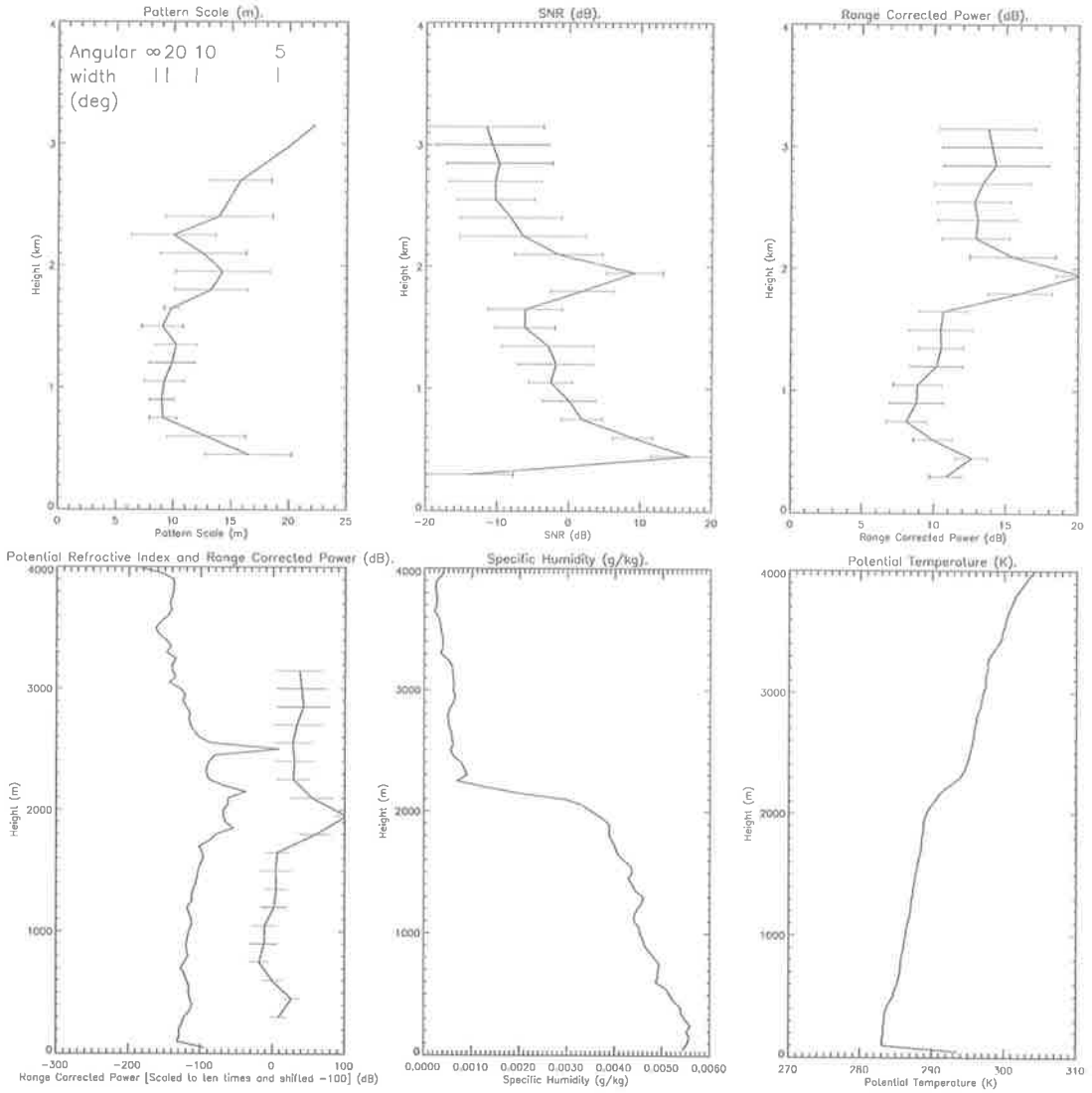

Figure 5.5: Comparison of radar with GPS radiosonde data for the radiosonde launch at 12:36 CST on 31/07/97. The combined diagram of profiles of potential refractive index and range corrected power, have had the magnitude of the power scaled to make it legible on the same graph.

Two interesting features emerge when the pattern scale plots is examined in Figure 5.5. The first is that, at the top of the mixed layer at 2 km, there is almost a 50 % increase in the size of the pattern scale which corresponds to a significant reduction of the angular spectrum of the irregular scatterers. The second feature is that the pattern scales tend to increase with height in the free air region above the top of the mixed layer. An increase in the magnitude of the pattern scale would be expected in the lower regions of the troposphere above the mixed layer due to a reduction in clear air turbulence above the transition from the frictional effects of terrain to the free air region.

Since the angular spectrum at altitudes around 3 km is quite narrow ($\sigma(s) \sim 5 - 10°$), returned echoes would be expected to have a high returned power. This has in fact occurred, though this is partially due to the range correction to the power. The mean SNR of around -10 dB was recorded in the highest range gates for this record.

The sonde launch of 19:21 CST on 31/07/97 (Figure 5.6) is another prime example where there is a weak transition to the free air region. Where this occurred the returned echoes were generally stronger at higher altitudes than usual, due to a broad entrainment zone bringing moisture into the free atmosphere. This moisture would then enhance the wet component of the reflectivity for the lowest region of the free atmosphere.

The sonde launch of 23:24 CST on 31/07/97 showed a thoroughly mixed layer up to about about 1.5 km, then near 2 km there is a thin moist layer. In this case the regions near 1 km and above 2.2 km have low SNR. The almost complete lack of moisture above 2.2 km is probably the main reason for this low SNR.

All of the sonde launches of the 01/08/97 from 02:06 CST to 15:22 CST are characterised by an extremely dry atmosphere above the mixing layer, with sharp changes in specific humidity and potential temperature at the top of the boundary layer. Another characteristic of these sharp changes is the corresponding changes in the gradients of the potential refractive index and the accompanying increase in echo strength.

The distinctive enlarging of the pattern scales at the location of the transition

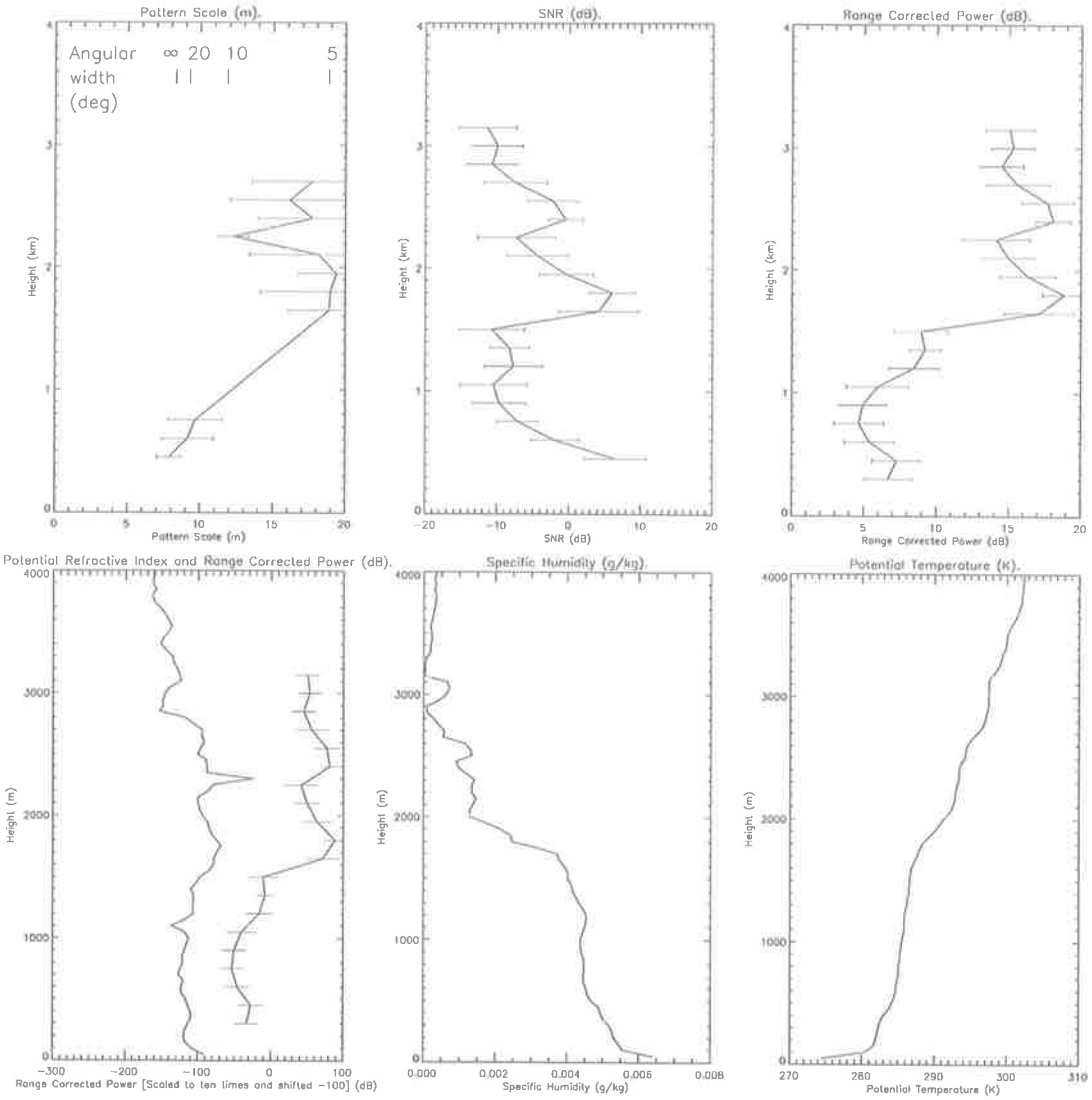

Figure 5.6: As for Figure 5.5 but for the launch at 19:21 CST on 31/07/97.

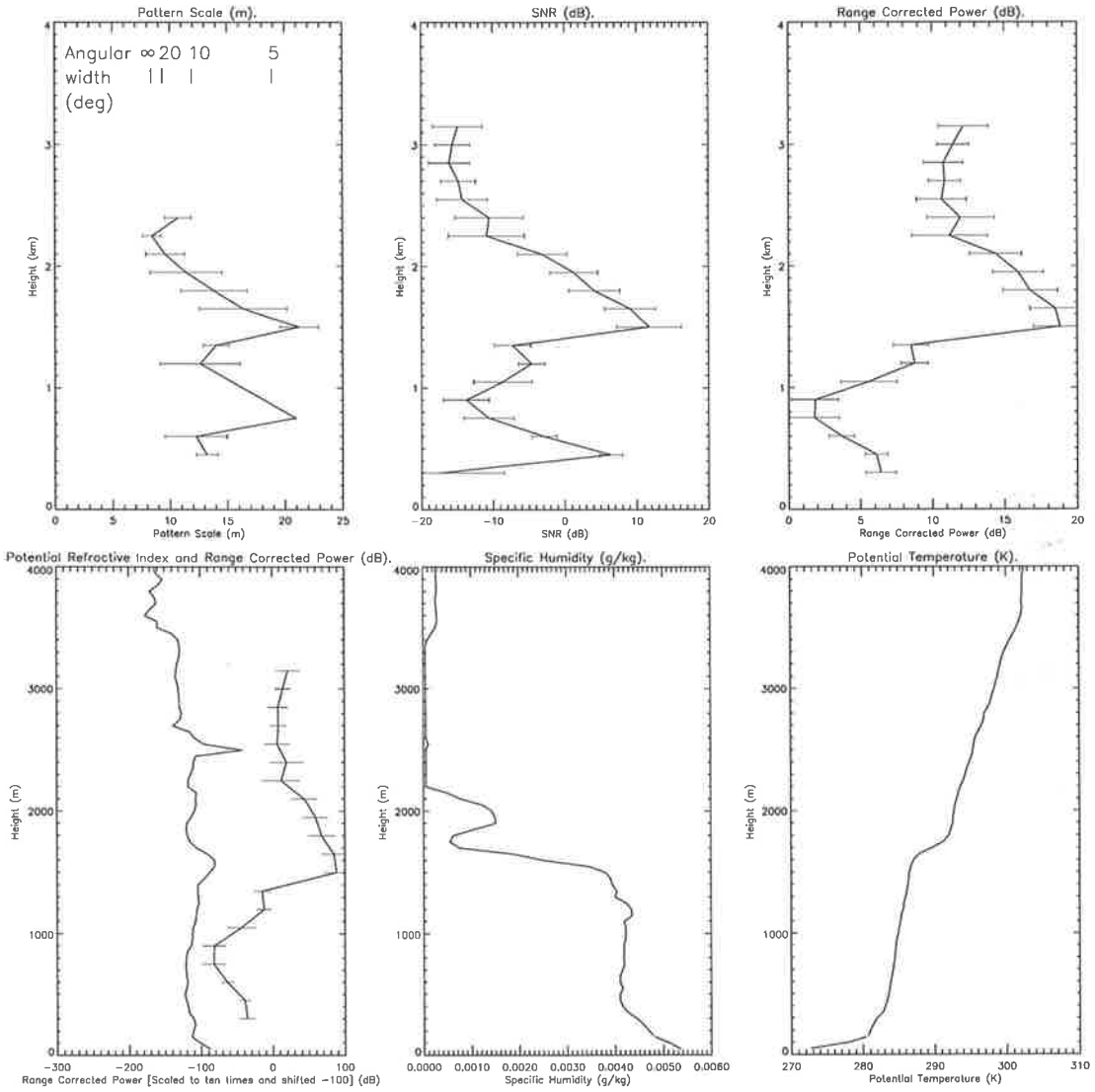

Figure 5.7: As for Figure 5.5 but for the launch at 23:24 CST on 31/07/97.

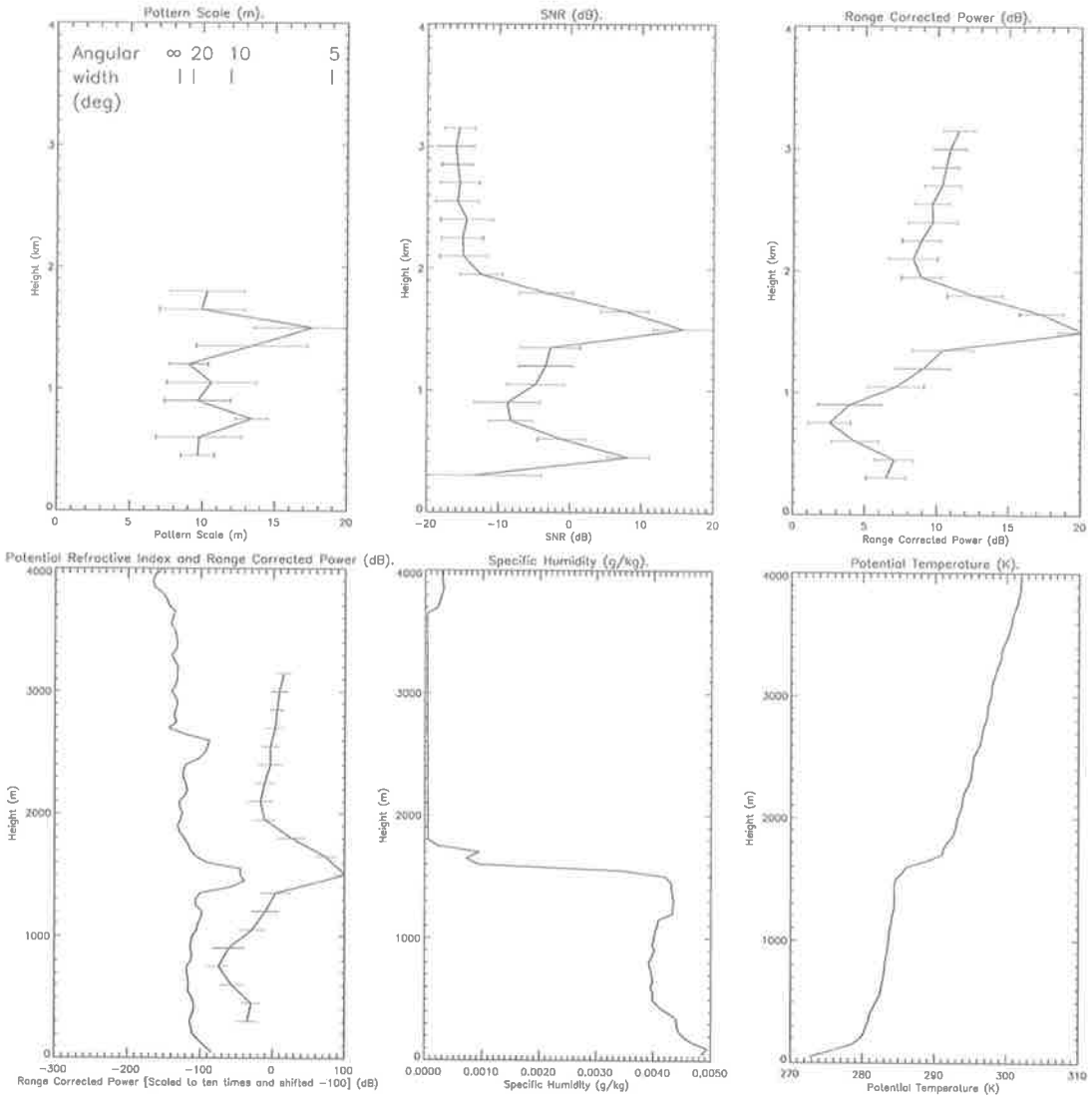

Figure 5.8: As for Figure 5.5 but for the launch at 02:06 CST on 01/08/97.

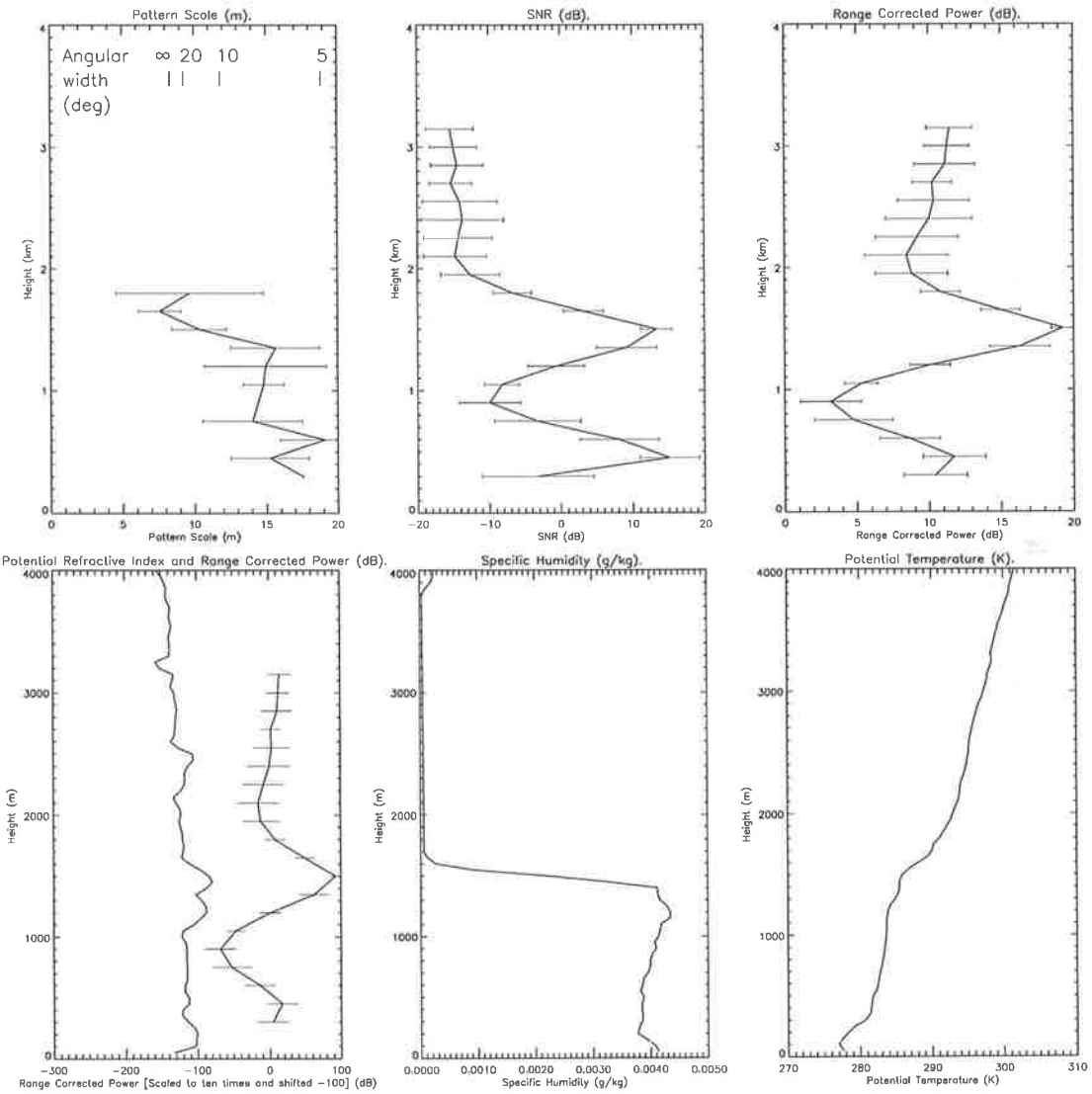

Figure 5.9: As for Figure 5.5 but for the launch at 04:57 CST on 01/08/97.

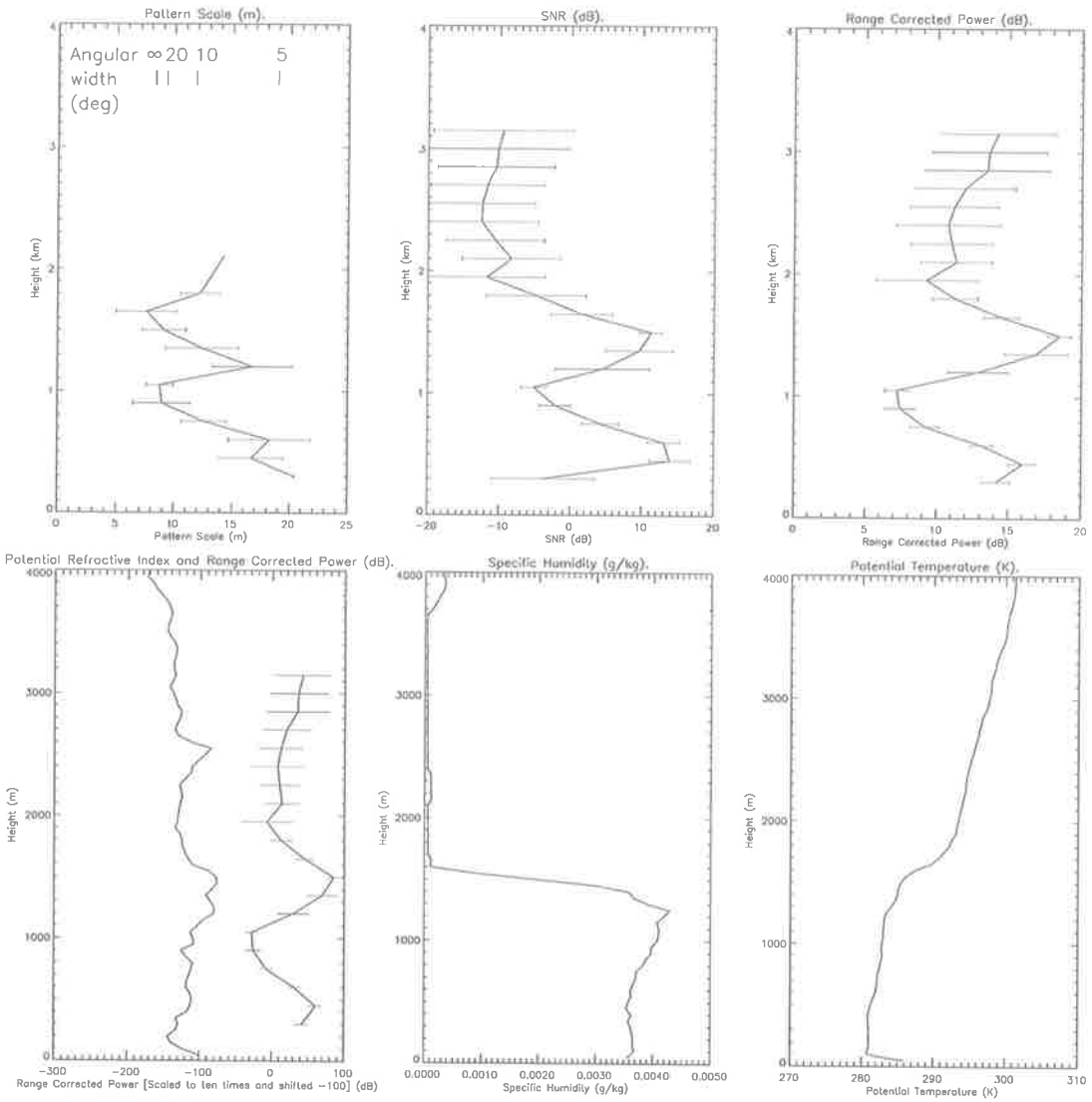

Figure 5.10: As for Figure 5.5 but for the launch at 08:07 CST on 01/08/97.

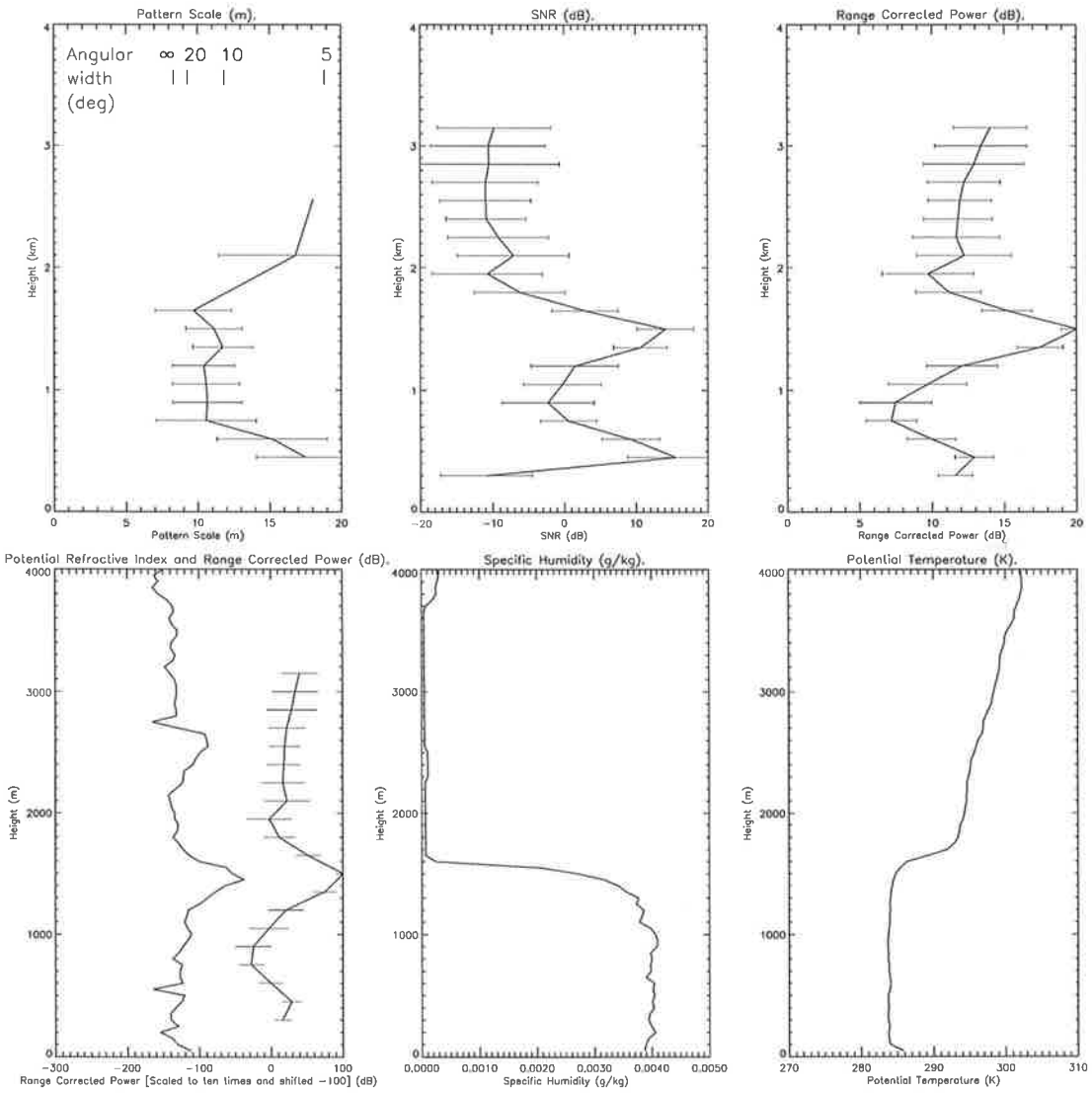

Figure 5.11: As for Figure 5.5 but for the launch at 10:25 CST on 01/08/97.

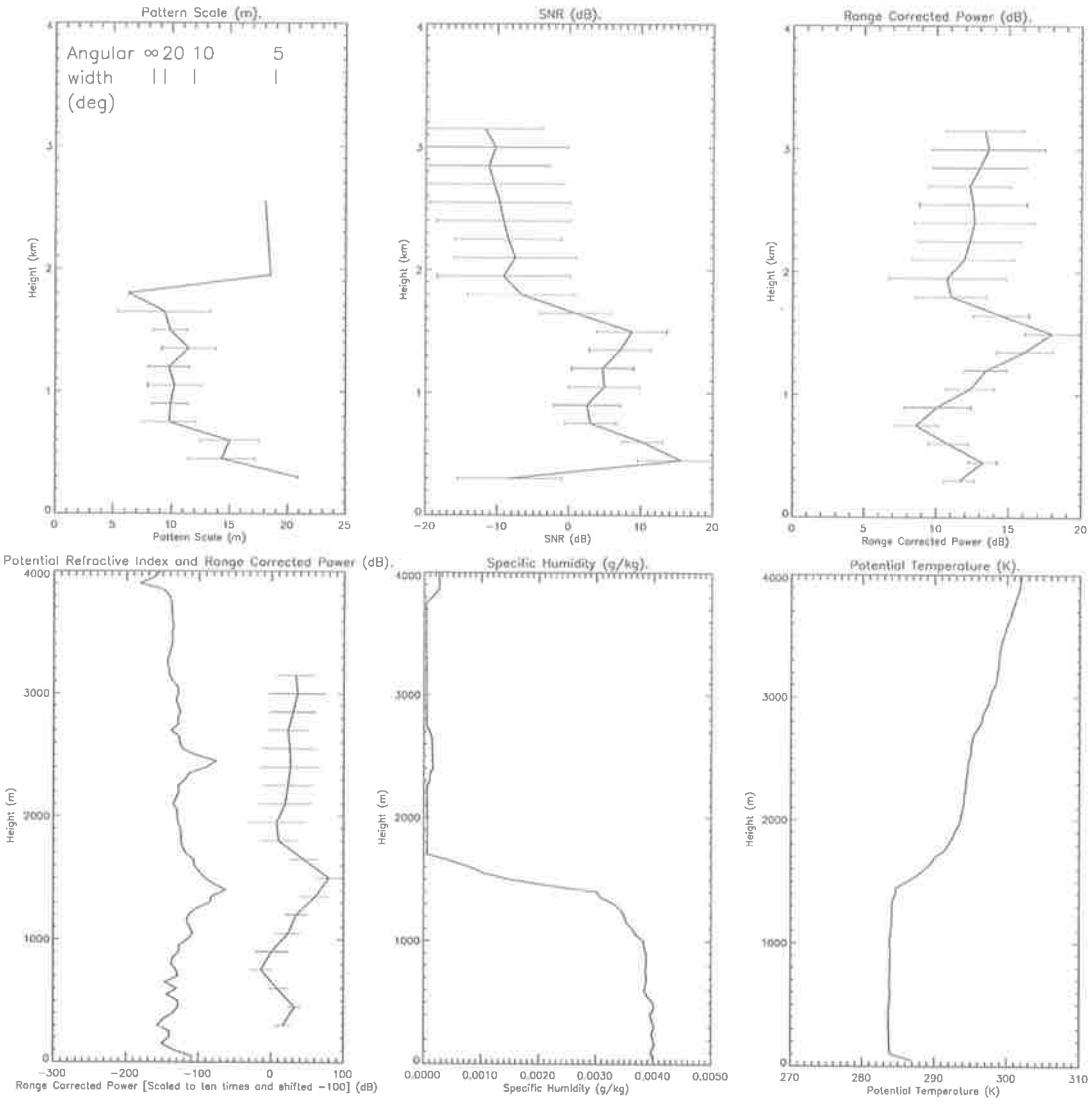

Figure 5.12: As for Figure 5.5 but for the launch at 13:30 CST on 01/08/97.

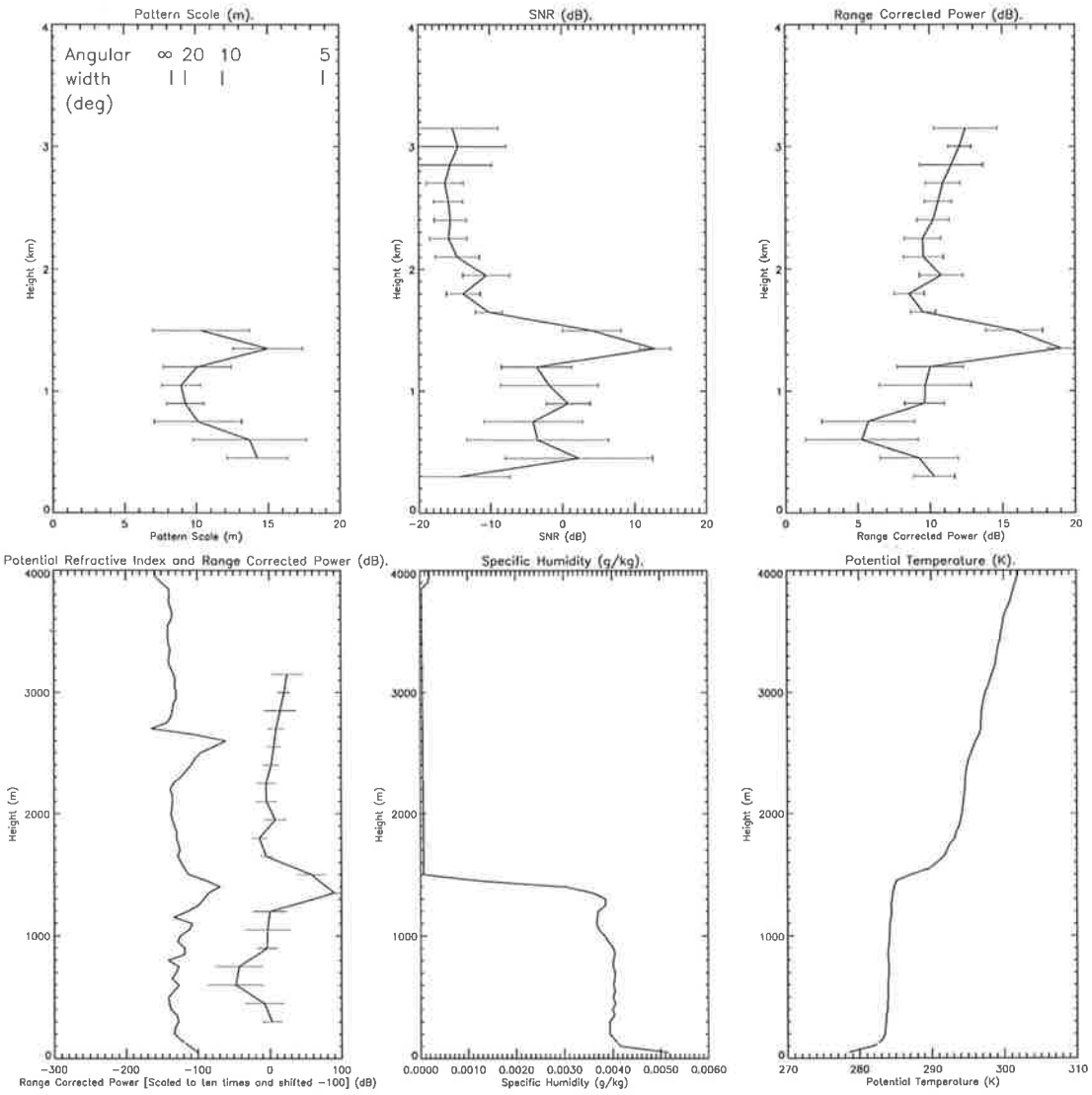

Figure 5.13: As for Figure 5.5 but for the launch at 15:22 CST on 01/08/97.

region is again a characteristic of the echoes around the launches of 02:06 CST and 15:22 CST.

5.2.2.2 Campaign 2: September 12 to September 14, 1997

The second campaign which ran from 18:48 CST on 12/09/97 to 15:06 CST on 14/09/97 used Omega Navaid radiosondes. During the campaign in mid September there was markedly more moisture in the lower troposphere than in July. Another difference is that thermal inversions are less evident than in the July campaign. This campaign was conducted while a cut-off low passed through the region of the radar.

The first sonde launching at 18:48 CST on 12/09/97 detected a thick moist layer (Figure 5.14) above the transition level. This was typical up until the sonde launching of 18:56 CST on 13/09/97. From 23:48 CST onwards to 15:06 CST on 14/09/97 there is a steady decline in the specific humidity with altitude from ground level, and a steady increase in the potential temperature.

As a result of these atmospheric conditions, the returned power is considerably higher than when an enhanced boundary layer exists. The resulting SNR above 3 km may have a mean of -10 dB but commonly exceeds even 0 dB.

5.2.2.3 Campaign 3: September 26 to September 27, 1997

The third campaign had Omega Navaid launchings from 15:20 CST on 26/09/97 to 06:05 CST on 27/09/97. The results are summarised in Figures 5.25 - 5.30. A typical characteristic of this campaign is the extremely dry conditions above the boundary layer, similar to the first campaign in late July to early August.

The first sonde launching shown in Figure 5.25 shows that even though the atmosphere is not thoroughly mixed near ground level, there is still an enhancement of the mean power and SNR near the capping inversion. Similar to the July campaign, there is an enlarging of the pattern scale in the region of the top of the mixed layer.

The second sonde launching shown in Figure 5.26 displays a strong capping to the convective boundary layer at 1.9 km, and a corresponding increase in the potential

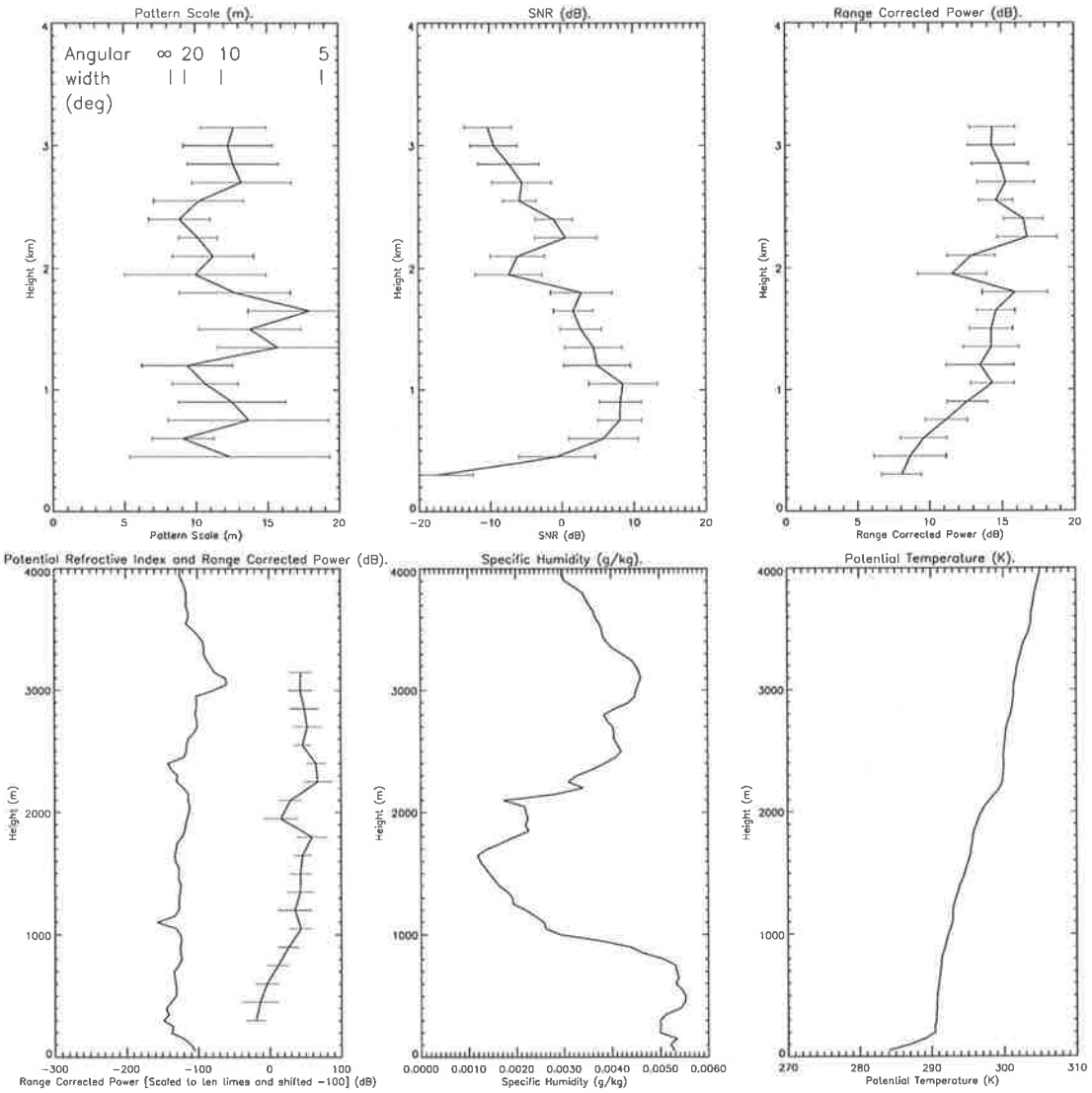

Figure 5.14: Comparison of radar with Omega Navaid radiosonde data for the radiosonde launch at 18:48 CST on 12/09/97. The combined diagram of profiles of potential refractive index and range corrected power, have had the magnitude of the power scaled to make it legible on the same graph.

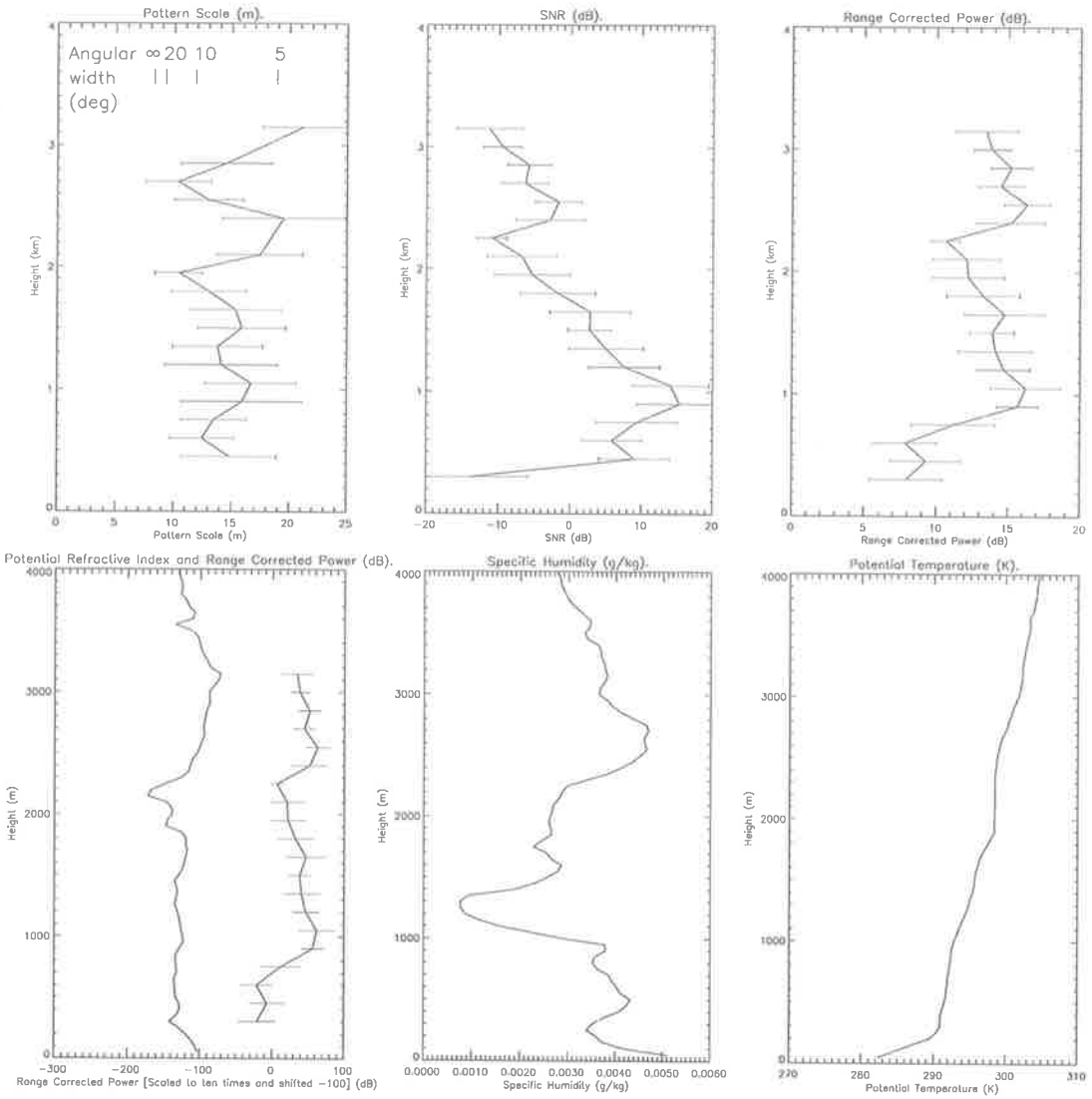

Figure 5.15: As for Figure 5.14 but for the launch at 22:59 CST on 12/09/97.

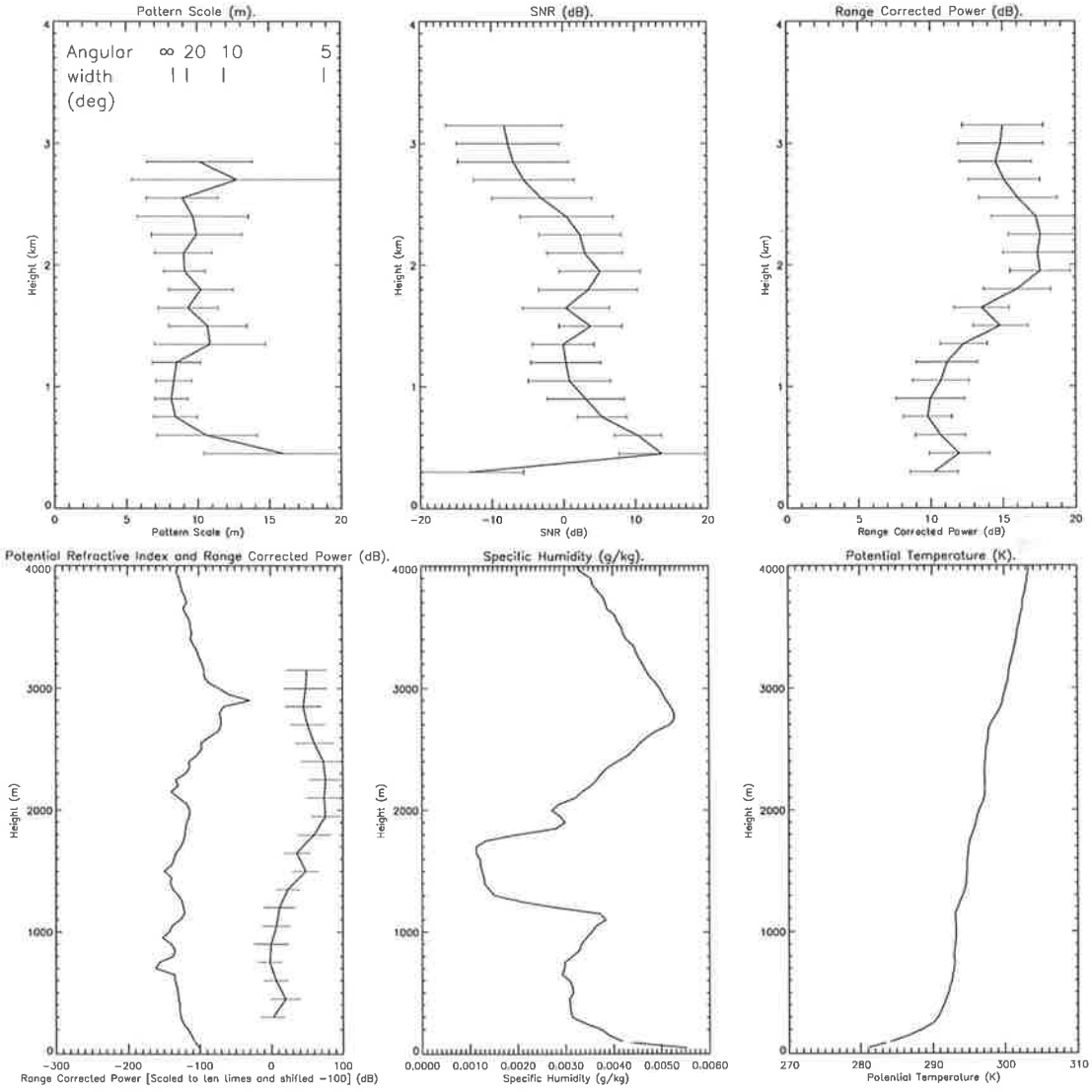

Figure 5.16: As for Figure 5.14 but for the launch at 07:10 CST on 13/09/97.

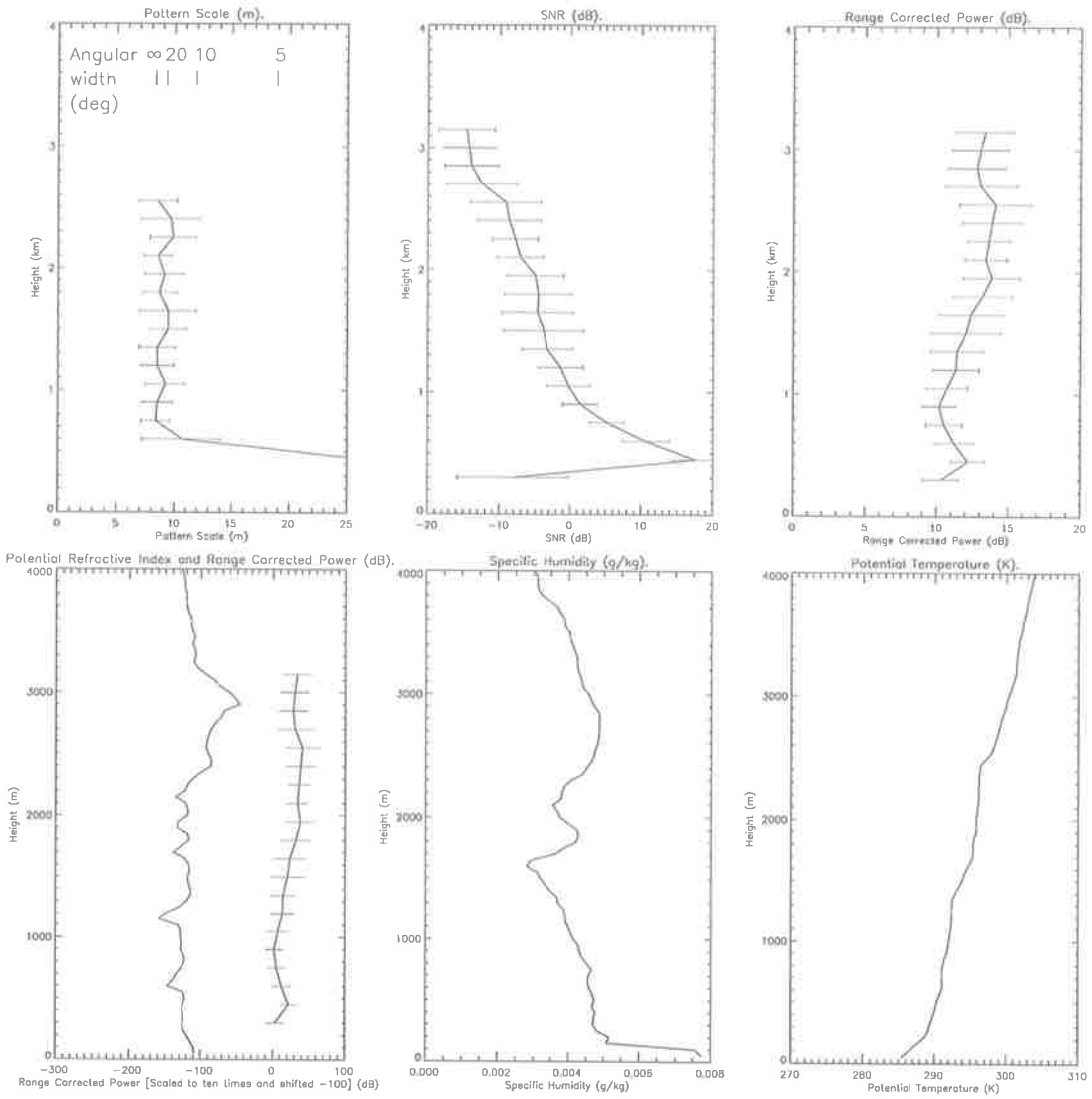

Figure 5.17: As for Figure 5.14 but for the launch at 10:57 CST on 13/09/97.

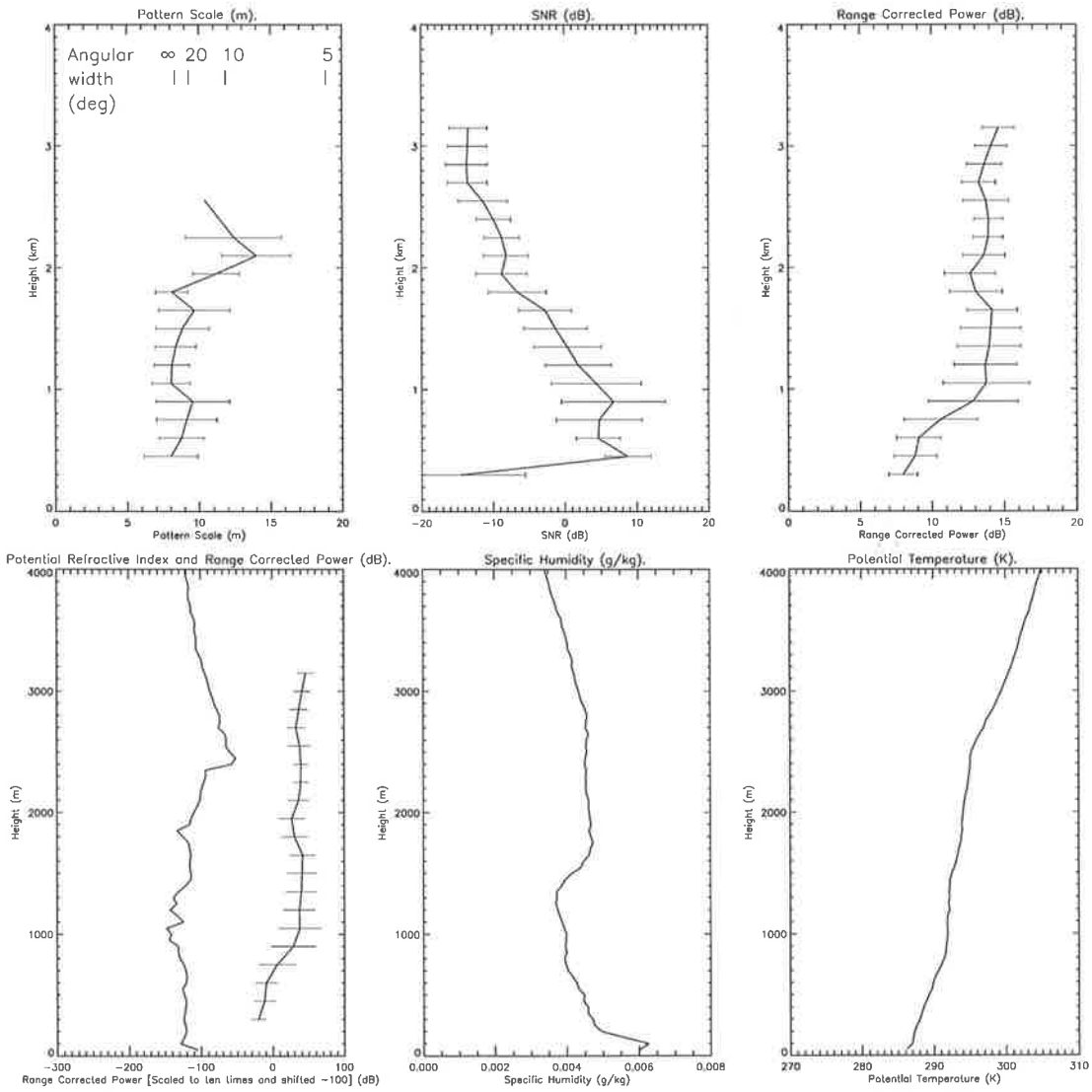

Figure 5.18: As for Figure 5.14 but for the launch at 15:07 CST on 13/09/97.

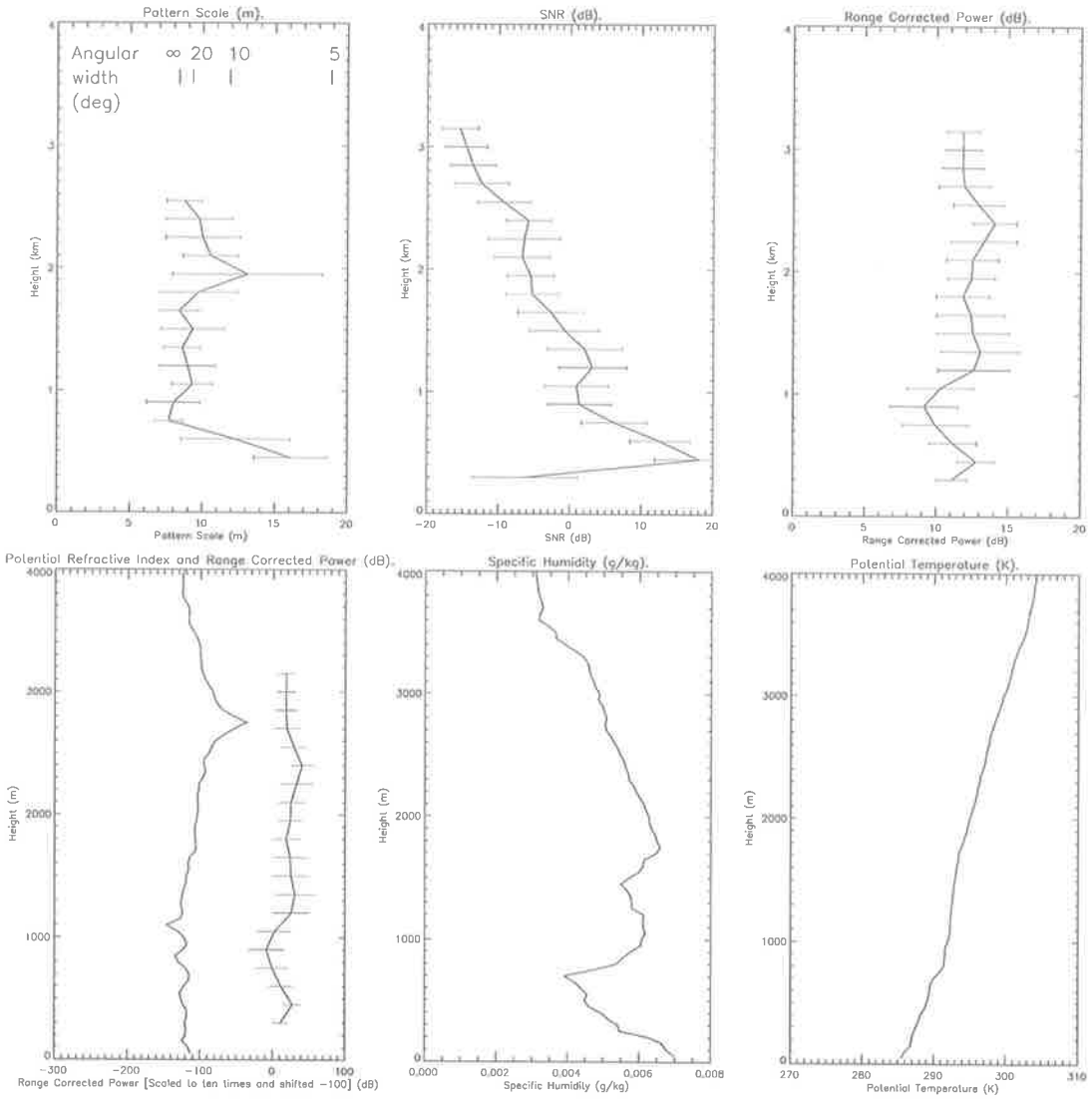

Figure 5.19: As for Figure 5.14 but for the launch at 18:56 CST on 13/09/97.

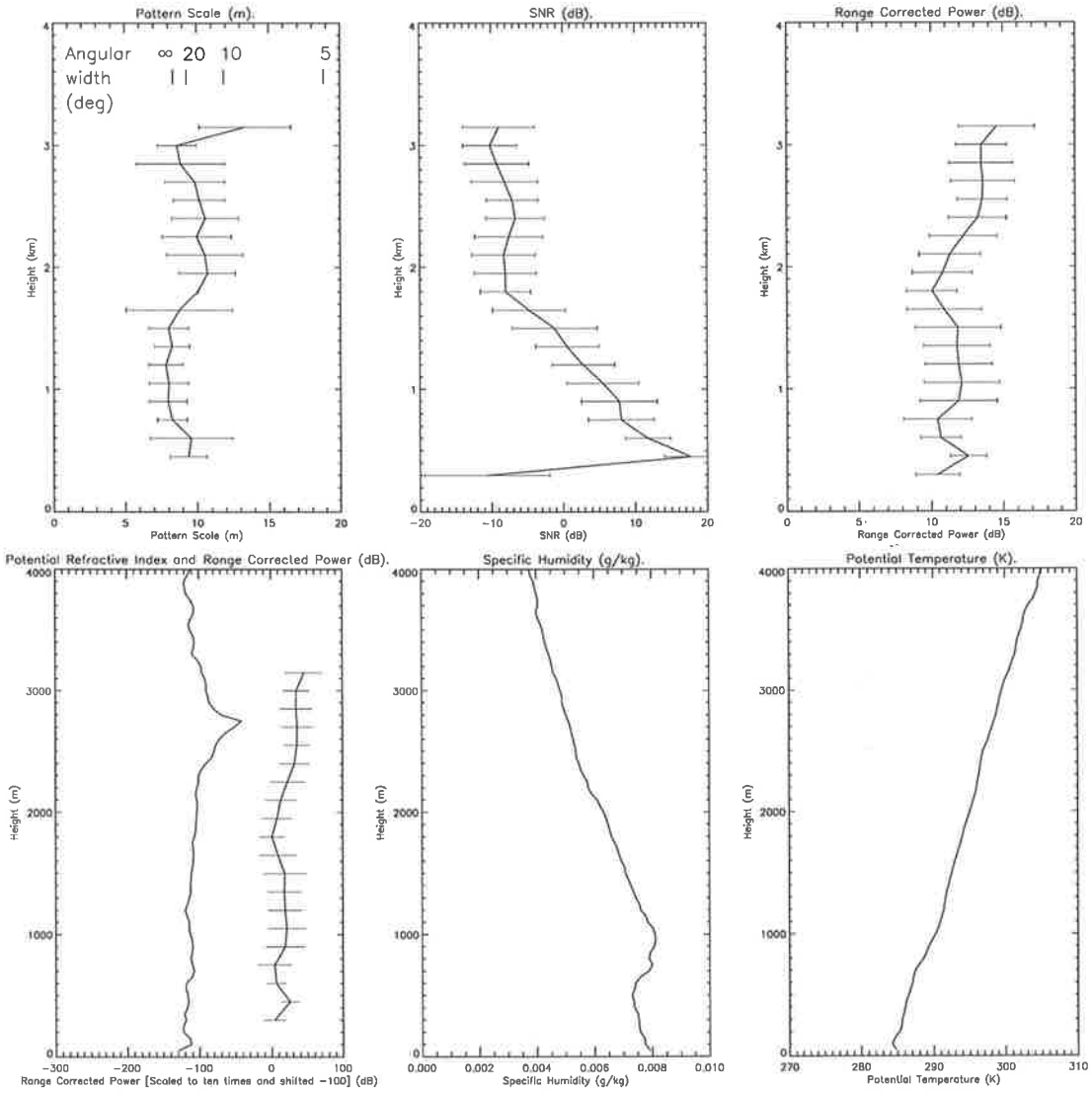

Figure 5.20: As for Figure 5.14 but for the launch at 23:48 CST on 13/09/97.

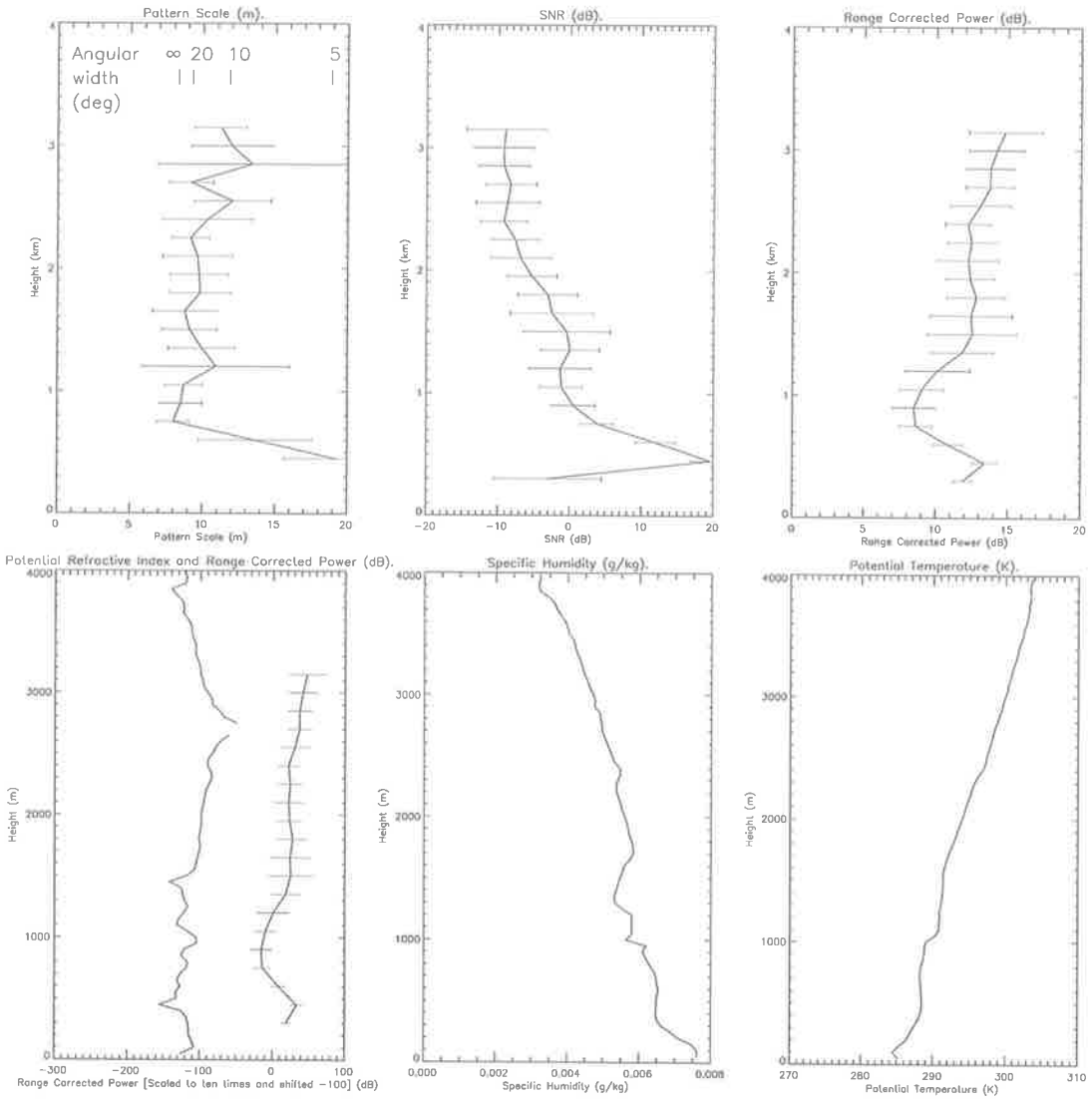

Figure 5.21: As for Figure 5.14 but for the launch at 03:18 CST on 14/09/97.

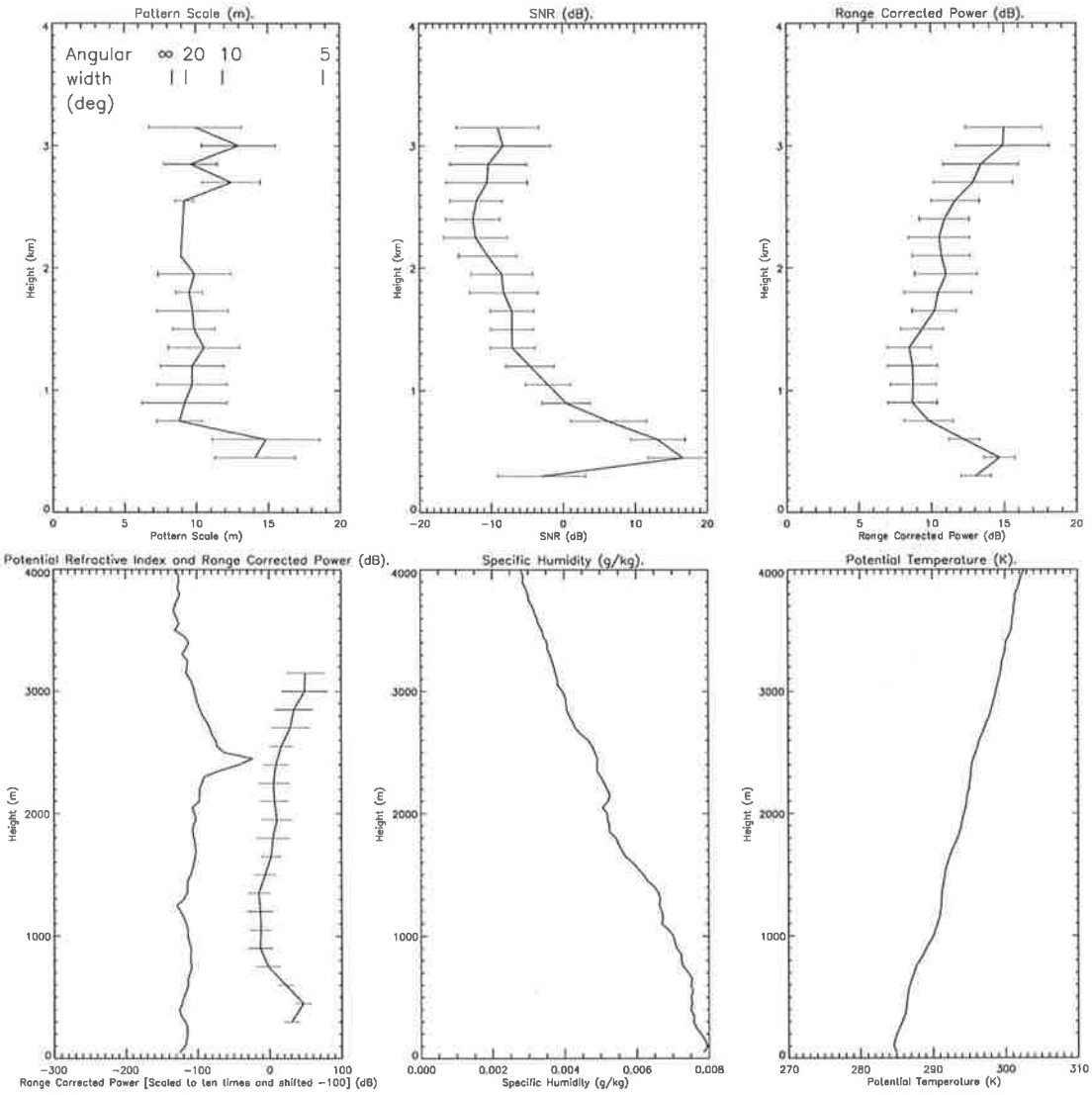

Figure 5.22: As for Figure 5.14 but for the launch at 07:29 CST on 14/09/97.

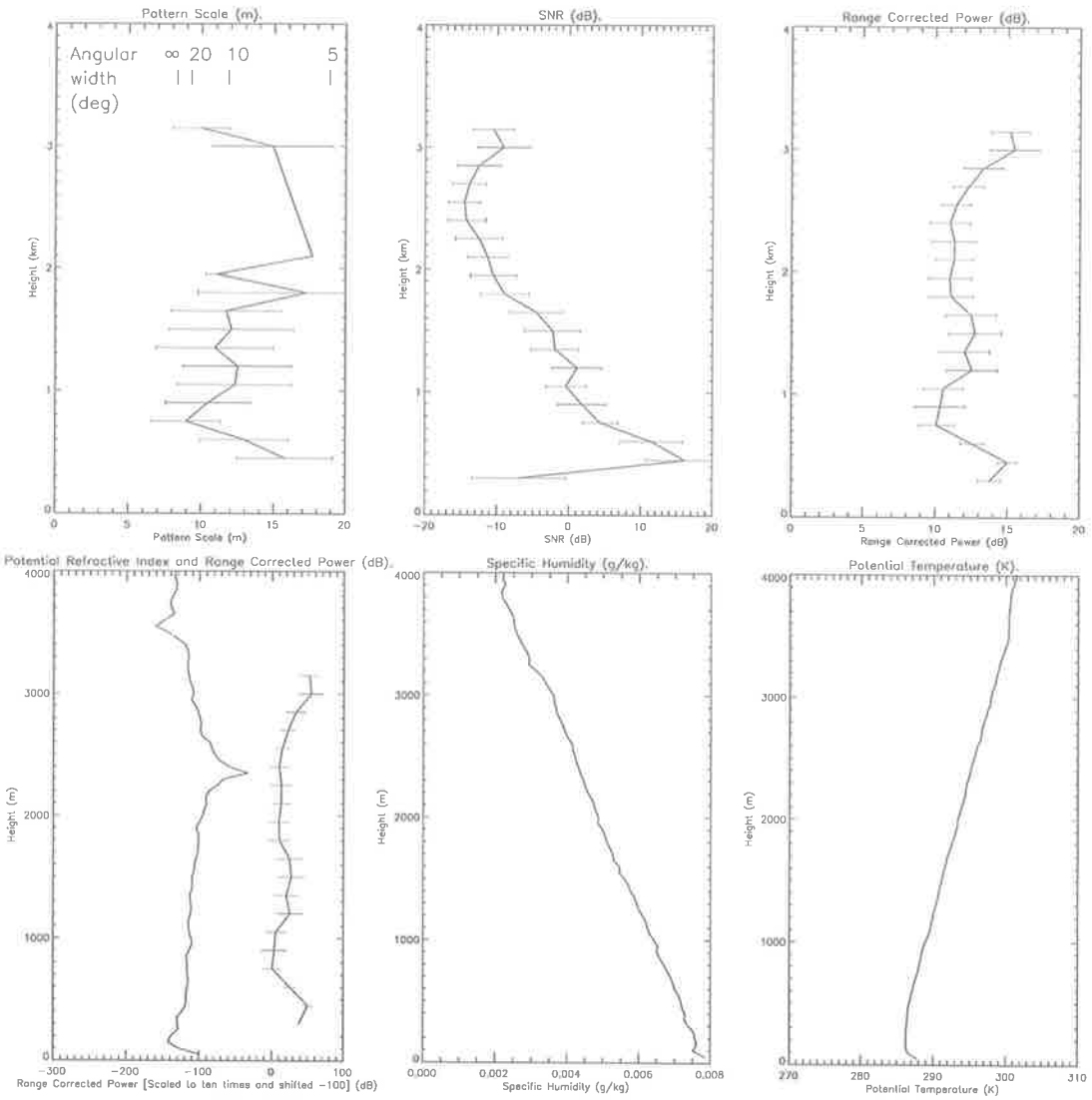

Figure 5.23: As for Figure 5.14 but for the launch at 11:03 CST on 14/09/97.

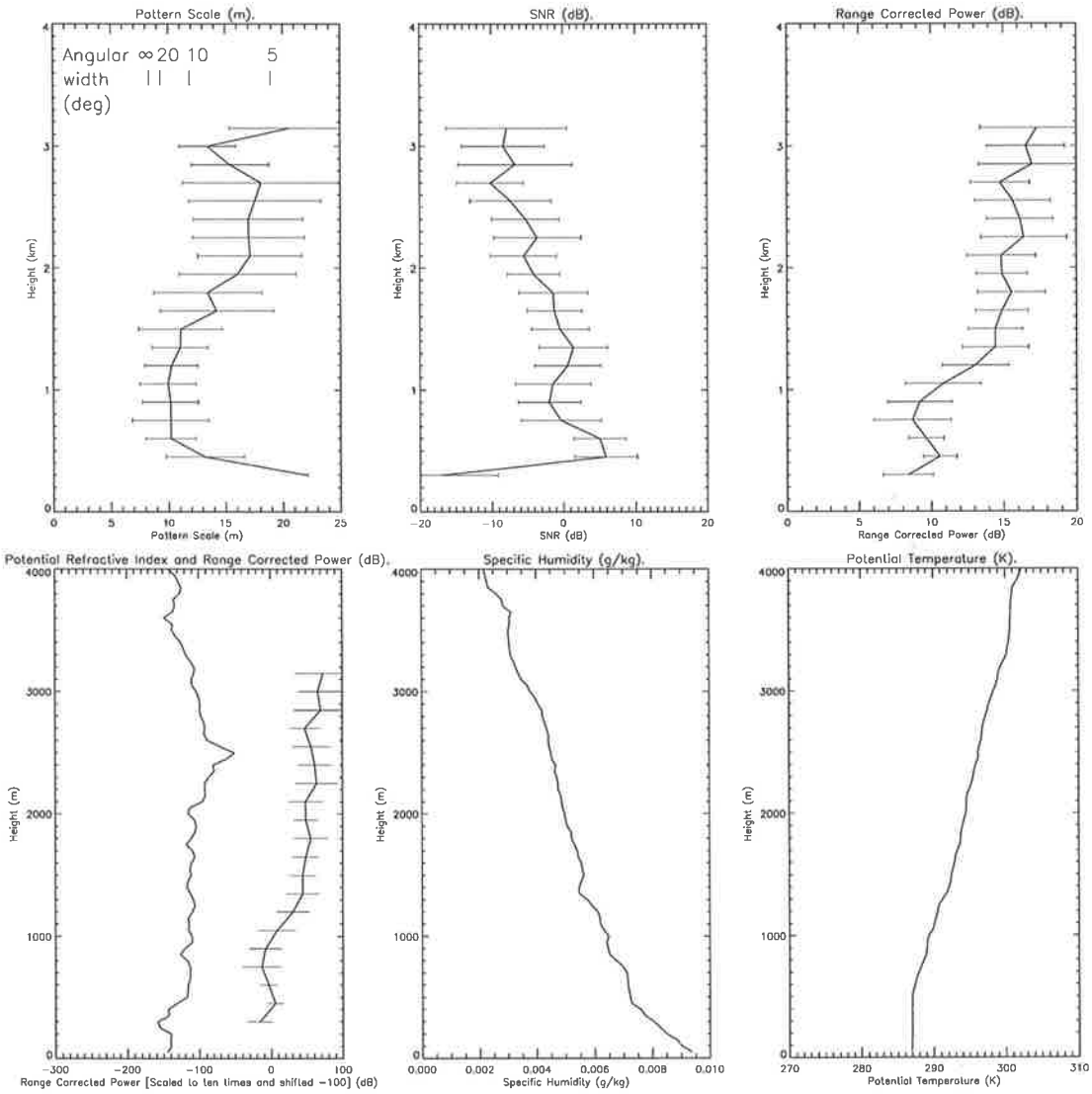

Figure 5.24: As for Figure 5.14 but for the launch at 15:06 CST on 14/09/97.

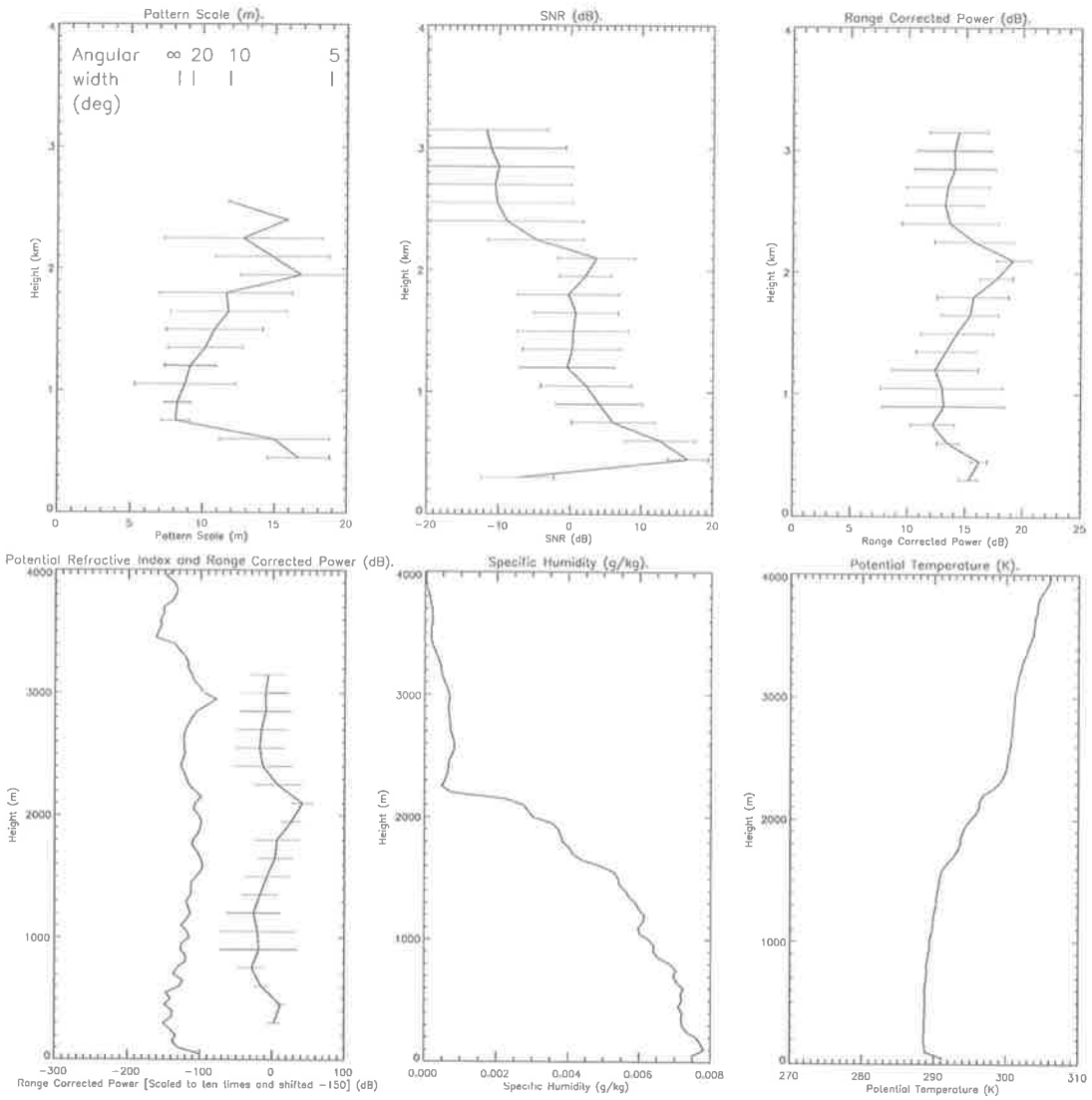

Figure 5.25: Comparison of radar with Omega Navaid radiosonde data for the radiosonde launch at 15:20 CST on 26/09/97. The combined diagram of profiles of potential refractive index and range corrected power, have had the magnitude of the power scaled to make it legible on the same graph.

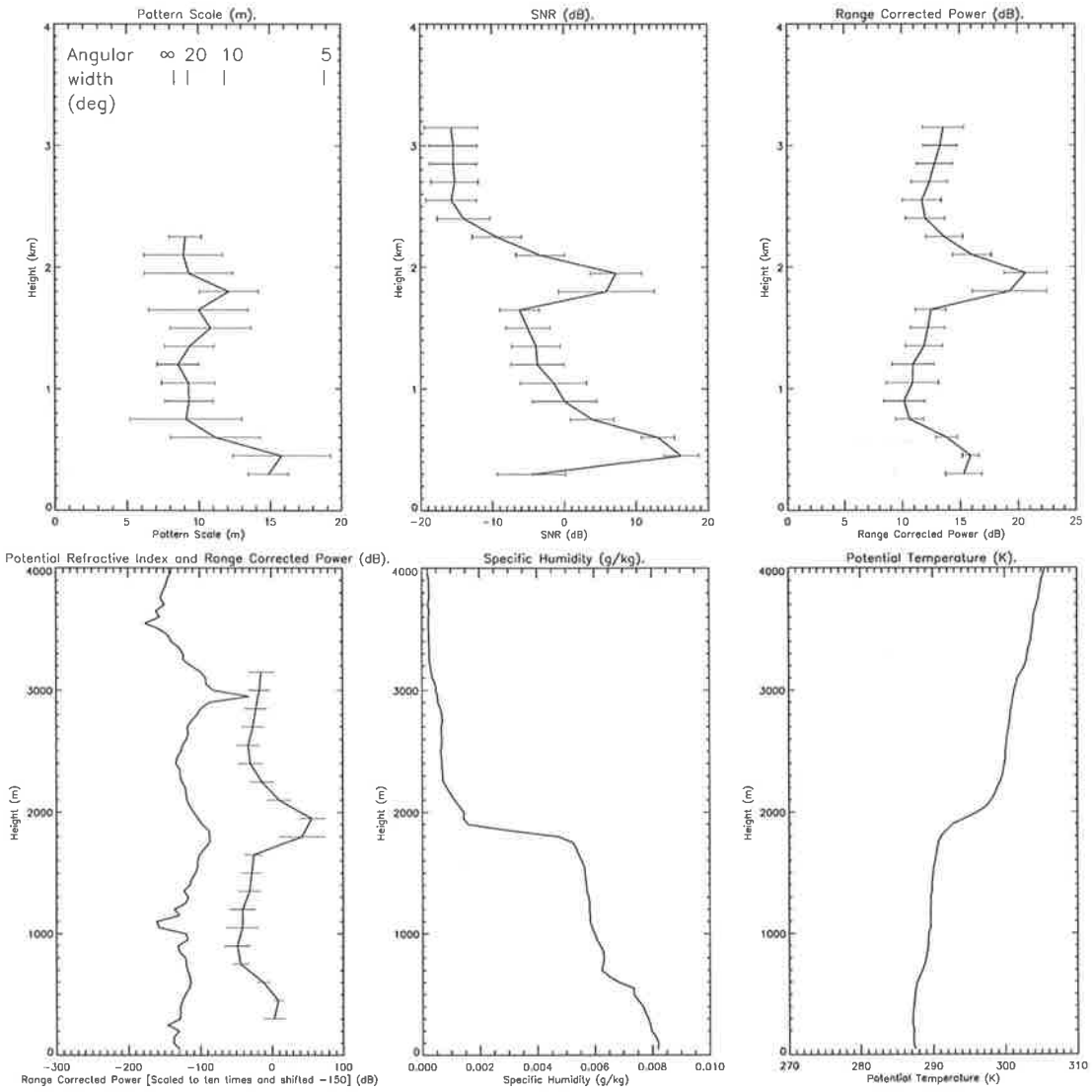

Figure 5.26: As for Figure 5.25 but for the launch at 18:06 CST on 26/09/97.

refractive index. This results in a very strong enhancement of the range corrected power and the signal to noise ratio. There is also a small increase in the pattern scale at this altitude.

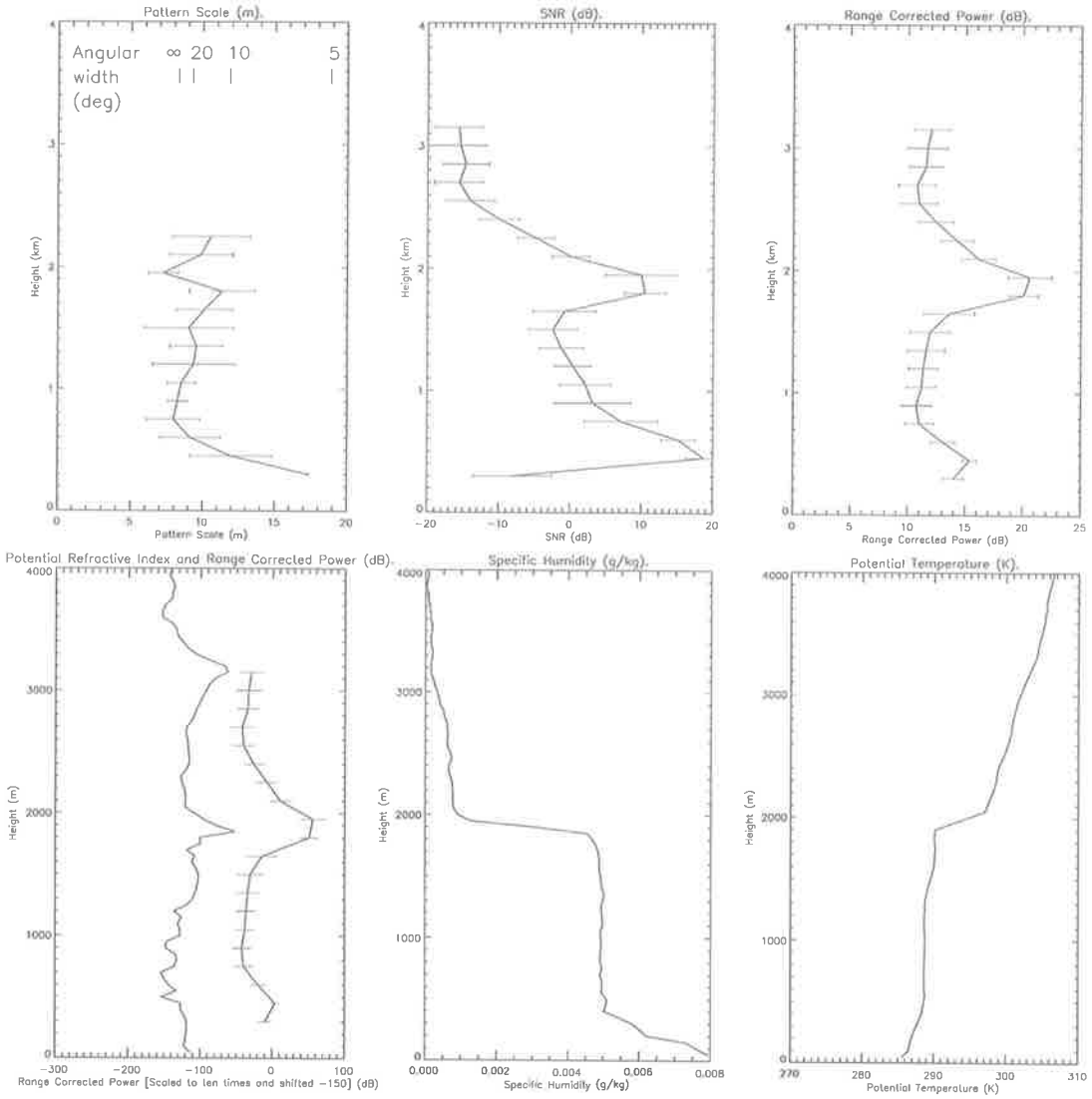

Figure 5.27: As for Figure 5.25 but for the launch at 21:01 CST on 26/09/97.

The third sonde launching shown in Figure 5.27, displays similar features near the top of the convective boundary layer, and above it. The sonde data indicates the commencement of a low-level nocturnal inversion at 400 metres.

From the fourth sonde launching displayed in Figure 5.28, the stable nocturnal layer has resulted in effective mixing up to only 400 metres. This decrease in moisture

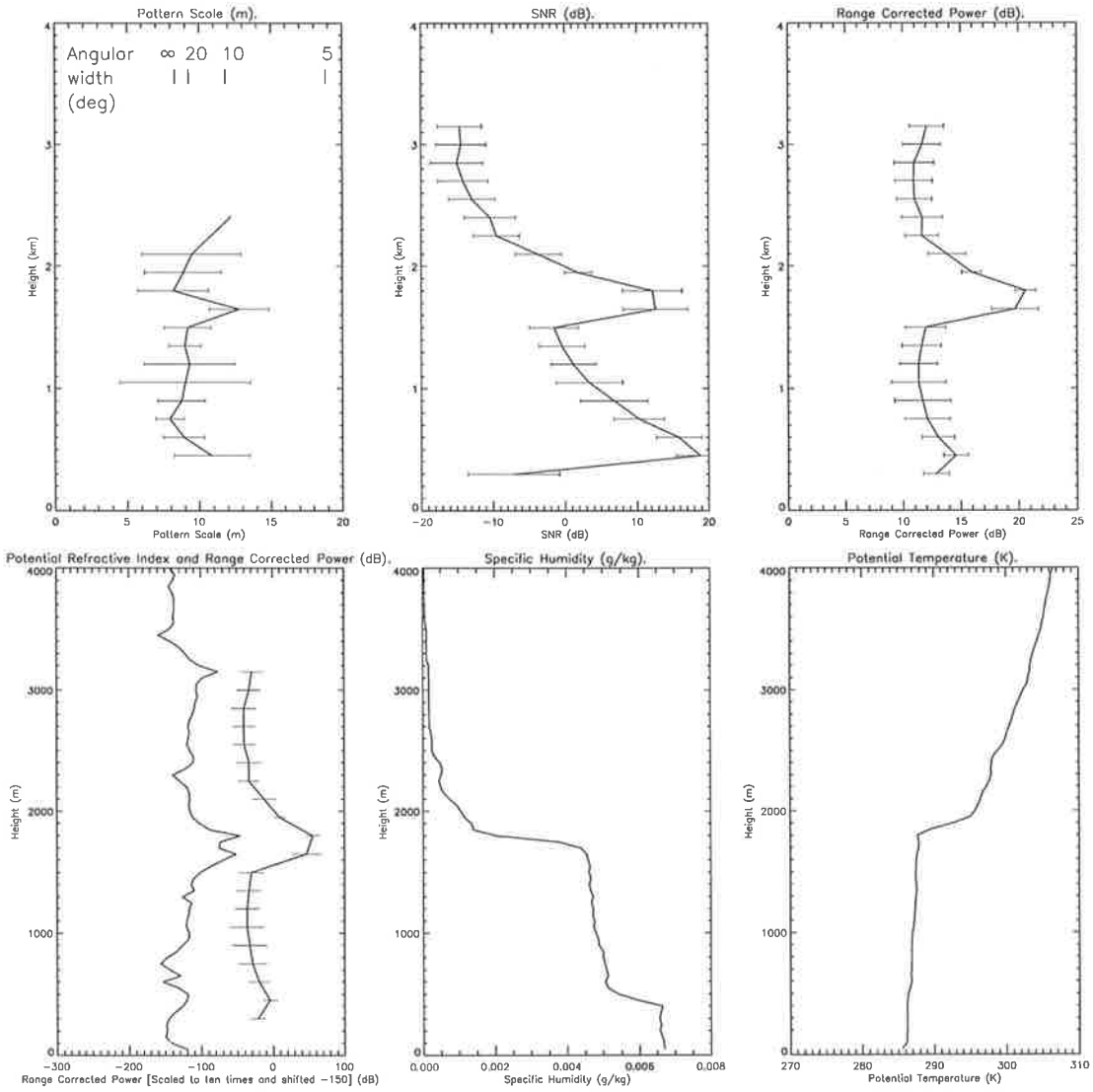

Figure 5.28: As for Figure 5.25 but for the launch at 00:05 CST on 27/09/97.

at 400 metres causes a small fluctuation in the potential refractive index, which resulted in signal to noise ratios exceeding 20 dB in the 450 metre range gate. There still exists a strong capping inversion at 1.8 km, which results in similar signal enhancement as observed in the early sondes of the campaign.

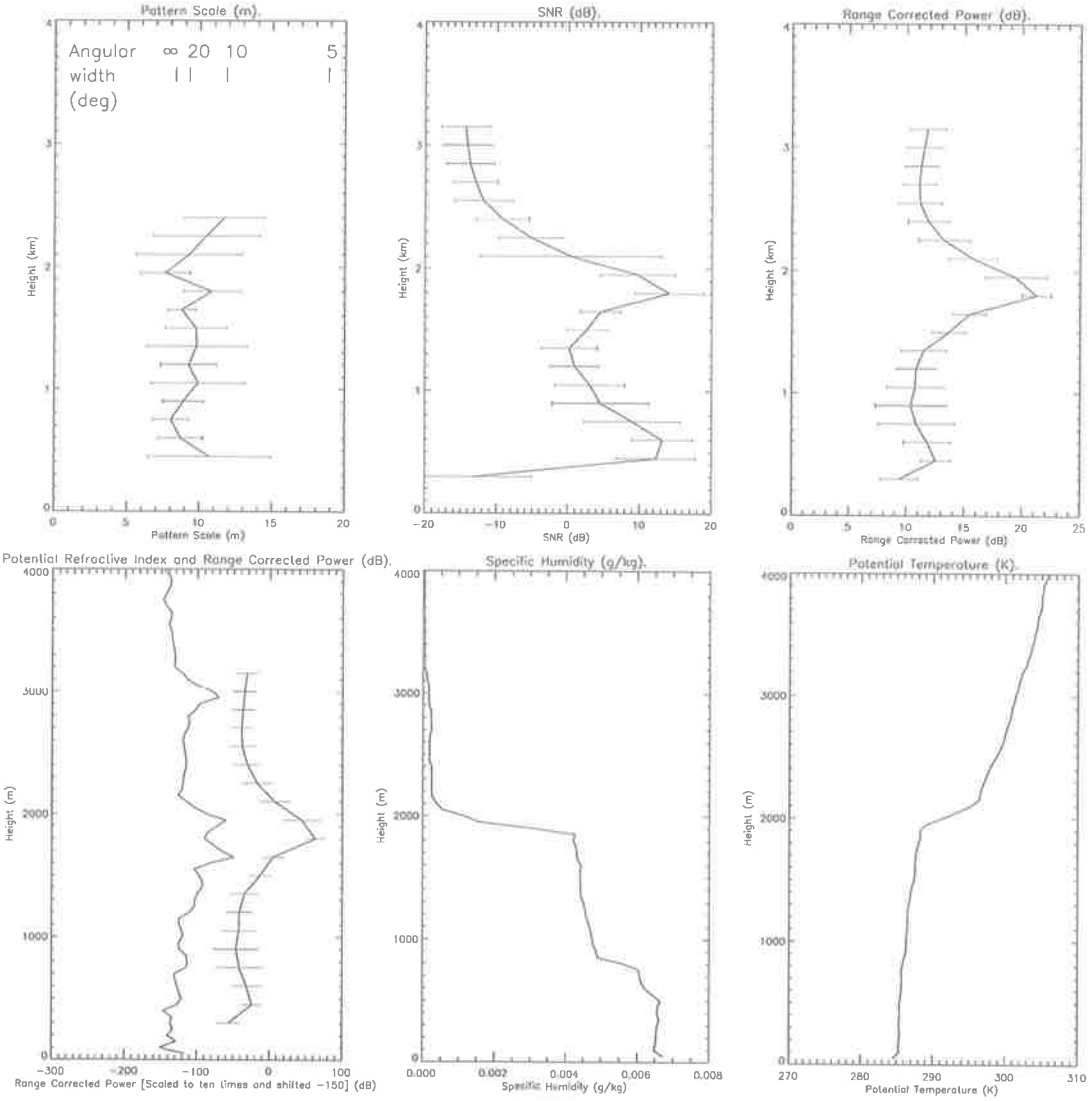

Figure 5.29: As for Figure 5.25 but for the launch at 03:03 CST on 27/09/97.

At the fifth sonde launching, it can be seen in Figure 5.29 that the thorough mixing level has propagated from 400 metres up to 800 metres.

In the final sonde launching seen in Figure 5.30 the capping inversion is at about 1.7 km. It can be seen again that the results support the early observations of enhanced

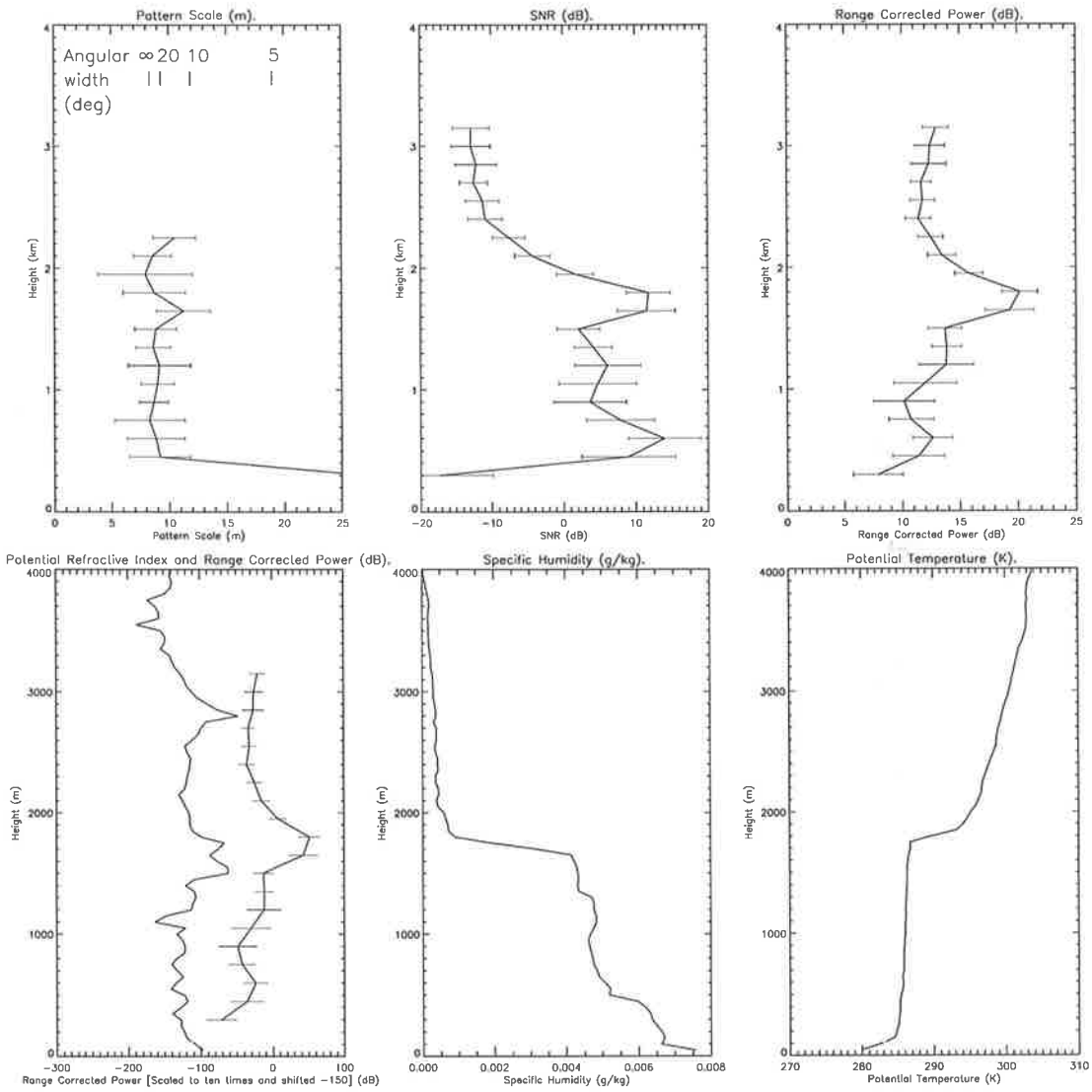

Figure 5.30: As for Figure 5.25 but for the launch at 06:05 CST on 27/09/97.

returned echoes and SNR at the same height detected by the boundary layer radar, and a small, but noticeable increase in the pattern scale.

5.2.2.4 Pattern Scales Profiles from the Joint Campaigns

This thesis has shown a consistent trait of an enlarged pattern scale occurrence at the top of the convective boundary layer. This would then make the pattern scale a possible indicator of the boundary of the mixed layer in many weather conditions including heavy precipitation.

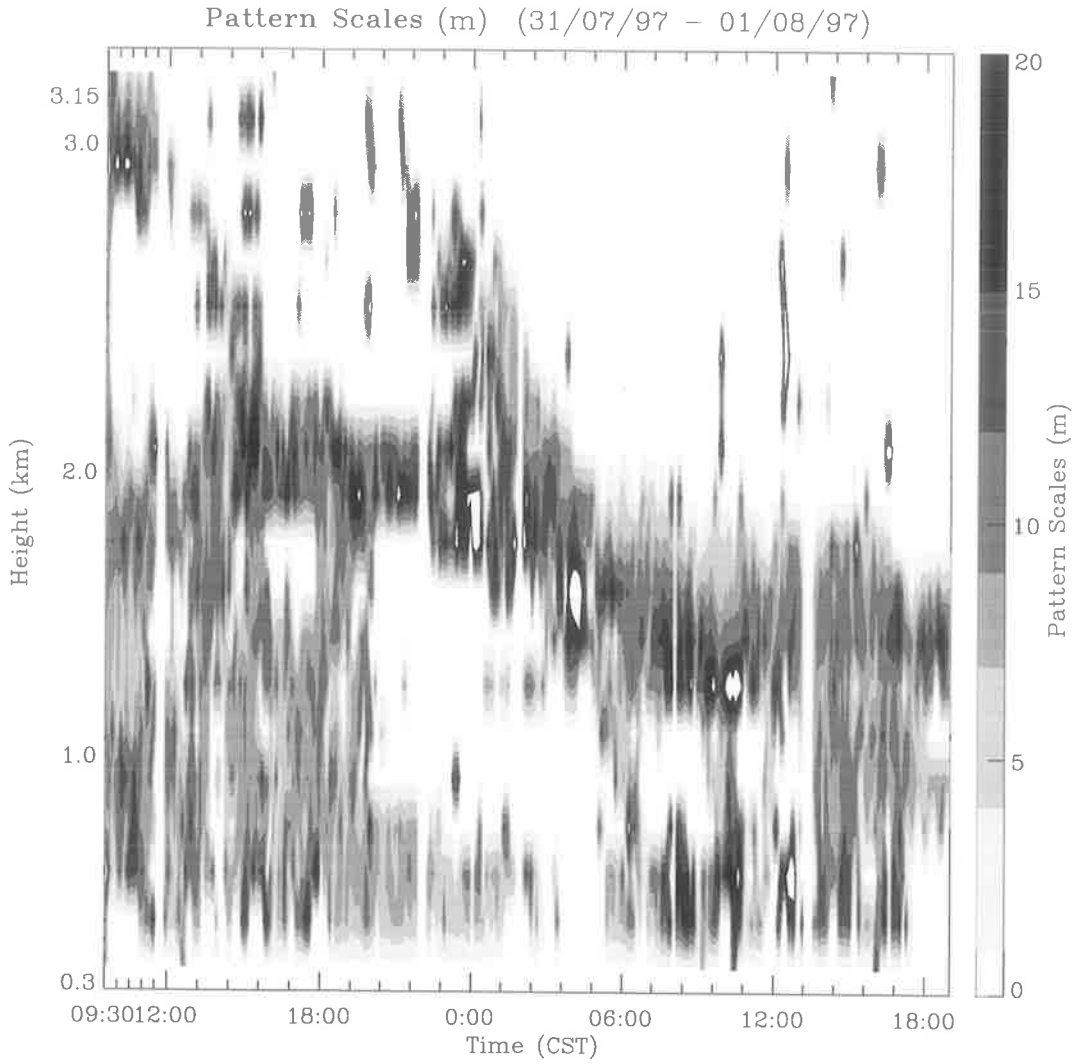

Figure 5.31: Pattern Scale for 31/07/97 to 01/08/97

The pattern scales for the entire first campaign are seen in the contoured image plot of Figure 5.31. The pattern scales were smoothed using a ten minute average.

The top of the convective boundary layer is clearly the location of the enlarged pattern scales between 1.4 and 2.0 km for this campaign. These enlarged pattern scales are at the same locations as the enhanced SNR, and the temporal variations in the pattern scales coincide with the same variation of SNR as shown in Figure 6 of *Vincent et al.* [1998] in Appendix B.

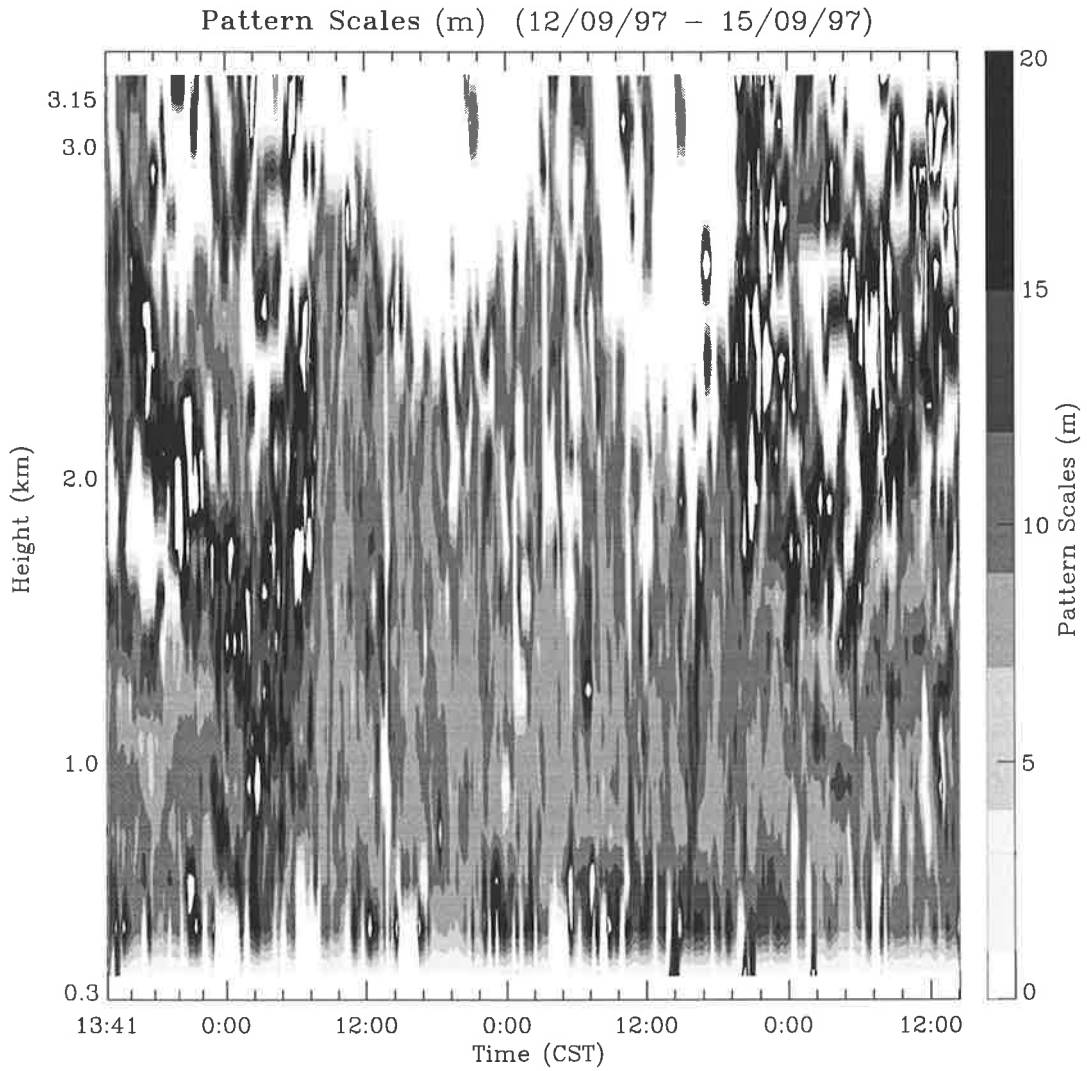

Figure 5.32: Pattern Scale for 12/09/97 to 15/09/97

The contoured image plot of the pattern scales for the second campaign can be

seen in Figure 5.32. It can be seen that generally the pattern scales are between 7 metres and 9 metres, although during low nocturnal activity the pattern scales can exceed 15 metres.

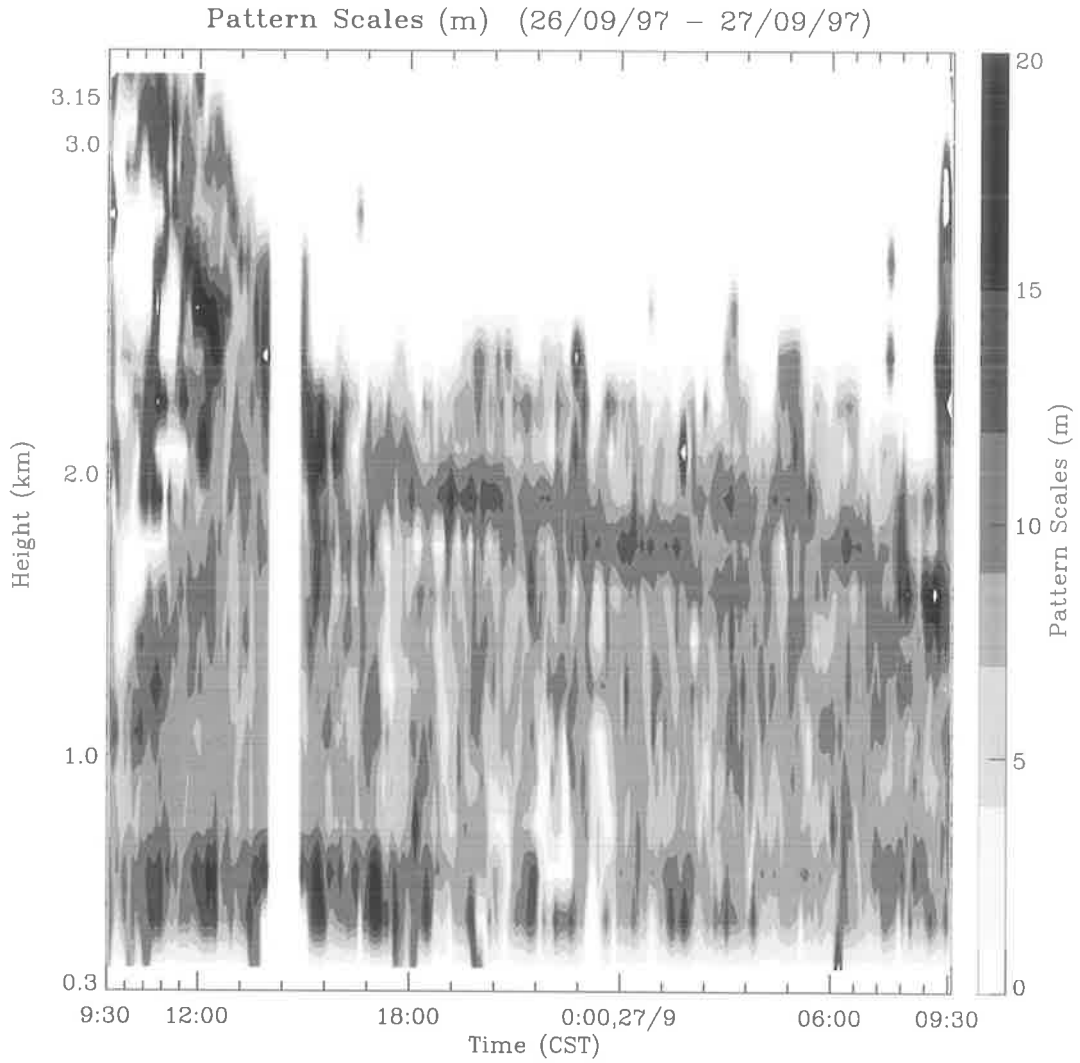

Figure 5.33: Pattern Scale for 26/09/97 to 27/09/97

The contoured image plot of the pattern scale for the final campaign in late September, Figure 5.33, clearly shows strong support of an enlarging of the pattern scales at the top of the convective boundary layer. The gradients of refractive index must be on the scale of a half-wavelength of the radar to obtain the detected quasi-specular nature for the returned echoes.

5.3 Summary

The first testing of the boundary layer radar as a vertically pointing Doppler radar in Spaced Antenna mode, showed that signal to noise ratios frequently exceeded 10 dB at the top of the mixing layer. This enabled calculations of the winds up to the free air region, and occasionally over 3 km high.

The three campaigns of radiosondes all located at the site of the boundary layer radar were useful in verifying the new radar's ability to detect the top of the convective boundary layer. The measurements of the pattern scales also verified that the correct spacing for the radar is on average 1.5 λ. Although the pattern scale can be larger and the angular widths narrower on occasions, the winds calculated from the Spaced Antenna analysis do not appear to be affected when compared with the sonde results. More research needs to be performed to compare statistics for low and high pattern scales to determine the full extent that narrower widths would have on wind determination.

Chapter 6

Conclusions and Future Research

6.1 Conclusions

This thesis discusses the development of a VHF wind profiling radar to enable all-weather monitoring of the lowest part of the atmosphere. This was achieved.

An important aspect of any radar system is the suitability of the antenna system. In this case, it involved optimising the relationship between the beamwidth and the directivity of the antenna array. This was necessary to ensure that the beamwidth was wide enough so that low heights were probed, but was also restricted enough to ensure that the directivity still resulted in high gains of the signal returns. The relatively narrow beamwidths for the full system were also useful in restricting the ground clutter entering sidelobes of the beam.

The large VHF radars previously used for studies of the troposphere and lower stratosphere suffered significant ringing. This means that echoes from the lowest heights are not observed. A key factor of this project was the careful matching of the baluns and combiner boxes to minimise this effect. Drifting of impedances with time is generally small unless weathering of components has occurred. This enables circuits which are carefully tuned to remain so for extended periods.

The removal of ground clutter from data is necessary to ensure that weak atmospheric echoes are detected, and so that there is no contamination of winds from

correlation techniques.

The determination of the aspect sensitivity of the lower atmosphere was used to find the pattern scales of the scatterers. This was used to determine the correct spacing of the antenna modules so that there would be no biasing of winds from the triangle size effect for wind determination using the full correlation analysis.

Probing of the atmosphere through the development of this system showed interesting phenomena. Initially aircraft echoes were clearly detected in the data by the characteristic movement of echoes down then up in range and by their characteristic Doppler Shift. The very high power of echoes from aircraft are easily removed from the weaker atmospheric returns.

The radar clearly detected the top of the mixing-layer. This was noticed by the presence of a strong echo when compared with the mixing occurring in the lower atmosphere as recorded by the radiosondes, through a strong reflective layer due to the changes in the potential refractive index. An unexpected result, was the observation of the top of the boundary layer through a considerable enlarging of the pattern scales. This corresponds, through the Fourier transform to a narrow angular spectra. Profiles of pattern scales from VHF radars may be an easier way to detect the top of the mixing-layer than locating the reflectivity peak using UHF radars [*Angevine and Grimsdell* 1998], [*Angevine* 1998].

This radar used similar principles to that used in the French VHF radar to reduce the minimum observable height [*Crochet* 1993]. This includes incorporating in the system a large bandwidth to enable use of a short pulsewidth (typically $1\mu s$) for improvement of the range resolution and reduction of the minimum observable height. However instead of receiving on a single mini-array of antennas, this project received on three modules of antennas in spaced antenna mode for wind determination using the full correlation analysis.

This project successfully showed the ability of a small portable system to give useful real-time results of the convective boundary layer from heights as low as 300 metres up to 4 km. By alternating radar parameters, including the pulse width and receiver

gain, it would be possible depending on atmospheric conditions, to probe higher into the atmosphere though there would be a slight loss of resolution in time.

6.2 Future Research

It is possible to incorporate additional transmitter modules into this system, due to its modular solid state design. This would add to the capability of the system of probing both the convective boundary layer and well into the free air regions of the troposphere. It is also possible to incorporate automatic gain control into the receiver system to ensure that lower altitudes are not saturated when high power is transmitted from the system.

A restriction on such a system would be that antenna ringing, which was reduced in the current system by careful matching of the impedances of the different components from the antennas through to the transmit/receive system, would probably become a problem as high powers were transmitted. This would need to be investigated further.

Other possibilities for modifying the system include introducing pulse coding for improved range resolution, and interferometric techniques to enable postset beam-steering studies of the atmosphere.

A radio acoustic sounding system has now been integrated into the boundary layer system, see *Vincent et al.* [1998] in Appendix B for further details. Studies using the RASS system once these modifications have been put in place would give a very powerful system for studying the general dynamics of the lower atmosphere in different locations through the entire system's portability. Meteorological phenomena including frontal activity which cross the Great Australian Bight into South Australia could also be carefully studied in conjunction with the ST radar system located at Buckland Park.

Studies capitalising on the flexibility of this system, once fully modified, would then enable good determination of the atmospheric conditions during precipitation, and indeed of the precipitation itself [*Rajopadhyaya et al.* 1993]. This could also be enhanced through adding additional antenna modules for reception for investigations

with this system of the polarisation of hydrometeor echoes and ground clutter.

Further investigation of the scale pattern technique for determining the boundary layer depth, would be an area of research of high practicality. Benefits include improved accessibility in determining the dynamics of the boundary-layer of the atmosphere, and importantly for meteorological purposes, applications including improved real-time continuous pollution monitoring.

Appendix A

Transmitter and Receiver Data Acquisition System Description

These systems were contracted out for initial construction to firms that were spawned from the atmospheric physics group of the university. The electronics for the transmitter were constructed by Tomco, the receiver and radar controllers were built by Genesis, and the on-line software suite was developed by ATRAD.

The allowable parameters for this system, though they are limited by the maximum duty cycle of the equipment of 10 %, and the usefulness of certain combinations are :

Table A.1: Transmitter and receiver allowable parameters.

Parameter	Setting
Pulse Repetition Frequency	1 - 500 000 Hz
Number of Coherent Integrations	1 - 4096
Number of Data Points	1 - 2^{31}
Enable Phase Inversion	Yes
Number of Channels	3 (upgradable to 16)
Contiguous Data Sets	1 - 2^{31}
Individual Rx Gain Values	62 - 122
Sampling Start Height	200 m
Sampling Resolution	$\geq$ 50 m
Sampling Range	$\geq$ 50 m
Transmitter Pulse Length	$\geq$ 100 m
Receiver Filter Setting	0.25 to 2 MHz

The modular solid state transmitter modules connected to each antenna module

used each have an output of 350 Watts PEP.

Appendix B

A VHF boundary layer radar: First Results

This is a reprint of the paper:

Vincent, R. A., Dullaway, S. N. M., MacKinnon, A., Reid, I. M., Zink, F., May, P. T., Johnson, B. H. (1998), 'A VHF boundary layer radar: First results', *Radio Science* **33**(4), 845-860.

Radio Science, Volume 33, Number 4, Pages 845–860, July–August 1998

A VHF boundary layer radar: First results

R. A. Vincent, S. Dullaway, A. MacKinnon, I. M. Reid, and F. Zink
Department of Physics, University of Adelaide, Adelaide, South Australia, Australia

P. T. May
Bureau of Meteorology Research Centre, Melbourne, Victoria, Australia

B. H. Johnson
Atmospheric Radar Systems, Adelaide, South Australia, Australia

Abstract. The development of a novel VHF radar designed to measure winds and temperatures in the planetary boundary layer is described. The radar operates at 54.1 MHz and is compact and easily transportable. The antenna system consists of 12 Yagis grouped into three subarrays arranged in the form of an equilateral triangle. Transmission takes place on the whole array, and reception takes place on the three subarrays, with winds measured by the spaced antenna technique over a height range between 300 and 3000 m. Results from field trials conducted in southern Australia in a variety of meteorological conditions are presented. Comparisons with high-resolution radiosondes launched from the radar site show excellent agreement, with rms differences between radiosonde and radar wind components being about 1.5 m s^{-1}. Observations carried out in rain show that echoes from precipitation are clearly distinguishable from clear-air echoes. Unlike UHF radars, this means that vertical air velocities can be measured during precipitation, and the evolution of drop-size distributions can be studied down to low altitudes. It is shown that temperatures derived from a radio acoustic sounding system are measured up to heights near 2 km, depending on background wind conditions.

1. Introduction

Stratosphere-troposphere (ST) radars or wind profilers are powerful tools for atmospheric research and operational meteorology [e.g., *Gage*, 1990]. While the ST radar field is relatively mature, development has proceeded in step with advances in technology. In the last few years, the advent of cheap, powerful computers, together with inexpensive computer memory for storing raw data and reliable solid-state transmitters, have opened up new possibilities for ground-based radar studies of the atmosphere. Developments in conceptual techniques include the use of interferometry to improve estimates of pointing directions and correct such important parameters as vertical air velocity. The ultimate aim is to derive as many atmospheric parameters as possible in real time to aid research and forecasting.

The last decade has seen the development and large-scale deployment of boundary layer (BL) profilers. These low-power systems have been designed for the express purpose of observing many of the important meteorological phenomena that occur in the lowest part of the troposphere. Typically, frequencies near 1 GHz are used for UHF boundary layer radars. Examples are the widely used radar system developed at NOAA's Aeronomy Laboratory which uses a frequency of 915 MHz [e.g., *Ecklund et al.*, 1988, 1990; *Carter et al.*, 1995] and the L-band (1.357 GHz) system developed by the Kyoto University group [e.g., *Hashiguchi et al.*, 1995]. Systems such as these are being used to investigate boundary layer wind and temperature fields and, since they are sensitive to hydrometeors, the precipitation field.

Paper number 98RS00828.
0048-6604/98/98RS-00828$11.00

Radars operating in the lower VHF band (~50 MHz) have primarily been used to measure winds to as high an altitude as possible, which requires the use of physically large antennas and high transmitter powers. However, effects such as long recovery times in transmit-receive systems and reflections or ringing in antennas and transmission cables mean that these larger systems generally cannot make measurements in the lowest 1–2 km of the atmosphere. However, pioneering work by the French group in Toulon show that it is possible to use small antennas and make useful BL measurements at VHF [e.g., *Crochet et al.*, 1994; *Fillot et al.*, 1997].

Operating at UHF offers many advantages. These include (1) the use of antennas that are physically small but relatively large compared with the radar wavelength, so that narrow beams can be generated; (2) low external noise; and (3) the availability of wide bandwidths, which means good height resolution. On the other hand, when precipitation or heavy cloud is present, echoes from hydrometeors dominate echoes from the clear air, which makes measurements of vertical velocity difficult. This is a particular limitation when radio acoustic sounding systems (RASS) are used to measure atmospheric temperatures at UHF with vertical pointing beams, since the sound velocity should be corrected for the vertical wind [e.g., *Angevine et al.*, 1994a]. Another limitation with RASS at UHF is that the acoustic frequencies (~0.8–1.6 KHz) suffer rapid attenuation, which limits the upper height to which temperatures can be obtained [*May et al.*, 1988].

The advantages in operating at VHF include the following:

1. Precipitation echoes are comparable in strength to, or weaker than, the clear-air echoes, and the precipitation and clear-air echoes are usually well separated in the Doppler spectrum. Hence a single VHF radar can simultaneously study the dynamics and cloud microphysics of precipitating clouds [e.g., *Rajopadhyaya et al.*, 1993].

2. Measurement of the vertical gradient of the vertical velocity gives the divergence of the wind field, especially in storm conditions when the vertical motions and gradients are large.

3. VHF BL radars are unlikely to suffer the problems with contamination by bird and bat echoes that UHF BL radars often encounter [*Wilczak et al.*, 1995; *May*, 1995].

4. A VHF/RASS boundary layer system should also have a better height coverage than a similar UHF system because the lower-frequency sound waves used suffer much less attenuation.

Thus a 50-MHz BL system has many advantages for the study of shallow weather systems, such as summertime cold fronts across southern Australia [*Wilson and Stern*, 1985]. Other applications include sea-breeze fronts which trigger convection. Finally, there is much that we do not understand about scattering processes from the atmosphere. Measurements should be made at a range of frequencies in the VHF and UHF bands to investigate these processes as well as exploit the research and operational potential of all systems.

The Atmospheric Physics group at the University of Adelaide has been developing radars at MF/HF and VHF for studies of both the upper and lower atmospheres. A major design goal has been to develop systems that have as many features in common as possible. Here we describe a VHF (54.1 MHz) radar that has been developed since 1994 for boundary layer studies. The aim is to study winds and temperatures in the lowest 2–3 km of the atmosphere with good height and time resolution and to extend the scope of boundary layer studies to include precipitation and vertical air motions in the presence of precipitation. The overall system design is briefly described in section 2, and some of the first wind and RASS measurements are presented and discussed in section 3.

2. System Design

A number of factors were taken into account in the development of the Adelaide VHF boundary layer (BL) radar. The prime requirements were that the system should be flexible in operation, relatively easy to transport, and power efficient so that it could be used at remote sites. A lower height limit of about 300 m was specified, and it was required to measure winds regularly to heights of 2–3 km in order to overlap with observations made with a ST VHF radar located at the Buckland Park field site [*Vincent et al.*, 1987].

To achieve these aims, the system shares a number of features common to other radar systems recently developed by our group in Adelaide. In order to obtain high mean power it was decided to use a compact, modular, solid-state transmitter that is capable of a high duty cycle (10%). The modular nature of the transmitter means that transmit-receive antennas can be configured in different ways to allow differ-

ent wind measuring techniques (e.g., Doppler, spaced antenna, and interferometric) to be investigated and used as appropriate. A receiver and data acquisition system (RDAS) was developed with wide dynamic range and sufficient amounts of memory (RAM) for the temporary storage of raw data. The data are then downloaded to the host computer for on-line analysis/permanent storage while the next sequence of data is being acquired. For operational flexibility, as many operating parameters (e.g., receiver gain, height range, height increment, etc.) as possible are placed under computer control. This enables a wide range of experiments to be configured in software and operated sequentially. System control and data analyses are undertaken with a PC computer that is easily networked. It is therefore both simple and inexpensive to add more computing power as required. Data are analyzed with a proprietary data analysis and display package and stored on disk for further off-line processing. Raw data can also be stored for later analysis in other ways.

2.1. Antenna Configuration

The low-height performance of 50-MHz ST systems is limited by the use of large antenna arrays and problems associated with ringing after the transmitter pulse, which hampers receiver recovery. Thus a VHF BL radar requires small antennas, which implies wide beam widths, so that ground clutter and interference to and from other operators may be a problem. Fast transmit-receive switches must be used and antenna ringing minimized to ensure reception at low heights. It was decided to utilize a spaced antenna (SA) configuration so that only vertically pointing beams are used. This arrangement is more compact than Doppler systems, and it eliminates the height-smearing problem that occurs when obliquely pointing wide beams are used for Doppler sounding [*Fillot et al.*, 1997] as well as potential problems associated with anisotropic backscatter which complicate wide-beam Doppler measurements [*Röttger*, 1984]. Another potential advantage of the SA configuration is that the data can be used for interferometric studies as well as conventional spaced antenna wind measurements. Interferometric techniques can then be used to study the scattering irregularities and have the potential to correct for possible contamination of the vertical velocity measurements caused by tilted layers [*Vincent and Röttger*, 1980].

Figure 1 shows the antenna configuration adopted for initial measurements with the VHF BL system. The arrangement is a compromise between making the subarrays as small as possible to minimize ringing and large enough to ensure an adequate power-aperture product. Three subarrays, each consisting of groups of four three-element Yagis, are arranged in an equilateral triangle. The whole array is used for transmission and each group is used for reception. An equilateral triangle arrangement reduces the chances of systematic biases in SA wind measurements, as can occur if other configurations, such as a right-angle triangle, are used. The optimum spacing of antennas in SA mode is when the mean cross correlation at zero lag is about 0.5 [*Briggs*, 1984]. Preliminary trials showed that the basic spacing should be at least 1.5λ (8.32 m), and this was chosen as the initial spacing. A reevaluation of the spacing took place after the radar had operated in a variety of meteorological conditions, as discussed in section 3.1.

The configuration adopted ensures that grating lobes on transmission are not significant. Figure 2 shows plots of the one-way polar diagrams for the receiving and transmitting arrays. The transmitting array has a half-power half width of 10°, corresponding to an effective area of about 250 m^2, while the respective values for the receiving antennas are 18° and about 80 m^2. However, as *May* [1990] has shown, the overall effective area of the system depends on the scattering mechanism. For the situation of isotropic volume-scatter the effective area is given by

$$A_{\text{eff}} = \frac{2A_T A_R}{(A_T + A_R)} \tag{1}$$

where A_T and A_R are the respective areas for the transmitting and receiving antennas. In this case, $A_{\text{eff}} \approx 120$ m^2. One problem with such relatively wide beams is the possible effects of ground clutter, but by suitably spacing and orientating the Yagi antennas it is possible to partly null out clutter and interference that arrive at low elevations.

2.2. Operating Parameters

Table 1 summarizes the range of possible operating parameters. In the evaluation of the system a 1-μs pulse length was used to achieve the desired 150-m range resolution, and a 2-MHz receiver bandwidth was selected to ensure that fast receiver recovery occurs and the desired lower height limit of about 300 m is attained. A particular feature of the system is the high degree of computer control of the system configuration, such as height coverage, range resolution, and so on. If necessary, a number of different ex-

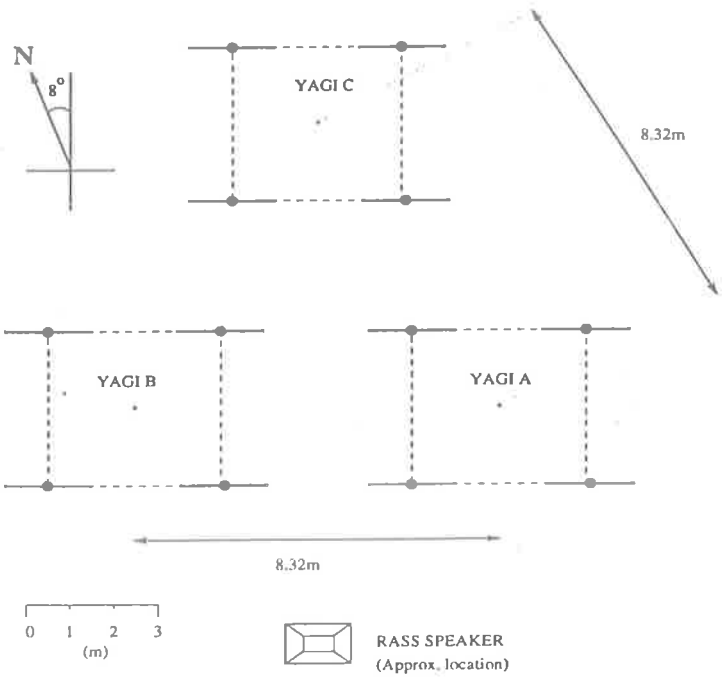

Figure 1. Plan view of VHF boundary layer radar antennas.

periments can be programmed to take place in any desired sequence. This is particularly useful while, as at present, the optimum operating parameters for SA wind and RASS measurements were being determined.

Initial tests suggest that in the spaced antenna mode the operating parameters shown in Table 2 give satisfactory performance. These values give a lower detectable wind speed of $\sim$1 m s^{-1} and an upper limit of about 80 m s^{-1}. With these settings the mean power is about 20 W, giving a power-aperture product of at least 2500 W m^2. The complex amplitudes received at the three antennas are analyzed in the standard method using the full correlation analysis (FCA) discussed by *Briggs* [1984]. The quality of the data was assessed using the standard criteria described by *Briggs* [1984], although only data with signal-to-noise ratios (SNR) greater than 0 dB (after coherent integration) were accepted, as modeling studies show that the accuracy of SA wind determinations decreases rapidly for smaller signal-to-noise ratios [*Holdsworth*, 1995].

3. Initial Results

Initial tests of the BL system were carried out at the University of Adelaide's Buckland Park field station (35°S, 138°E), where it is located immediately adjacent to a VHF ST profiler [*Vincent et al.*, 1987]. The site is very flat and upwind of any significant topography. However, the site is rather crowded with buildings, antenna masts, etc., and there is the potential for significant ground clutter, which can make the detection of the clear-air echoes difficult. Fortunately, clutter has not proved to be a major problem, except at the lowest range gates of 300–450 m, and is easily distinguished from atmospheric echoes by its characteristic slow fading. A number of algorithms are being tested to reduce the effects of ground clutter and intermittent clutter due to aircraft, including the use of wavelet transforms [*Jordan et al.*, 1997].

In order to assess the performance of the radar, a series of intercomparisons were made during the period July 31 to September 26, 1997, with simultaneous measurements made with high-resolution ra-

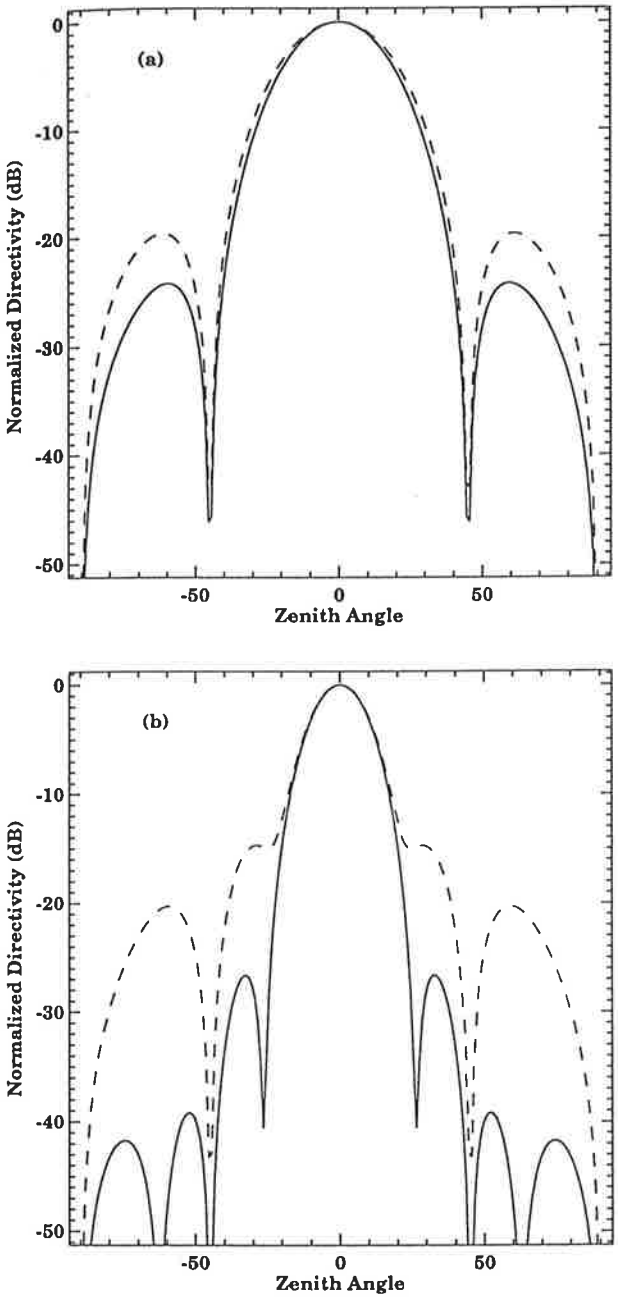

Figure 2. Antenna polar diagrams. The solid lines indicate the E plane, and the dashed lines indicate the H plane. (a) Receiving antenna. (b) Transmitting antenna.

diosondes (Vaisala RS80-15) launched from Buckland Park. Three campaigns were carried out in a variety of meteorological conditions, including significant precipitation. Campaign I occurred between July 31 and August 1, campaign II took place between September 12 and 15, and the final campaign occurred on September 26, 1997. Results from all three campaigns were used to evaluate the performance of the radar, such as accuracy of wind measurements. To illustrate the capabilities of the system, we focus on some of the results from the first two campaigns, which were conducted under very different weather conditions.

Table 1. Operating Parameters of the VHF Boundary Layer Radar

Parameter	Value
Transmitter power	3×350 W peak envelope power
Transmit/receive switch	passive, ~1-μs recovery time
Antenna bandwidth	~4 MHz
Receiver bandwidth*	2 MHz to 250 kHz
Pulse length*	0.7–10 μs
Maximum duty cycle	10%
Sample height*	100-m minimum, 25-m increments
Pulse repetition frequency*	up to 50 kHz
Coherent integration*	up to 4096 points
Digitizers	12-bit
Signal averagers	24-bit
Memory	1 Mbyte per receiver

*Software selectable.

Table 2. Typical Spaced Antenna Parameters Used in Campaigns

Parameter	Value
Parameter	Value
Pulse repetition frequency*	20,480 Hz
Number of coherent integrations*	1,024
Number of data points per sample*	1,024
Height coverage*	300–3200 m
Record length*	52.4 s
Range resolution*	150 m
Maximum lag*	4 s
Sample rate	0.05 s

*Software selectable.

3.1. Radar and Radiosonde Wind Comparisons

A primary goal of the campaigns was to assess the accuracy of the radar wind measurements by comparing them with radiosondes equipped with medium- to high-resolution wind-finding systems. For campaign I a Global Positioning System (GPS) tracking system was used, while for the campaigns starting on September 12 and 26, the balloons were tracked using VLF Omega navigation signals. For each flight the radar winds at each 150-m range gate were averaged over a period of 20 min, centered on the time at which the balloon had reached an altitude of 1 km. At least three radar observations were required at a given level to produce a mean value. No consensus averaging [*Strauch et al.*, 1984] was used in producing the mean wind velocities. In all, there were 29 flights and 144 samples.

Figure 3 shows scatterplots of the zonal (u) and meridional wind (v) components. It is apparent that the observations are highly correlated ($r = 0.95$), with the points distributed reasonably evenly around the line of unit slope. Only in the case of the v component are there any significant outliers, with six points lying about 5 m s^{-1} away from the line. These points came from two consecutive soundings in which there appeared to be significant curvature in the wind field. Table 3 summarizes the results of the comparisons. There are two lines for each wind component, with the second line corresponding to the case where the two soundings mentioned previously were discounted. Whether these soundings are included or not, the comparisons are very good, with rms differences between the radar and radiosonde winds being about 1.5 m s^{-1}.

These results compare very favorably with the results from similar studies. Many earlier comparisons were between profiler and radiosonde release sites separated by many tens of kilometers, and so some of the differences could be ascribed to spatial variability. For example, *Vincent et al.* [1987] compared 50-MHz ST profiler winds measured at Buckland Park with radiosondes released from Adelaide Airport, situated some 36 km to the south. They found rms speed differences in the 2–6 km height range of 3–4 m s^{-1}. The most extensive intercomparison using collocated soundings is that of *Weber and Wuertz* [1990], who compared 915-MHz profiler and radiosonde observations conducted at Stapleton Airport in Denver, Colorado, over a 2-year period. After editing their data to remove outliers, they found rms component differences of about 2.5 m s^{-1}.

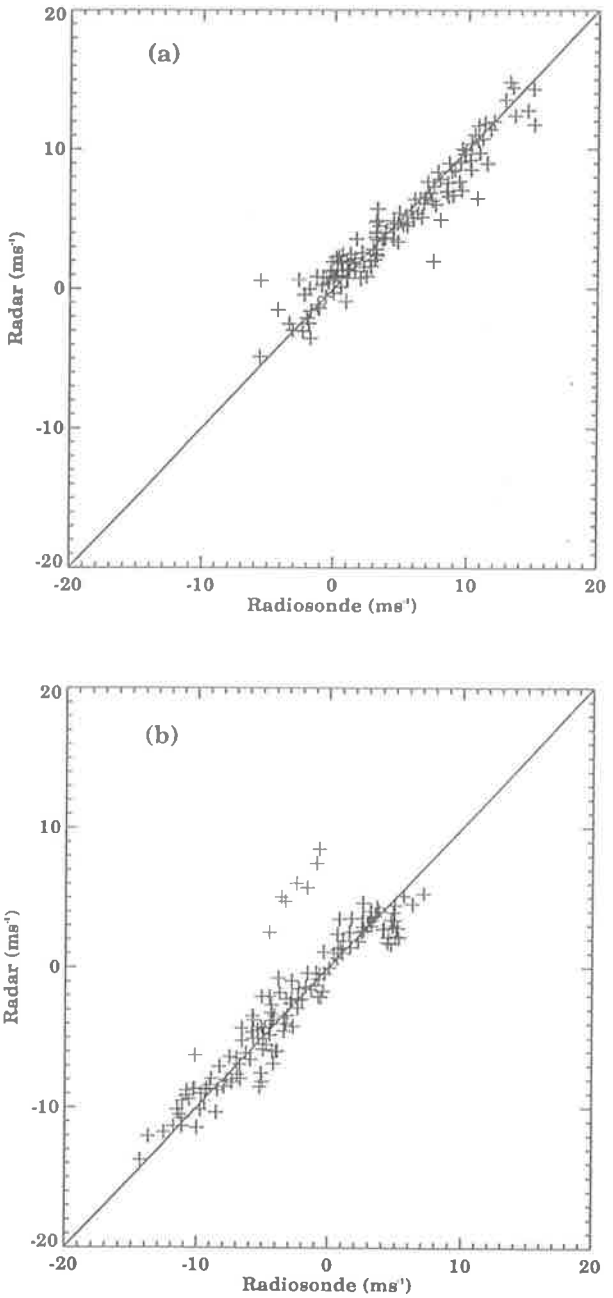

Figure 3. Scatterplot of wind velocities measured by radar and radiosondes. (a) zonal component and (b) meridional component. Lines of unit slope are shown.

There are fewer comparisons of boundary layer measurements. *Hashiguhi et al.* [1995] report rms

Table 3. Statistics of Radiosonde/Profiler Comparisons for Zonal (u) and Meridional (v) Wind Components

	Correlation	Mean Difference, ms^{-1}	Intercept, ms^{-1}	Slope	RMS, ms^{-1}
u	0.96	-0.05	0.72	0.86	1.4
	(0.96)	(-0.10)	(0.74)	(0.83)	(1.4)
v	0.94	-0.47	0.12	0.93	2.2
	(0.98)	(-0.13)	(0.26)	(0.94)	(1.3)

Profiler observations are averaged over 20 min from the time of launch of the radiosondes, and comparisons were made at each radar range bin whenever there were three or more radar observations in that bin. There were a total of 29 profiles for each instrument. The intercept and slope refer to the weighted least squares fit straight line to the scatterplots shown in Figure 3, while the rms values indicate root-mean-square difference between radiosonde and radar data. The values in parentheses refer to comparisons with two flights removed (see text).

component differences of better than 3 m s^{-1} when they compared L-band boundary layer profiler winds with winds derived from radiosondes released from the radar site. An extensive comparison using Tropical Ocean-Global Atmosphere/Coupled Ocean-Atmosphere Response Experiment (TOGA-COARE) data taken with 915-MHz profilers and radiosondes reveals rms differences of less than 1 m s^{-1} [*Riddle et al.*, 1996]. *Angevine and MacPherson* [1995] compared 915-MHz profiler wind measurements with simultaneous aircraft observations and found rms differences of less than 1 m s^{-1}. The differences are site dependent. For example, *May* [1995] found differences of ~2–3 m s^{-1} in a highly convective boundary layer during the day in central Australia. Comparisons were even worse at night because of scattering from bats.

The excellent agreement between the wind velocities measured here by the two techniques probably reflects the low spatial variability inherent in this comparison. As noted, Buckland Park is situated on the flat Adelaide Plains upwind of any significant topography, so spatial variability was minimized as the balloons drifted away from the site. It should be noted, however, that this comparison ignores the errors inherent in the radiosonde soundings. One factor that is often ignored in these comparisons is the smoothing required to reduce the effects of the pendulum motion of the sonde package. This smoothing acts as a low-pass filter that reduces the amplitude of short-vertical-wavelength wind variations. The length of the filter in the GPS-sonde measurements was 60 s and was 240 s in the Omega-sonde wind determinations. Given the ~4 m s^{-1} ascent rate of the balloons, the effective height resolution of the radiosondes is several hundred meters. This reduces the small-scale wind variations relative to those observed by the radar. Some of the Omega-sonde data were reprocessed with a shorter filter length of 150 s to see how significant this effect was. The rms deviation from the wind speeds processed with the normal 240-s filter was about 0.7–1 m s^{-1}. As expected, the deviations were largest where the wind curvature was greatest.

There are a number of factors that influence the accuracy of radar wind measurements using the spaced antenna technique. As noted above, the optimum antenna spacing is where the spatial correlation is about 0.5. Ground-pattern statistics obtained from the full correlation analysis (FCA) were used to test how well this was satisfied with the present arrangement, as well as to provide other useful information on the scattering irregularities. In the FCA, the ground diffraction pattern is modeled as a series of concentric ellipses of constant correlation, ρ. The size and orientation of the characteristic ellipse for which $\rho = 0.5$ are convenient measures of the average pattern scale and orientation. Pattern-scale statistics obtained from spaced antenna measurements in the three campaigns are summarized in Table 4. The most probable value of 8.5 m is identical to the antenna spacing of 8.3 m (1.5λ), which shows that the spacing was close to optimal. Table 4 also shows another useful pattern parameter, the axial ratio, which

Table 4. Characteristics of Ground Diffraction Pattern

	Most Probable	Mean
Pattern scale, m	8.5	11.2
Axial ratio	1.125	1.48

is a measure of the elongation of the characteristic ellipse. The most probable and mean values are both less than 1.5, which in practice means that the average pattern is not significantly different from circular [*Wright and Pitteway*, 1978].

Profiles of the pattern scale with height, such as those given in Figure 4 for the first two campaigns, suggest that there is a small increase in pattern scale with increasing height. As the pattern scale and the angular spectrum or width of the backscattered radiation are a Fourier transform pair [e.g., *Briggs*, 1992], this indicates that there is a narrowing of the angular spectrum with height and hence a change in the aspect sensitivity of the scattering irregularities. In order to make a quantitative estimate of the width of the angular spectrum it is necessary to make some assumptions about the angular dependence of the antenna polar diagrams and of the angular spectra. The almost circular nature of the correlation functions suggests that energy is backscattered almost uniformly from around the zenith and is just a function of the zenith angle φ. Assuming that the antenna polar diagrams and angular spectrum have a Gaussian dependence and that the irregularities are confined to narrow layers, then the relationship between the spatial correlation function and angular spectrum has the simple form given by

$$\rho(r) = \exp(-\pi s_o^2 r^2), \tag{2}$$

where $s_o = \sin\varphi_o$ and r is the antenna separation in radar wavelengths [*Briggs*, 1992]. If

$$\sigma(s) \propto \exp(-s^2/s_I^2), \tag{3}$$

$$G_T(s) \propto \exp(-s^2/s_T^2), \tag{4}$$

$$G_R(s) \propto \exp(-s^2/s_R^2), \tag{5}$$

describe the angular spectrum s_I of the irregularities and G_T and G_R are the transmitter and receiver polar diagrams as a function of $s = \sin\varphi$, respectively, then

$$\frac{1}{s_o^2} = \frac{1}{s_I^2} + \frac{1}{s_T^2} + \frac{1}{s_R^2}. \tag{6}$$

In the present case, $\varphi_T = 12°$ and $\varphi_R = 21.8°$, so, from the measured values of pattern scale, $\rho_{0.5}$, it is straightforward to estimate φ_I, the angular width of the atmospheric echoes.

The scale at the top of Figure 4 gives the conversion of the pattern scale to angular width. An infinite value corresponds to isotropic scatter. The rather narrow angular widths observed in the lowest range gates are probably caused by incomplete removal of slow fading clutter. However, the decrease in φ_I with height is most likely real. There are at least two reasons for the effect. First, the backscattering irregularities may be more aspect sensitive in the more stable free atmosphere above the well-mixed boundary layer. Second, it is possibly a selection effect, as irregularities which scatter energy preferentially from overhead are more likely to be observed by the vertically pointing radar at longer ranges, where the SNR are smallest.

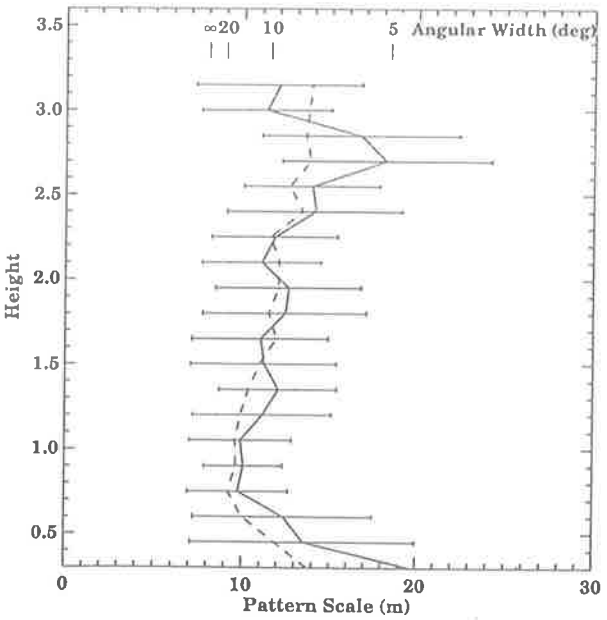

Figure 4. Vertical profiles of mean pattern scale for campaign I (solid line) and campaign II (dashed line). The scale at the top gives the angular width of the backscattered echoes.

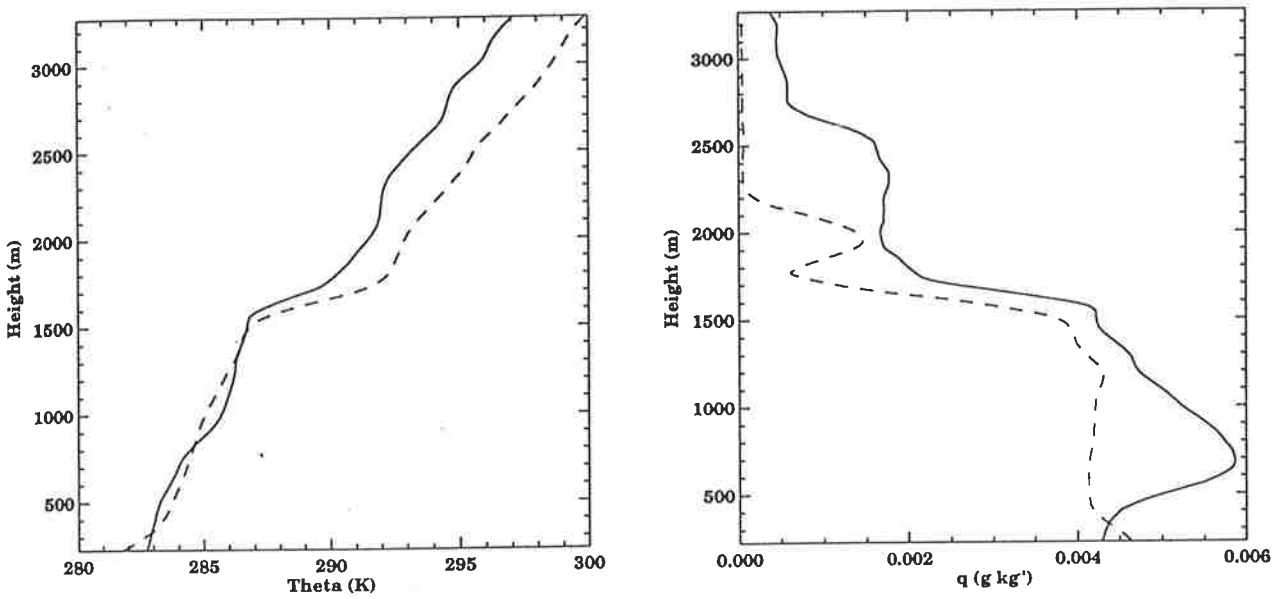

Figure 5. Vertical profiles of (left) potential temperature and (right) specific humidity derived from radiosonde soundings at 1206 LT (solid line) and 0206 LT (dashed line).

3.2. Campaign I

During this period a strong high-pressure region (~1035 hPa) was centered over the site. The BL observations were interleaved with observations with another radar also undergoing tests at Buckland Park, so the effective sample period was 2 min. Eleven radiosondes were launched at intervals of approximately 3 hours.

Day and night profiles of potential temperature and specific humidity q are shown in Figure 5. There is a marked subsidence inversion clearly evident in all profiles. The daytime boundary layer is reasonably well mixed but contains a localized stable layer at a height of about 800 m and a corresponding maximum in specific humidity. The nighttime profile shows a residual mixed layer overlying a typical ground-based radiation inversion. Figure 6 shows the time-height cross section of the signal-to-noise ratios (SNR). Values were smoothed over 30 min to reduce some of the short-term variability. There is a clear relationship between the strong subsidence inversion and the layer of enhanced reflectivity, analogous to the results of *Angevine et al.* [1994b] with a 915-MHz profiler. This example is particularly clear compared with typical 915-MHz estimates of boundary layer depth, but it is not evident if it is the result of the difference in radar frequency or of the intense subsidence inversion. The nighttime profiles show the growth of a nocturnal inversion at altitudes below 400 m and a fossil mixed layer (residual layer) that is very evident in q at heights below 1200 m. During the night, there is no heating from below to produce turbulent fluctuations of temperature and moisture (and hence scattering irregularities) in the fossil mixed layer, a condition exacerbated by the light winds.

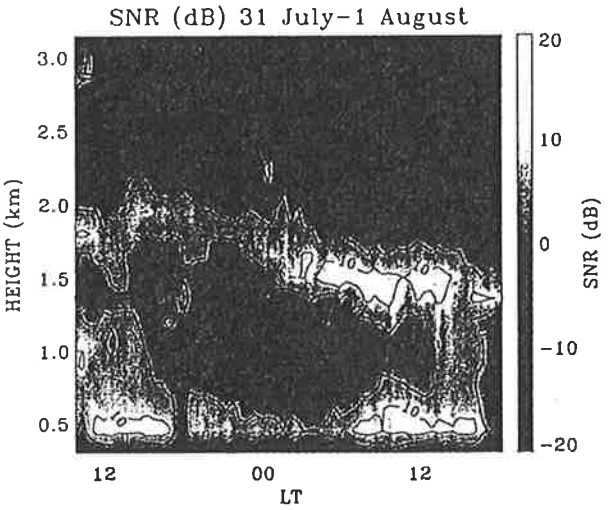

Figure 6. Time-height cross section of 30-min average signal-to-noise ratios observed in campaign I.

Meteorological parameters recorded during the radiosonde ascents can be used to gain some insight into radar performance. The received power P_R is related to the range R and radar reflectivity η by

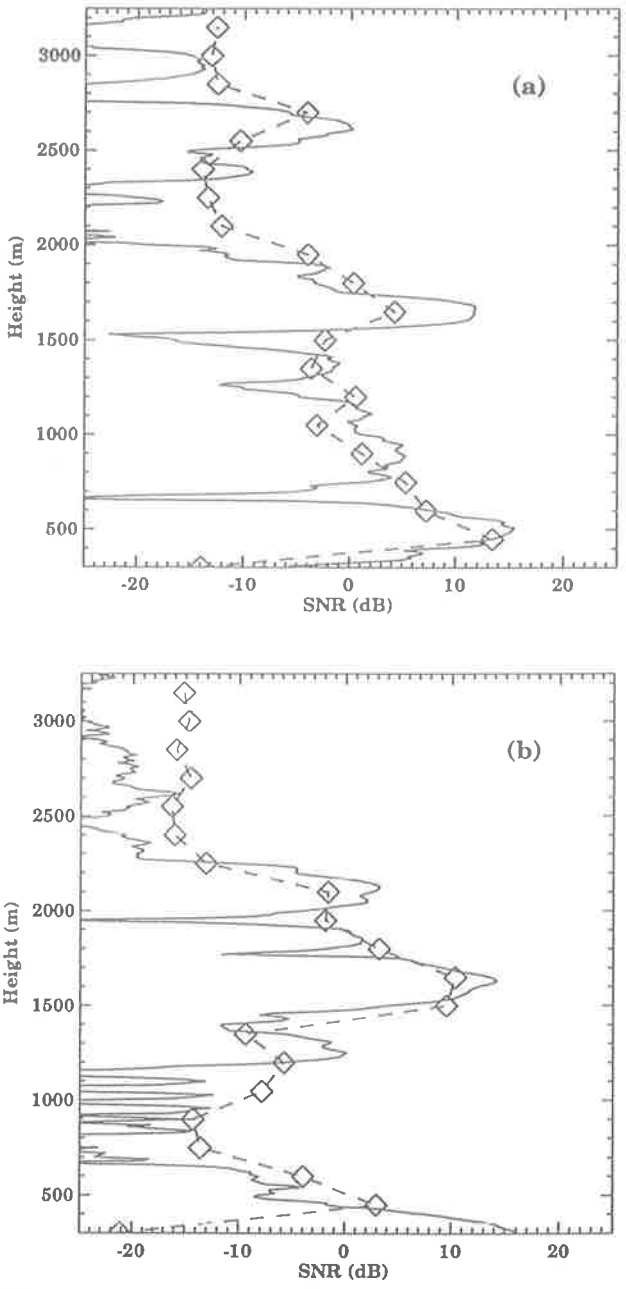

Figure 7. Vertical profiles of refractivity from radiosondes (solid line) and radar (dashed line) measurements for (a) 1200 LT July 31, 1997, and (b) 0206 LT August 1, 1997.

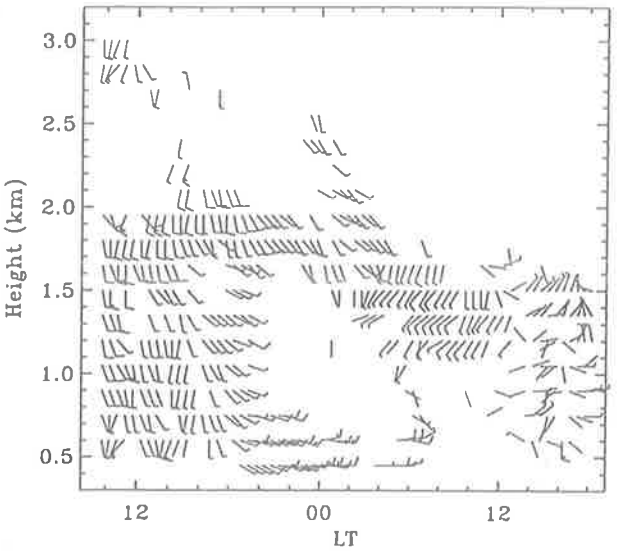

Figure 8. Half-hour average horizontal winds measured between July 31 and August 1, 1997. A half barb represents 2.5 m s^{-1}, and a full barb represents 5 m s^{-1}.

$$P_R \propto \frac{\eta}{R^2} \tag{7}$$

The reflectivity is related to the turbulent refractive index C_n^2, which, in turn, can be expressed in terms of the outer scale of turbulence and the gradient of radio refractive index, M, where

$$M = -77.610^{-6}\frac{p}{T}\left(\frac{\partial ln\theta}{\partial z}\right)\left[1+\frac{15500q}{T}\left(1-\frac{1}{2}\frac{\partial lnq/(\partial z)}{\partial ln\theta/(\partial z)}\right)\right] \tag{8}$$

and z is height [*VanZandt et al.*, 1978]. Vertical profiles of M^2 were constructed from profiles of temperature T, pressure p (measured in hectopascals), potential temperature q, and specific humidity. The observations were made with 2-s time resolution, equivalent to approximately 8–10 m height resolution.

Figure 7 compares SNR values in decibels observed by the radar and estimated from the radiosonde soundings during both day and night conditions. The range-corrected reflectivity profiles constructed from the sonde values have been smoothed to give a height resolution comparable to the radar and have been increased by an arbitrary factor of 175 dB to bring them into approximate coincidence with the radar

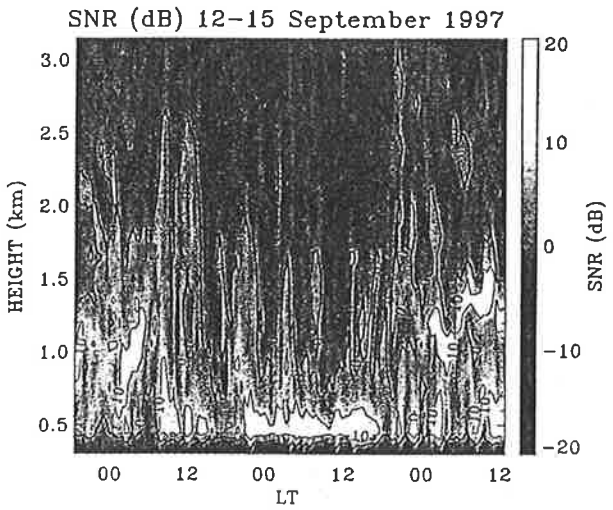

Figure 9. Same as for Figure 6, but for campaign II.

values. It is evident that the profiles agree rather well in shape and indicate that the time delays in the radar system were calibrated reasonably correctly. Both the sonde and radar profiles are characterized by strong peaks at heights near 1500 m and very weak reflectivities at night at heights between 500 and 1200 m.

The corresponding horizontal wind field is shown in Figure 8. The winds were very light, rarely exceeding 5 m s^{-1}. No winds were recorded in the lowest range gate at 300 m due to slower recovery in one of the receivers. However, winds were frequently measured at the second lowest range gate at 450 m, and observations extended to heights near or above 2 km. Noticeable gaps in the wind measurements occurred during periods centered on 0000 and 1000–1200 LT on August 1. In the latter interval, no winds were measured at heights near 0.5 km, despite the fact that the SNR was near 10 dB. The cause was the presence of stronger than average slow fading ground clutter superimposed on the atmospheric echoes. This emphasizes the need for improved clutter suppression. The gap centered on midnight was caused by SNR values that fell as low as -20 dB in the height range between 600 and 1500 m.

3.3. Campaign II

The second case study centered on the passage of a cutoff low across the radar site. A time-height cross section of SNR is shown in Figure 9, and Figure 10 shows the wind field, where its vortex nature is clearly evident. The SNR plot shows little evidence of the layering so evident in Figure 6, and this is also evident in profiles of potential temperature and humidity (Figure 11), which show a much smoother variation with height than is evident in the profiles in Figure 5. The high SNR means that there were often sufficient useful echoes to produce winds at most times at heights between 450 m and 3000 m.

During this campaign, quite heavy rain fell on occasion. The rain gave the opportunity to test the capability of the profiler to distinguish rain echoes from the signals scattered from the clear air despite the expected large amount of spectral broadening due to the wide beam width. That rain echoes can be detected is illustrated in Figure 12, which shows stacked plots of Doppler spectra normalized to the strongest signal in each spectrum. The spectra, which were constructed by averaging nine spectra obtained in a 16-min interval, show strong precipitation echoes with downward velocities in the range 5–10 m s^{-1} in the height range between 500 and 2000 m. At this time the precipitation system was quite shallow. Satellite measurements of cloud top temperatures over Adelaide at this time were only about -10°C, with deeper cloud about 300 km to the east.

The important point is that the clear-air echo can be used to measure the vertical air velocity as a function of height. The ability to distinguish the clear-air and precipitation echoes is also an impor-

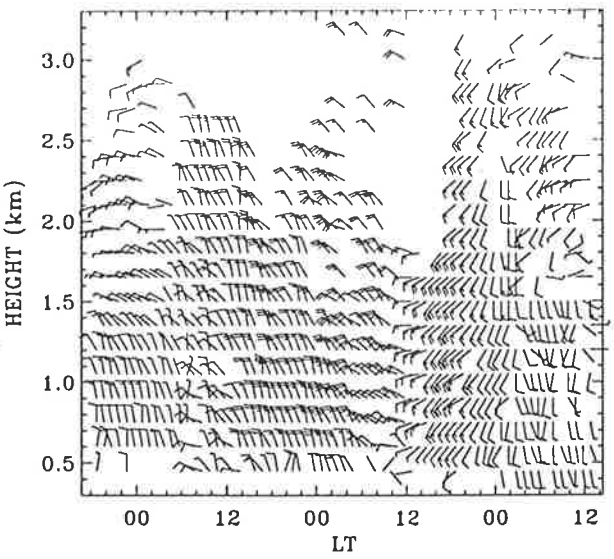

Figure 10. Same as for Figure 8, but for campaign II.

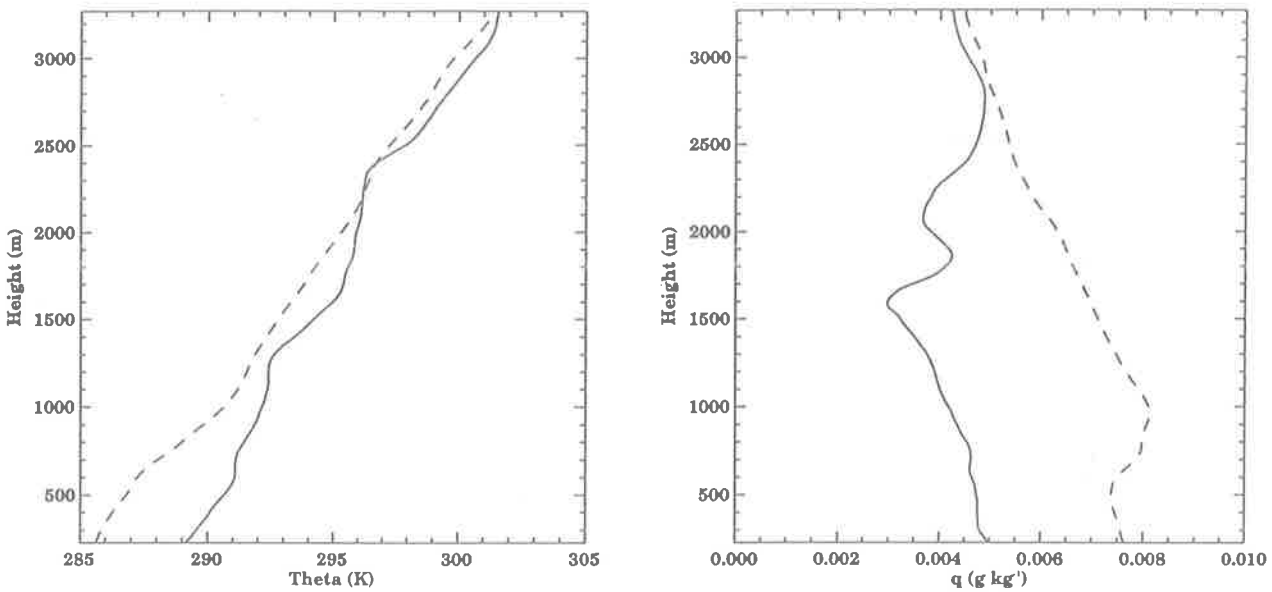

Figure 11. Velocity profiles of (left) potential temperature and (right) specific humidity derived from soundings on September 13 at 1057 LT (solid line) and 2348 LT (dashed line).

tant factor in the deconvolution procedures required to deduce drop-size distributions [*Rajopadhyaya et al.*, 1993]. All these factors illustrate the capability of the VHF profiler for observing mesoscale detail within weather systems, including vertical wind measurements in rain.

3.4. RASS Measurements

In common with other profiler-based RASS systems, the Adelaide BL RASS uses a FM CW acoustic excitation to ensure that a range of temperatures can be measured [*May et al.*, 1990]. Pseudorandom, sawtooth, and triangular sweep types are software selectable, together with appropriate bandwidths and dwell times to ensure a good match at the Bragg frequency [*May et al.*, 1990; *Angevine et al.*, 1994a]. The use of fast digitizers, and limited amounts of coherent integration give an effective sample rate of 320 Hz and ensure a Nyquist frequency significantly higher than the acoustic echo. The power spectra computed from the 1024 point samples at each height encompass both the acoustic-echo peak near 120 Hz and the clear-air echo near 0 Hz.

A number of different modes of operation of the RASS have been evaluated. The acoustic source, which is free running to ensure a flat spectrum over the range of operation [*Angevine et al.*, 1994a], is fed to a 1-kW audio amplifier which drives a vertically pointing stadium horn. Table 5 summarizes the mode of operation currently in use. Data are recorded for 6.4 s and then transferred to the computer; allowing for data transfer and power spectral analysis, the effective sample time is about 10 s. Usually, about 20–30 spectra are incoherently summed to improve the signal-to-noise ratios, which means that the time resolution of the temperature retrievals is 4–5 min. The spectral parameters for the acoustic echo are computed by the moment method, and the vertical velocity derived from the clear-air echo is used to correct the sound speed before it is converted to virtual temperature [e.g., *Angevine et al.*, 1994a].

Comparisons with RASS measurements and virtual temperatures computed from the temperature and humidity profiles derived from collocated radiosonde soundings are shown in Figure 13. RASS measurements were made over a period of 15–20 min near the time of the release of the sondes, and the values shown are the result of averaging four to five data sets so that the bars give an idea of the degree of variability in the retrieved temperatures. It is apparent that the agreement is excellent. The plots also illustrate that temperatures can be measured from heights as low as 500 m to as high as at least 2500 m. However, they also illustrate some of the difficulties that can be encountered with the present experimental setup. *Bauer and Peters* [1993] and *May*

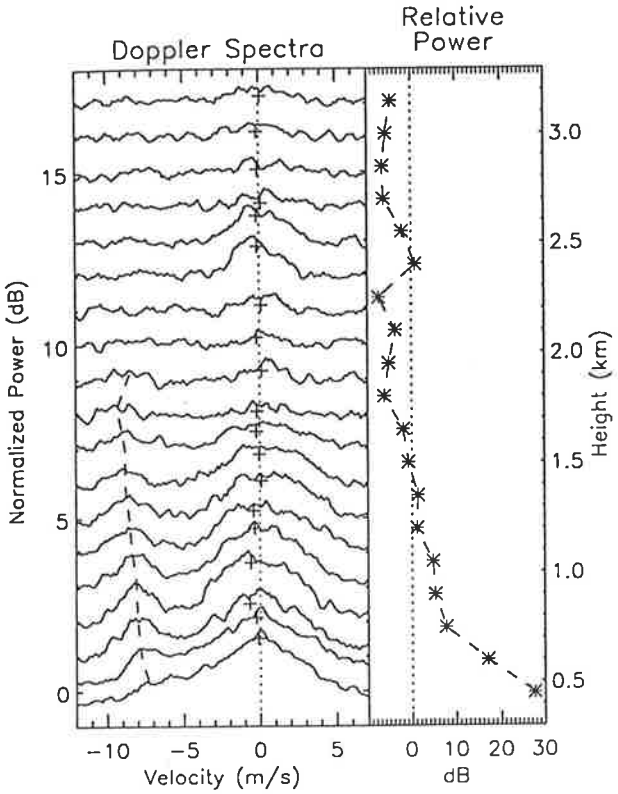

Figure 12. Stacked Doppler spectra obtained between 0400 and 0416 LT on September 14, 1997. At each height the first moment of the clear-air spectral peak, indicated by a plus sign, gives the vertical velocity. The dashed line shows the position of the peak of the precipitation echo. The vertical profile of relative echo power of the clear air peak is shown in the right panel.

et al. [1996] have shown that the RASS signal is focused onto a diffraction-limited spot approximately the size of the transmitting antenna. The small antennas used here mean that the acoustic spot is also small and is easily advected out of the radar beam by the background horizontal winds. It was necessary to carefully place the speaker upwind of the transmitting array to ensure the good height coverage evident in Figure 13a. Future developments include multiple acoustic sources.

4. Conclusions

Here we have discussed the development of a VHF (50 MHz) boundary layer radar and illustrated its capabilities with some of the first results obtained with the system. The system is compact and modular in nature so that it can be operated to use a range of wind-measuring techniques. A notable feature is that very useful wind and temperature measurements were obtained with quite small antennas for transmission and reception. The antennas are a compromise between wanting to make them as small as possible to minimize ringing and thus achieve the desired lower height limit and making them large enough to obtain sufficient gain to attain the desired upper height limit and to reduce clutter and interference.

Initial measurements made with the new boundary layer VHF radar show that its performance meets the design specifications, with wind and temperature measurements being made with good accuracy on a regular basis to over 2 km in altitude. The ability to distinguish rain echoes from the clear-air echo has also been demonstrated. This is an important attribute, which will allow the study of precipitation drop-size distributions to be extended downward into the boundary layer. Overall, the performance compares well with UHF profilers operating near 1 GHz at a similar stage of their development [*Ecklund et al.*, 1990; *Hashiguchi et al.*, 1995].

The next stage is to improve the height coverage. Wind and temperature measurements are made reg-

Table 5. Typical Radio Acoustic Sounding System Operating Parameters

Parameter	Value
Pulse repetition frequency*	20,480 Hz
Number of coherent integrations*	64
Number of data points per sample*	2,048
Height coverage*	100–3100 m
Record length	6.4 s
Range resolution*	150 m
Nyquist frequency	160 Hz
Acoustic frequency range*	118–126 Hz
Acoustic power	~150 W
Acoustic excitation*	FM CW sawtooth sweep
Acoustic steps*	200
Frequency step*	0.04 Hz
Dwell time (per frequency step)*	100 ms

*Software selectable.

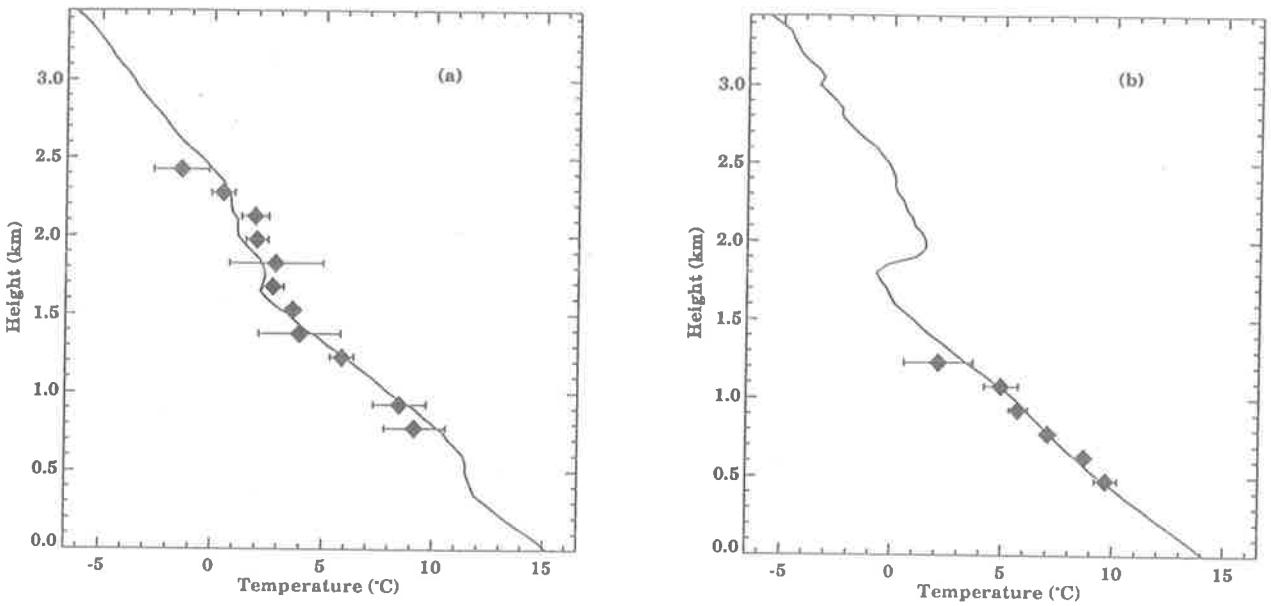

Figure 13. (a) Profile of virtual temperature derived from a radiosonde sounding at 1530 LT on October 18, 1997. Radio acoustic sounding system measurements made from 1500 to 1515 LT are indicated by diamonds. (b) Same as for (a), but for 1750 LT on October 19, 1997 with RASS measurements made from 1732 to 1805 LT.

ularly to heights as low as 450 m and sometimes as low as 300 m. Recent testing shows that it is possible to get to lower heights by using pulse lengths of 0.75 μs and exploiting the capacity of the system to make observations with a 100-m range resolution. Similarly, the upper height limit is improved by increasing the mean power, either by using pulse coding or using longer pulses to give a 300-m resolution. Using 300-m pulses, it has been possible to achieve observations as high as 5000 m. It should also be possible to use somewhat larger antennas for both transmission and reception, which will improve the power-aperture product and hence over-all system sensitivity. Tests of the system with these improvements are now in progress, as are tests using interferometric techniques to better define the dominant directions of scatter and correct the vertical velocities.

Acknowledgments. The development of the radar was made possible by the support of grant A69331543 from the Australian Research Council. The help and provision of radiosonde equipment by J. Stickland, Australian Bureau of Meteorology, and M. J. Reeder, Monash University, are gratefully acknowledged.

References

Angevine, W. M., and J. I. MacPherson, Comparison of wind profiler and aircraft wind measurements at Chebogue Point, Nova Scotia, *J. Atmos. Oceanic Technol., 12*, 421-426, 1995.

Angevine, W. M., W. L. Ecklund, D. A. Carter, K. S. Gage, and K. P. Moran, Improved radio acoustic sounding techniques, *J. Atmos. Oceanic Technol., 11*, 42-49, 1994a.

Angevine, W. M., A. B. White, and S. K. Avery, Boundary layer depth and entrainment zone characterization with a boundary layer profiler, *Boundary Layer Meteorol., 68*, 375-385, 1994b.

Bauer, M., and G. Peters, On the altitude coverage of temperature profiling by RASS, in *26th International Conference on Radar Meteorology*, pp. 487-489, Am. Meteorol. Soc., Boston, Mass., 1993.

Briggs, B. H., The analysis of spaced sensor records by correlation techniques, in *Handbook for MAP*, vol. 13, edited by R. A. Vincent, pp. 166-186, SCOSTEP, Secr. Univ. of Ill., Urbana, 1984.

Briggs, B. H., Radar measurements of aspect sensitivity of atmospheric scatterers using spaced-antenna correlation techniques, *J. Atmos. Sol. Terr. Phys., 54*, 153-165, 1992.

Carter, D. A., K. S. Gage, W. L. Ecklund, W. M. Angevine, P. E. Johnston, A. C. Riddle, J. Wilson, and C. R. Williams, Developments in UHF lower tropospheric wind profiling at NOAA's Aeronomy Laboratory, *Radio Sci., 30*, 977-1001, 1995.

Crochet, M., C. Bourdier, and E. Spano, VHF ST radar for low altitude investigations, in *Proceedings of the 6th Workshop on Technical and Scientific Aspects of MST Radar*, edited by B. Edwards, pp. 128-131, SCOSTEP, Secr. Univ. of Ill., Urbana, 1994.

Ecklund, W. L., D. A. Carter, and B. B. Balsley, A UHF wind profiler for the boundary layer: Brief description and initial results, *J. Atmos. Oceanic Technol., 5*, 432-441, 1988.

Ecklund, W. L., D. A. Carter, B. B. Balsley, P. E. Currier, J. L. Green, B. L. Weber, and K. S. Gage, Field tests of a lower tropospheric wind profiler, *Radio Sci., 25*, 899-906, 1990.

Fillol, J.-M., P. Broche, and M. Crochet, Retrieval of stratified atmospheric reflectivity and wind velocity using inverse methods: Application to a VHF ST mini-radar, *J. Atmos. Sol. Terr. Phys., 59*, 1159-1177, 1997.

Gage, K. S., Radar observations of the free atmosphere: Structure and dynamics, *Radar in Meteorology*, edited by D. Atlas, pp. 534-565, Am. Meteorol. Soc., Boston, Mass., 1990.

Hashiguchi, H., S. Fukao, T. Tsuda, M. D. Yamanaka, D. L. Tobing, T. Sribimati, S. W. Harijono, and H. Wiryosumarto, Observations of the planetary boundary layer over equatorial Indonesia with an L-band clear-air Doppler radar: Initial results, *Radio Sci., 30*, 1043-1054, 1995.

Holdsworth, D. A., Signal analysis with applications to atmospheric radars, Ph.D. thesis, 371 pp., Univ. of Adelaide, Adelaide, South Aust., Australia, 1995.

Jordan, J. R., R. J. Lataitis, and D. A. Carter, Removing ground and intermittent clutter contamination from wind profiler signals using wavelet transforms, *J. Atmos. Oceanic Technol., 14*, 1280-1297, 1997.

May, P. T., Spaced antenna versus Doppler radars: A comparison of techniques revisited, *Radio Sci., 25*, 1111-1119, 1990.

May, P. T., The Australian nocturnal jet and diurnal variations of boundary-layer winds over Mt. Isa in north-eastern Australia, *Q. J. R. Meteorol. Soc., 121*, 987-1003, 1995.

May, P. T., R. G. Strauch, and K. P. Moran, The altitude coverage of temperature measurements using RASS with wind profiler radars, *Geophys. Res. Lett., 15*, 1381-1384, 1988.

May, P. T., R. G. Strauch, K. P. Moran, and W. L. Ecklund, Temperature sounding by RASS with wind profiler radars: A preliminary study, *IEEE Trans. Geosci. Remote Sens., 28*, 19-28, 1990.

May, P. T., T. Adachi, T. Tsuda, and R. J. Lataitis, The spatial structure of RASS echoes, *J. Atmos. Oceanic Technol., 13*, 1275-1284, 1996.

Rajopadhyaya, D., P. T. May, and R. A. Vincent, A general approach to the retrieval of rain drop-size distributions from VHF wind profiler Doppler spectra: Modelling results, *J. Atmos. Oceanic Technol., 10*, 710-717, 1993.

Riddle, A. C., W. M. Angevine, W. L. Ecklund, E. R. Miller, D. B. Parsons, D. A. Carter, and K. S. Gage, In situ and remotely sensed horizontal winds and temperature intercomparisons obtained using integrated sounding systems during TOGA COARE, *Beitr. Phys. Atmos., 69*, 49-61, 1996.

Röttger, J., The MST radar technique, in *Handbook for MAP*, vol. 13, edited by R. A. Vincent, pp. 187-232, SCOSTEP, Secr., Univ. of Ill., Urbana, 1984.

Strauch, R. G., D. A. Merritt, K. P. Moran, K. B. Earnshaw, and D. Van de Kamp, The Colorado wind profiling network, *J. Atmos. Oceanic Technol., 1*, 37-49, 1984.

VanZandt, T. E., J. L. Green, K. S. Gage, and W. L. Clark, Vertical profiles of refractivity turbulence structure constant: Comparison of observations by the Sunset radar with a new theoretical model, *Radio Sci., 13*, 819-829, 1978.

Vincent, R. A., and J. Röttger, Spaced antenna VHF radar observations of tropospheric velocities and irregularities, *Radio Sci., 15*, 319-335, 1980.

Vincent, R. A., P. T. May, W. K. Hocking, W. G. Elford, B. H. Candy, and B. H. Briggs, First results with the Adelaide VHF radar: Spaced antenna studies of tropospheric winds, *J. Atmos. Sol. Terr. Phys., 49*, 353-366, 1987.

Weber, B. L., and D. A. Wuertz, Comparison of rawinsonde and wind profiler radar measurements, *J. Atmos. Oceanic Technol., 7*, 157-174, 1990.

Wilczak, J. M., et al., Contamination of wind profiler data by migrating birds: Characteristics of corrupted data and potential solutions, *J. Atmos. Oceanic Technol., 12*, 449-467, 1995.

Wilson, K. J., and H. Stern, The Australian summertime cool change, 1, Synoptic and sub-synoptic aspects, *Mon. Weather Rev., 113*, 177-201, 1985.

Wright, J. W., and M. L. V. Pitteway, Computer simulations of ionospheric radar drift measurements and their analysis by correlation methods, *Radio Sci., 13*, 189-210, 1978.

S. Dullaway, A. MacKinnon, I. M. Reid, R. A. Vincent, and F. Zink, Department of Physics, University of Adelaide, Adelaide, SA 5005, Australia. (e-mail: rvincent@physics.adelaide.edu.au)

B. H. Johnson, Atmospheric Radar Systems, 1/12 Sterling St., Thebarton, SA 5031, Australia. (e-mail: bjohnson@atrad.com.au)

P. T. May, Bureau of Meteorology Research Centre, PO Box 1289K, Melbourne, VIC 3001, Australia. (e-mail: p.may@bom.gov.au)

(Received December 17, 1997; revised March 5, 1998; accepted March 10, 1998.)

References

Angevine, W. M. (1998), Boundary layer height measurements with UHF profilers: Toward automated recognition and quality control, *in* 'Fourth International Symposium on Tropospheric Profiling: Needs and Technologies', pp. 13–15.

Angevine, W. M. and Grimsdell, A. W. (1998), Turbulence measurements with UHF profilers: Lessons from the Flatland Boundary Layer Experiments, *in* 'Fourth International Symposium on Tropospheric Profiling: Needs and Technologies', pp. 10–12.

Briggs, B. H. (1968*a*), 'On the analysis of moving patterns in geophysics, Part I, Correlation Analysis', *Journal of Atmospheric and Terrestrial Physics* **30**, 1777–1788.

Briggs, B. H. (1968*b*), 'On the analysis of moving patterns in geophysics, Part II, Dispersion Analysis', *Journal of Atmospheric and Terrestrial Physics* **30**, 1789–1794.

Briggs, B. H. (1980), 'Radar observations of atmospheric winds and turbulence: a comparison of techniques', *Journal of Atmospheric and Terrestrial Physics* **42**, 823–833.

Briggs, B. H. (1984), The analysis of spaced sensor records by correlation techniques, *in* 'Handbook for the Middle Atmosphere Program', Vol. 13, Special Committee for Solar-Terrestrial Physics Secretariat, pp. 166–186.

Briggs, B. H. (1992), 'Radar measurements of aspect sensitivity of atmospheric scatterers using spaced-antenna correlation techniques', *Journal of Atmospheric and Terrestrial Physics* **54**(2), 153–165.

Briggs, B. H. (1993), 'Observations of atmospheric dynamics using radar techniques', *Australian Journal of Physics* **46**(2), 127–147.

Carter, D. A., Gage, K. S., Ecklund, W. L., Angevine, W. M., Johnston, P. E., Riddle, A. C., Wilson, J. and Williams, C. R. (1995), 'Developments in UHF lower tropospheric profiling at NOAA's Aeronomy Laboratory', *Radio Science* **30**(4), 977–1001.

Clifford, S. F., Wang, T. and Priestley, J. T. (1978), 'Spot size of the radar return from a radar-acoustic sounding system (RASS) due to atmospheric refractive turbulence', *Radio Science* **13**(6), 985–989.

Cohn, S. A., Rogers, R. R., Jascourt, S., Ecklund, W. L., Carter, D. A. and Wilson, J. S. (1995), 'Interactions between clear-air reflective layers and rain observed with a boundary layer wind profiler', *Radio Science* **30**(2), 323–341.

Cohn, S. A., Susedik, M., Holloway, C. L. and Doviak, R. J. (1998), Boundary layer Spaced Antenna wind measurements, *in* 'Fourth International Symposium on Tropospheric Profiling: Needs and Technologies', pp. 61–63.

Crescenti, G. H. (1997), 'A Look Back on Two Decades of Doppler Sodar Comparison Studies', *Bulletin of the American Meteorological Society* **78**, 651–673.

Crochet, M. (1993), 'VHF ST radar for low altitude investigations', *Proceedings of the Sixth Workshop on Technical and Scientific Aspects of MST Radar* pp. 128–131.

Currier, P. E., Avery, S. K., Balsley, B. B., Gage, K. S. and Ecklund, W. L. (1992), 'Combined use of 50 MHz and 915 MHz wind profilers in the estimation of rain-drop size distributions', *Geophysical Research Letters* **19**, 1017–1020.

Doviak, R. J. and Zrnić, D. S. (1993), *Doppler Radar and Weather Observations*, 2nd edn, Academic Press, San Diego, California.

Ecklund, W. L., Carter, D. A., Balsley, B. B., Currier, P. E., Green, J. L., Weber, B. L. and Gage, K. S. (1990), 'Field tests of a lower tropospheric wind profiler', *Radio Science* **25**(5), 899–906.

Fillol, J. M., Broche, P. and Crochet, M. (1997), 'Retrieval of stratified atmospheric reflectivity and wind velocity using inverse methods: application to a VHF ST mini-radar', *Journal of Atmospheric and Terrestrial Physics* **59**(10), 1159–1177.

Frankel, M. S. and Peterson, A. M. (1976), 'Remote temperature profiling in the lower atmosphere', *Radio Science* **11**(3).

Gage, K. S. (1981), Wind measurement techniques available for the middle atmosphere program, *in* 'Handbook for the Middle Atmosphere Program', Vol. 2, Special Committee for Solar-Terrestrial Physics Secretariat, pp. 21–29.

Gage, K. S. and Balsley, B. B. (1980), 'On the scattering and reflection mechanisms contributing to clear air radar echoes from the troposphere, stratosphere, and mesosphere', *Radio Science* **15**, 243–257.

Gage, K. S., Balsley, B. B. and Green, J. L. (1981), 'Fresnel scattering model for the specular echoes observed by VHF radar', *Radio Science* **16**, 1447–1453.

Gage, K. S. and Green, J. L. (1978), 'Evidence for specular reflection from monostatic VHF radar observations of the stratosphere', *Radio Science* **13**, 991–1001.

Gage, K. S., Green, J. L. and VanZandt, T. E. (1980), 'Use of Doppler radar for the measurement of atmospheric turbulence parameters from the intensity of clear-air echoes', *Radio Science* **15**(2), 407–416.

Gage, K. S., Williams, C. R., Ecklund, W. L. and Johnston, P. E. (1998), 'Use of two profilers during MCTEX for unambiguous identification of Bragg scattering and Rayleigh scattering', *Journal of the Atmospheric Sciences* . In press.

Golley, M. and Rossiter, D. (1970), 'Some tests of methods of analysis of ionospheric drift records using an array of 89 aerials', *Journal of Atmospheric and Terrestrial Physics* **32**(7), 1215–1233.

Hocking, W. K. (1983*a*), 'On the extraction of atmospheric turbulence parameters from radar backscatter Doppler spectra–I. theory', *Journal of Atmospheric and Terrestrial Physics* **45**(2/3), 89–102.

Hocking, W. K. (1983*b*), 'The Spaced Antenna Drift method', *Handbook for the Middle Atmosphere Program* **9**, 171–186. SCOSTEP Secretariat, University of Illinois, Urbana, Illinois.

Hocking, W. K. and Mu, P. K. L. (1997), 'Upper and middle tropospheric kinetic energy dissipation rates from measurements of $\bar{C}_n^2$ - review of theories, *in-situ* investigations, and experimental studies using the Buckland Park atmospheric radar in Australia', *Journal of Atmospheric and Terrestrial Physics* **59**(14), 1779–1803.

Holdsworth, D. A. (1995), Signal analysis with applications to atmospheric radars, PhD thesis, University of Adelaide, Adel., Australia.

Holton, J. R. (1992), *An Introduction to Dynamic Meteorology*, 3rd edn, Academic Press, San Diego.

Houghton, J. T. (1986), *The physics of atmospheres*, 2nd edn, Cambridge University Press, London.

Kelleher, R. F. (1966), 'Some statistical properties of the ground diffraction patterns of vertically reflected radio waves', *Journal of Atmospheric and Terrestrial Physics* **28**, 213–224.

Larsen, M. F. and Röttger, J. (1989), 'The Spaced Antenna Technique for Radar Wind Profiling', *Journal of Atmospheric and Oceanic Technology* **6**(6), 920–938.

Liu, C. H., Röttger, J., Pan, C. J. and Franke, S. J. (1990), 'A model for Spaced Antenna observational mode for MST radars', *Radio Science* **25**(4), 551–563.

Low, D. J. (1995), Some applications of a VHF wind profiler to studies in dynamic and mesoscale meteorology, PhD thesis, University of Adelaide, Australia.

Masuda, Y., Awaka, J., Nakamura, K., Adachi, T. and Tsuda, T. (1992), 'Analysis of the radio acoustic sounding system using a chirped acoustic wave', *Radio Science* **27**(5), 681–691.

May, P. T. (1986), VHF radar studies of the Troposphere, PhD thesis, University of Adelaide, Adel., Australia.

May, P. T., Holland, G. J. and Ecklund, W. L. (1994), 'Wind Profiler Observations of Tropical Storm Flow at Saipan', *Weather and Forecasting* **9**, 410–426.

May, P. T., Strauch, R. G. and Moran, K. P. (1988), 'The altitude coverage of temperature measurements using RASS with wind profiler radars', *Geophysical Research Letters* **15**(12), 1381–1384.

Merritt, D. (1995), 'A Statistical Averaging Method for Wind Profiler Doppler Spectra', *Journal of Atmospheric and Oceanic Technology* **12**(3), 985–995.

Ohno, Y., Williams, C. R. and Gage, K. S. (1998), Statistical study of rain types using UHF wind profilers, *in* 'Fourth International Symposium on Tropospheric Profiling: Needs and Technologies', pp. 240–242.

Rajopadhyaya, D. K. (1994), Meteorological studies using a VHF radar, PhD thesis, University of Adelaide, Adel., Australia.

Rajopadhyaya, D., May, P. T. and Vincent, R. A. (1993), 'A general approach to the retrieval of rain dropsize distributions from VHF wind profiler Doppler spectra: Modelling results', *Journal of Atmospheric and Oceanic Technology* **10**, 710–717.

Richner, H., Kretzschmar, R. and Griesser, T. (1998), Neural network techniques for identifying and eliminating bird signals in 1290 MHz wind profiler spectral data, *in* 'Fourth International Symposium on Tropospheric Profiling: Needs and Technologies', pp. 270–272.

Rogers, R. R., LeBlanc, S. G., Cohn, S. A., Ecklund, W. L., Carter, D. A. and Wilson, J. S. (1996), 'Profiler measurements of turbulence and wind shear in a snowstorm', *Contributions to Atmospheric Physics* **69**(1), 27–36.

Röttger, J. (1984), 'The MST radar technique', *Handbook for the Middle Atmosphere Program* **13**, 187–232. SCOSTEP Secretariat, University of Illinois, Urbana, Illinois.

Röttger, J. and Liu, C. H. (1978), 'Partial Reflection and Scattering of VHF Radar Signals Fom the Clear Atmosphere', *Geophysical Research Letters* **5**(5), 357–360.

Sato, T. and Woodman, R. (1982), 'Spectral parameter estimation of cat radar echoes in the presence of fading clutter', *Radio Science* **17**, 817–826.

Tatarskii, V. I. (1961), *Wave propagation in a turbulent medium*, McGraw-Hill. Translated by R. A. Silverman.

Tsuda, T., VanZandt, T. E. and Saito, H. (1997), 'Zenith-angle dependence of VHF specular reflection echoes in the lower atmosphere', *Journal of Atmospheric and Terrestrial Physics* **59**(7), 761–775.

U.S. Standard Atmosphere (1976), *US Standard Atmosphere, 1976*, US Government Printing Office, pgs 9 - 11.

Väisälä (1996), *RS80 Radiosondes: Information Release.*

Van Baelen, J. S., Tsuda, T., Richmond, A. D., Avery, S. K., Kato, S., Fukao, S. and Yamamoto, M. (1990), 'Comparison of VHF Doppler beam swinging and Spaced Antenna observations with the MU radar: first results', *Radio Science* **25**, 629–640.

Van Zandt, T. E., Warnock, J. M., Ecklund, W. L., Evans, W. R., Clark, W. L., Johnston, P. E. and Gage, K. S. (1998), Quantitative studies of the contributions to radar reflectivity from particulate and turbulent scatter using dual-wavelength radar, *in* 'Fourth International Symposium on Tropospheric Profiling: Needs and Technologies', pp. 353–355.

Vincent, R. A., Dullaway, S. N. M., MacKinnon, A., Reid, I. M., Zink, F., May, P. T. and Johnson, B. H. (1998), 'A VHF boundary layer radar: First results', *Radio Science* **33**(4), 845–860.

Vincent, R. A., May, P. T., Hocking, W. K., Elford, W. G., Candy, B. H. and Briggs, B. H. (1987), 'First results with the Adelaide VHF radar: Spaced Antenna studies of tropospheric winds', *Journal of Atmospheric and Terrestrial Physics* **49**, 353–366.

Vincent, R. A. and Röttger, J. (1980), 'Spaced Antenna VHF radar observations of tropospheric velocities and irregularities', *Radio Science* **15**, 319–335.

Wallace, J. M. and Hobbs, P. V. (1977), *Atmospheric Science: An Introductory Survey*, Academic Press, London.

Williams, C. R., Johnston, P. E., Ecklund, W. L. and Gage, K. S. (1998), Precipitation parameters derived using collocated UHF and S-band profilers, *in* 'Fourth International Symposium on Tropospheric Profiling: Needs and Technologies', pp. 335–337.

Woodman, R. F. (1981), Turbulence in the middle atmosphere: A review, *in* 'Handbook for the Middle Atmosphere Program', Vol. 2, Special Committee for Solar-Terrestrial Physics Secretariat, pp. 293–300.

Woodman, R. F. and Guillén, A. (1974), 'Radar observations of winds and turbulence in the stratosphere and mesosphere', *Journal of the Atmospheric Sciences* **31**, 493–505.